CALCIUM AS A SECOND MESSENGER IN DEVELOPING NERVE CELLS

Friedrich Zimprich

A thesis submitted for the degree of

Doctor of Philosophy

in the

University of London

Department of Physiology

University College London

October 1995

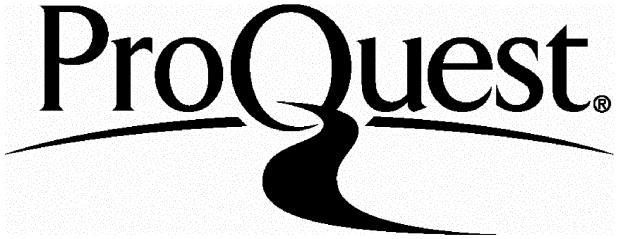

ABSTRACT

Calcium is thought to play a crucial role in the regulation of nerve cell development and growth cone behaviour. In this context I studied three aspects of calcium as a second messenger.

- In growth cones of the N1E-115 cell line I studied the properties and distribution of calcium channels and the pattern of calcium flux through these channels.

- In the same cells the effect of the cytosolic calcium concentration $[Ca^{2+}]_i$ on neurite outgrowth was investigated.

-Finally I monitored spontaneous calcium changes in life zebrafish embryos.

1) In imaging experiments, using the calcium indicator dye Fluo-3, I studied the calcium influx into club-shaped growth cones which are characteristically found on advancing neurites. Depolarisation caused the highest calcium influx near the distal, leading tip. This gradient is not altered by blocking calcium induced calcium release from internal stores. Using the voltage clamp technique in the cell attached mode I identified and characterised T type and L type calcium channels on the growth cones of this cell line. L channel density was significantly higher at the distal tip than at the more proximal growth cone. The calcium gradient in the depolarised growth cone can thus be explained by a gradient of calcium channel density.

2) In N1E-115 cells decreasing $[Ca^{2+}]_i$ below the resting value promoted neurite outgrowth monotonically unlike the situation in some other celltypes

which show rather a bell shaped dependence. Surprisingly, neurite outgrowth was also promoted when $[Ca^{2+}]_i$ was raised much above the resting levels.

3) In an attempt to study calcium dynamics in nerve cells in an intact, *in vivo,* preparation the calcium indicator dye calcium-green dextran was injected into one of the blastomeres of a 2 to 3 hour old zebra fish embryo which was then allowed to develop further. Studying 18 to 24 hour old embryos, using a confocal microscope, labelled nerve cells among the daughter cells of the injected blastomere could be clearly identified according to their shape and position.

When such 24 hour old embryos were dissociated and plated on culture dishes labelled nerve cells responded to a depolarisation with a fluorescence increase demonstrating that the dye was retained in the cytoplasm and still capable of reporting calcium changes. Spontaneous calcium changes were observed in developing motoneurons in situ.

CONTENTS

LIST OF FIGURES

ABBREVIATIONS

AM	acetoxymethyl ester
BAPTA	1,2-bis(o-aminophenoxy)-ethane-N,N,N',N'-tetraacetatic acid
$[Ca^{2+}]_i$	cytosolic free calcium concentration
$[Ca^{2+}]_o$	free calcium concentration in the bathing medium
CCD	charge coupled device
CICR	calcium induced calcium release
DHP	dihydropyridine
DMEM	Dulbecco's modification of Eagle's medium
DMSO	dimethyl sulphoxide
DRG	dorsal root ganglion
EGTA	ethylene glycol-bis(β-aminoethyl ether) N,N.N',N'-tetraacetic acid
FCS	foetal calf serum
GABA	γ-aminobuturic acid
HEPES	N-[2-hydroxyethyl]piperazine-N'-[2-ethanesulfonic acid]
hpf	hours post fertilisation
HVA	high voltage activated
LTP	long term potentiation
LVA	low voltage activated
NA	numerical aperture
NMDA	N-methyl-D-aspartate
PBS	phosphate buffered saline
PC	Personal computer
Po	single channel open probability
RMS	root mean square
TEA	tetraethyl-ammonium
TRIS	hydroxymethyl-aminomethane
TTX	tetrodotoxin
VDCC	voltage dependent calcium channels

ACKNOWLEDGEMENTS

Above all, I want to sincerely thank Stephen Bolsover, my supervisor, for his guidance, advice, objective criticism and encouraging support during this work. I would also like to thank Hugh Pearson at the Royal Free Hospital for introducing me to the practical aspects of single channel patch clamping and Steve Wilson at King's College for helping me get the zebrafish experiments started. I am grateful to Michael Duchen, Angus Silver and David Attwell for helpful discussion on this work. Thanks too, to the many people in the Physiology Department that made my time here so enjoyable. Finally, I am indebted to the dedicated people of Action Research who work hard raising money and thus made the funding for this project possible.

PUBLICATIONS

F. Zimprich, S. R. Bolsover (1995) Calcium channels in neuroblastoma cell growth cones. *Eur Journal Of Neuroscience* submitted

F. Zimprich, K. Torok and S. R. Bolsover (1995) Nuclear calmodulin responds rapidly to calcium influx at the plasmalemma. *Cell Calcium, 17,* 233-238

F. Zimprich, M. Gailey and S. R. Bolsover (1994) Biphasic effect of calcium on neurite outgrowth in neuroblastoma and cerebellar granule cells. *Developmental Brain Research, 80,* 7-12

F. Zimprich and S. R. Bolsover (1994) Two populations of high voltage-activated (HVA) calcium channels in cultured neuroblastoma-cells. *Journal Of Physiology London, 475p,* P 147-P 147

CHAPTER 1

INTRODUCTION

1.1 CALCIUM AND NERVE CELL DEVELOPMENT

Calcium is one of the most important second messengers in the regulation of normal cellular function. In recent years it has emerged that calcium plays a particularly prominent role during neuronal development. Almost every aspect of nerve cell development studied so far was shown to be influenced by calcium. During the formation of the nervous system cells undergo maturation from an uncommitted epidermal cell to a fully functioning and differentiated nerve cell. Several key processes can be identified during this development which determine the eventual fate of the neuron. In the following paragraphs I will try to give a summary of those processes which are thought to be regulated by calcium.

Neural Induction: In amphibians during late gastrulation ectoderm cells overlying the mesoderm are induced to differentiate into neural cells. A recent paper by Moreau et al. (1994) has demonstrated that the signal for this differentiation is an influx of Ca^{2+} through L -type calcium channels. If the associated rise in intracellular calcium $[Ca^{2+}]_i$ is inhibited ectoderm cells develop into epidermis instead. In vertebrates neurogenesis usually occurs in germinal centres from where postmitotic nerve cells have to migrate to their final positions (Jacobson, 1991). The migration of cerebellar granule cells along a radial Bergmann glia scaffolding is a particularly well studied example (Hatten & Mason, 1990). During this movement granule cells exhibit cyclic fluctuations of $[Ca^{2+}]_i$ and the inhibitions of these transients by NMDA or N type calcium channel

blockers curtails the migration (Komuro & Rakic, 1992; Komuro & Rakic, 1993; Rakic et al., 1994). Usually at an early stage in its differentiation a neuron decides which transmitter it will express. Calcium influx has been shown to influence this choice of neurotransmitter phenotype in many preparations such as in sympathetic neurones where it stabilises adrenergic differentiation (Walicke & Patterson, 1981) or in mouse spinal neurones where it promotes a cholinergic differentiation (Ishida & Deguchi, 1983). In *Xenopus* spinal neurones action potentials elicit much larger calcium transients during an early critical period than later on in the development (Holliday & Spitzer, 1990). These transients promote the differentiation into γ-aminobuturic acid (GABA) positive interneurons and also regulate the maturation of potassium channels (Desarmenien & Spitzer, 1991; Spitzer et al., 1993; Gu & Spitzer, 1995).

The most obvious morphological change during the development of a nerve cell is the outgrowth of neurites from an initially unpolarised cell. The structure at the tip of neurites, the growth cone, contains the cellular machinery responsible for finding the correct pathway by integrating attractive or repulsive guidance information from the environment (Goldberg & Burmeister, 1989, Davis et al., 1992; Tessier-Lavigne, 1994). Many studies have now extensively documented that signalling by calcium ions is central in the regulation of growth cone behaviour (Kater & Mills, 1991). To list a few of these experiments: depending on the cell type studied either small increases or decreases in the intracellular calcium level were shown to promote the formation of new neurites and the rate of elongation (Gunderson & Barrett, 1980; Reboulleau, 1986; Mattson & Kater, 1987; Robson & Burgoyne, 1989; Silver et al., 1989; Al-Mohanna et al., 1992; Zimprich et al., 1994). Local outgrowth of filopodia and turning of the growth cone towards chemoattractants or an electric field has been

linked to small local increases in calcium (Gunderson & Barrett, 1980; Silver et al., 1990; Bedlack et al., 1992; Davenport & Kater, 1992; Williams et al., 1994; Zheng et al., 1994). Guidance information transmitted to the growth cone via cell adhesion molecules is clearly associated with calcium influx through voltage operated L or N type calcium channels (Williams et al., 1992; Doherty & Walsh, 1994). Calcium oscillations in the growth cones of Xenopus spinal neurones and chick embryo DRG's seem to signal the arrest of neurite elongation (Gomez et al., 1995; Gu & Spitzer, 1995), spontaneous electrical activity induced calcium influx in Purkinje cells causes dendrites to branch (Schilling et al., 1991), and finally growth cone collapse or retraction is mediated by large increases of cytosolic calcium (Silver et al., 1989; Fields et al., 1990; Bandtlow et al., 1993).

When growth cones meet their postsynaptic target membrane they are transformed to synapses. A retrograde signal from the postsynaptic cell causes the calcium to rise presynaptically and to remain high, and this calcium change is essential for the morphological development of the synapse and the induction of transmitter release (Dai & Peng, 1993; Funte & Haydon, 1993; Zoran et al., 1993; Haydon & Zoran, 1994). After synaptic connections have been established neurones are linked together to coactive networks. In the cerebral cortex the formation of such domains is characterised by synchronous calcium transients in all participating cells (Yuste et al., 1992). In the subsequent development of these initial networks to a complex central nervous system, the detailed synaptic wiring needs to be modulated continuously even after the completion of the embryonic phase. Again calcium is a key second messenger in this process. Long term potentiation (LTP) in the hippocampus, which is the best studied example of synaptic plasticity, requires the activation of

NMDA-glutamate receptors and the subsequent influx of calcium into the postsynaptic cell (Madison et al., 1991; Bliss & Collingridge, 1993).

Neuronal survival and cell death: In recent years it has become generally accepted that at all times during the development from undifferentiated precursor cells to the establishment of functioning connections, neurones need to be kept alive by active signalling from the environment. Only those nerve cells that receive such signals continue to develop whereas the redundant rest - it seems a significant proportion of all cells - are rapidly removed by a process termed apoptosis or programmed cell death (Jacobson, 1991; Altman, 1992).

Early studies showed that depolarisation enhances the survival of neurones in culture (Scott & Fisher, 1970). This effect was shown to be due to the influx of calcium ions through voltage operated L type channels and the resulting increased levels of $[Ca^{2+}]_i$ (Collins et al., 1991; Larmet et al., 1992; Lampe et al., 1995). Other studies have shown the paradoxical result that increased intracellular calcium levels can signal cell death or apoptosis in embryonic neurones (Takei & Endo, 1994; Wolszon et al., 1994).

In conclusion these experiments demonstrate that calcium is a widely used second messenger in the development of the nervous system. What enables calcium to be such a central player? One reason for this may lie in the fact that calcium occupies a strategic position. It can respond to a wide variety of different stimuli. Calcium can not only act as a classical second messenger but also carries a current across the membrane which can produce important use dependent effects. On the other hand calcium also affects an exceptionally broad range of intracellular process either directly or indirectly via the activation of calcium dependent molecules such as protein kinase C, the calcium calmodulin kinases or other enzymes. In the

context of nerve cell development important effects of calcium include its influence on the cytoskeleton which may explain its many effects of calcium on growth cone behaviour. Large increases in intracellular calcium concentration destabilise the actin cytoskeleton (Bentley & O'Connor, 1994; Neely & Gesemann, 1994), whereas small local increases may trigger the induction of new filopodia (Bedlack et al., 1992; Davenport & Kater, 1992). Calcium also plays a key role at various stages of secretion and incorporation of new membrane into the plasmalemma which are important steps for the release of neurotransmitters and growth of membrane (Neher & Zucker, 1993; Burgoyne, 1995). Finally calcium can trigger a signalling cascade resulting in the expression of new genes (Sheng et al., 1988; Bading et al., 1993; Gallin & Greenberg, 1995). Such a calcium induced gene expression was demonstrated in neurotransmitter differentiation, apoptosis and calcium promoted cell survival (Spitzer et al., 1993; Takei & Endo, 1994; Galli et al., 1995).

1.2 Regulation of calcium signalling

Maybe the most striking aspect of the above investigations taken together is that apparently very similar calcium signals, such a rise in $[Ca^{2+}]_i$, can mediate many disparate biological events or even opposite effects such as neurite elongation versus growth cone collapse or neuronal survival versus cell death. How is the cell able to maintain the independence of different stimulus response pathways if they all share calcium as an element in the signalling cascade? Several explanations can be applied to resolve this problem.

The level of $[Ca^{2+}]_i$ is important

The observation that distinct calcium sensitive processes in neurite outgrowth require different narrow ranges of calcium levels led to the proposal of the "calcium optimum" or "set-point hypothesis" (Mattson & Kater, 1987; Kater & Mills, 1991). According to this hypothesis the cell or the growth cone would integrate the various stimuli acting on the cell in terms of the cytosolic calcium concentration, and the resulting calcium level would or would not be within the permissive range for the particular process. In support of this hypothesis it was shown that in some developing neurones low levels of calcium are associated with growth cone advance, somewhat higher levels with increased filopodial activity and yet higher concentration with growth cone collapse and retraction (Silver et al., 1989). In dorsal root ganglion cells or cerebellar neurones neurite outgrowth clearly shows a bell shaped dependence on $[Ca^{2+}]_i$ (Al-Mohanna et al., 1992; Zimprich et al., 1994). A similar calcium optimum hypothesis has been suggested for the calcium dependence of early neuronal survival or death (Koike et al., 1989; Larmet et al., 1992), or the events related to synaptogenesis (Dai & Peng, 1993; Zoran et al., 1993) but as outlined below for many other processes this theory is not an adequate explanation (Fields et al., 1993).

Spatial heterogeneity of calcium regulation.

Employing a spatial restriction to calcium signals seems to be another mechanism that allows specific cellular responses to be activated selectively as only those calcium responsive elements near to the calcium change would be activated. Action potentials in developing neurones were found to produce localised calcium hotspots of only a few micrometers in diameter under the plasmalemma of growth cones. Hotspots were thought

to be the result of L-type calcium channel clustering (Silver et al., 1990). Similarly electric field induced depolarisations caused calcium to rise only in small localised areas of the growth cone and marked the site of future outgrowth (Bedlack et al., 1992; Davenport & Kater, 1992). It was estimated that calcium may reach several hundred micromolar within such a domain, but due to the action of fast mobile calcium buffers such as calbindin these levels would be confined to a very small volume around the site of calcium entry (Roberts, 1994). On a bigger scale differences in $[Ca^{2+}]_i$ can also exist between the growth cone and the cell body. In grasshopper pioneer axons the leading growth cone has a higher $[Ca^{2+}]_i$ than the cell body during neurite elongation (Bentley et al., 1991) and in *Xenopus* spinal neurones spontaneous calcium transients can occur in isolation either in the growth cone or the cell body (Gu & Spitzer, 1995).

The mode of entry matters

Several lines of evidence suggest that the route of calcium entry into the cytosol and the kinetic characteristics of the calcium rise are important determinants of the nature of the response. In the migration of neuronal granule cells, blocking calcium influx through N type channels or NMDA receptors impairs movement whereas blockers of L or T -type channels have no effect (Komuro & Rakic, 1992; 1993). Bading et al. (1993) have shown that depending on whether calcium enters hippocampal neurones through L-type channels or NMDA receptors two distinct signalling pathways are activated that result in the transcription of different genes. Evidence for the importance of the kinetics of calcium entry comes from studies of calcium induced growth cone collapse in mouse dorsal root ganglion cells. After chronic electric stimulation growth cones become

resistant to collapse mainly because the rise time of the calcium increase is slowed (Fields et al., 1993).

Temporal regulation of calcium signalling

One simple form of temporal regulation is the alteration either of calcium responsive elements or of mechanisms that influence calcium levels over time. Changes to calcium levels during development are exemplified by the maturation of the action potential, which is associated in many neurones with a reduction in the calcium influx (Spitzer, 1991). Early *Xenopus* spinal nerve cells for instance were shown to express a higher density of low voltage activated calcium channels, which favours higher spontaneous calcium elevations during this short period (Gu & Spitzer, 1993). The susceptibility of certain processes to calcium can also change during development. This point is nicely illustrated in developing cerebellar granule cells. During the first day in culture calcium influx through N-methyl-D-aspartate (NMDA) receptors promotes mainly neurite outgrowth; during the following days general cell differentiation is stimulated, and after 5 days NMDA receptor stimulation is essential for cell survival (Burgoyne et al., 1993). Similarly the survival promoting effect of calcium in chick nodose neurones can only be observed during a restricted period (Larmet et al., 1992).

Encoding information in calcium oscillations.

It has only been discovered recently that many neurones show spontaneous oscillating calcium transients during development with a great variability in the time course of calcium rise, duration and extent of propagation (Holliday & Spitzer, 1990; Gu & Spitzer, 1993; Gu et al., 1994; Williams & Cohan, 1994; Gomez et al., 1995; Gu & Spitzer, 1995) Such

Table I: Properties of voltage operated calcium channels

Type	Electrophysiology	α_1-subunit cDNA class	Distribution	Blockers	References
HVA	high activation threshold (~-20 to-30 mV)				
L	single channel conduct.= 19-28 pS, slow inactivation during depol., resistance to steady state inactivation at -40mV. relatively slow deactivating.	C	Smooth mu, Heart, Brain, Pituitary	Dihydropyridines (class D also reversibly inhibited by ω-conotoxin)	Hess et al., 1984, Nature 311:538 Nowycky et al., 1985, Nature 316:440 Tanabe et al., 1988, Nature 366:134 Mikami et al., 1989, Nature 340:230 Hui et al., 1991, Neuron 7:35 Seino et al., 1992 PNAS 89:584
		D	Brain, Heart, Pituitary,Pancreas		
		S	Skeletal muscle		
N	single channel conduct. = 13-18 pS, intermediate fast inactivation, little steady state inactivation at -60 mV	B	Brain	irreversibly blocked by ω-conotoxin GVIA (a toxin from a cone snail)	Nowycky et al., 1985, Nature 316:440 Fox et al., 1987, J Physiol 394:149 Fox et al., 1987, J Physiol 394:173 Plummer et al., 1989, Neuron 2:1453 Dubel et al., 1992, PNAS 89:5058 Williams et al., 1992, Science 257:389
P	single channel conduct. = 9 - 19 pS no inactivation during depolarisation resist. to steady state inactiv. at neg. volt.	A	Brain	ω-agatoxin IVA (toxin from funnel web spider)	Mintz et al., 1992, Nature 355:827 Usowicz et al., 1992, Neuron :1185
Q	intermediate fast inactivation, no single channel data	? (A)	Brain	ω-conotoxin MVIIC (this toxin also blocks N and P-type). ω-agatoxin IVA (only in 100x higher conc. than for P channels)	Zhang et al., 1993, Neuropharmacol 32:1075 Wheeler et al., 1994, Science 264:107 Randall and Tsien, 1995, J Neurosci 15:2995
R	A current component in cerebellar granule cells resistant to DHP, conotoxins and agatoxins with rapid inactivation	? (E)	Brain, elsewhere?	?	Zhang et al., 1993, Neuropharmacol 32:1075 Randall and Tsien 1995, J Neurosci 15:2995
LVA	low voltage activation threshold (~ -60mV)				
T	single channel conduct. = 7-11 pS fast inactivation during depol. needs holding voltage > -80 mV to avoid steady state inactivation, slow deactivation	? (E)	many excitable and nonexcitable cells	No specific blockers Ni2+, amiloride, flunarizine,	Carbone and Lux, 1984, Nature 310:501 Fox et al., 1987, J Physiol 394:149 Fox et al., 1987, J Physiol 394:173

calcium oscillations are probably a sophisticated form of calcium signalling. It is thought that specific information is encoded in the number, frequency, amplitude or kinetics of the calcium transients which would permit a very complex signalling mechanism. In support of this theory Gu and Spitzer (1995) present evidence that in *Xenopus* neurones short calcium spikes promote neurotransmitter expression and channel maturation but longer lasting calcium waves regulate neurite extension.

1.3 VOLTAGE DEPENDENT CALCIUM CHANNELS IN DEVELOPING NERVE CELLS

The best characterised pathway for calcium entry into cells is across voltage dependent calcium channels (VDCC) on the plasmalemma and there is good evidence that from early on during nerve cell development these channels are expressed and critically influence the cytoslic calcium concentrations (Gottmann et al., 1988; McCobb et al., 1989; Silver et al., 1989). Not surprisingly, VDCCs are involved in almost all the developmental processes mentioned in the previous paragraphs. Their importance is maybe most clearly demonstrated in experiments where specific channel blockers interrupt various aspects of normal neuronal development such as growth cone extension, guidance, retraction, neuronal migration or early cell survival (Robson & Burgoyne, 1989; Komuro & Rakic, 1992; Williams et al., 1992; Moorman & Hume, 1993; Franklin et al., 1995).

VDCCs open in response to membrane depolarisations and according to their activation threshold are generally divided into low voltage activated (LVA) and high voltage activated (HVA) types (Hess, 1990; Scott et al.,

1991; Snutch & Reiner, 1992; Dolphin, 1995). LVA channels or T type channels from all studied tissues share very similar single channel characteristics although whole cell kinetic differences within the same cell type have been described (Kobrinsky et al., 1994). In contrast HVA channels are a very heterogeneous group and big differences can be found in biophysical properties such as activation and inactivation kinetics, voltage requirements or single channel conductances (Nowycky et al., 1985; Fox et al., 1987; Forti & Pietrobon, 1993). Currently it is thought that the most reliable tool to distinguish between HVA channel subtypes and defining criterion is their sensitivity to specific pharmacological agents. In neuronal preparations L, N, P and Q type channels have been described to date. L type channels are sensitive to dihydropyridines (Hess et al., 1984), N type channels are blocked by ω-conotoxin GVIA (Williams et al., 1992) and Q and P type channels are blocked at different concentrations by ω-agatoxin IVA (Mintz et al., 1992 ; Randall & Tsien, 1995). More channel types however may yet be discovered. The underlying basis for the marked diversity of calcium channels lies largely in their complex molecular composition. Neuronal VDCCs consist of at least four subunits . The large transmembrane α1 subunit forms the calcium permeable pore, carries the binding site for dihydropyridines, conotoxins and agatoxins and functions as the voltage sensor (Hofmann et al., 1994). The auxiliary transmembrane α2 and δ subunit and the intracellular β subunit are substantial for effective expression of the channel complex and profoundly influence the kinetics and voltage dependencies of activation and inactivation (Isom et al., 1994; Berrow et al., 1995). So far six different genes have been isolated that code for distinct α1 subunits and four different genes that code for β subunits. In addition differential splicing of some of these genes results in various isoforms which further increases the number of possible channel combinations (Hofmann et al., 1994). Besides the molecular heterogeneity

Examples of developmental changes in ion channel expression

Ion channel	Tissue	Type of change and functional consequence	References
AChR (nicotinic acetylcholine receptor)	bovine skeletal muscle	Replacement of the γ subunit in the fetal receptor by the ε subunit in the adult. This causes in the adult receptor an increased single channel conductance and a shorter channel open time.	Mishima et al. Nature 321: 406-11 (1986)
AChR (nicotinic acetylcholine receptor)	chick ciliary ganglion	Between embryonic stages E8 and E18 the density of AChRs and the ACh response per unit membrane increases whereas the affinity of receptors for ACh decreases. The 25pS conductance channel disappears and a 40 pS conductance becomes more abundant. The receptor becomes sensitive to a cAMP mediated mechanism that enhances the ACh response.	Margiotta et al. DevBiol 135:326-9 (1989)
$GABA_A$ (γ- aminobutyric acid) receptor	rat brain	From fetal and early postnatal to adult brain expression of the α_2, α_3, α_4, γ_1 and γ_3 subunits decreases whereas α_1 and β_2 subunits are more abundant in the adult brain. Over the same period there is a switch from the excitatory effect of GABA to an inhibitory effect.	McLennan et al. Neurosci 43:369-77 (1991) Cherubini et al TINS 14:515-9 (1991)
L -type calcium channels	rat heart	Two splice variants of the third membrane spanning region of the fourth motif (CaCh2a and CaCh2b) of the α1 subunit of the C class L channel are expressed in a mutually exclusive fashion in the fetal and adult heart. This correlates temporally with a change in the timecourse of the heart action potential and a lower sensitivity of the adult CaCh2a to the DHP antagonist nisoldipine.	Diebold et al. PNAS 89:1497-501 (1992) Wellington et al Cir-Res 73:974-80 (1993)
T-type calcium channels	*Xenopus* spinal cord	The percentage of cells expressing a T-type calcium current is high ~90% in young embryonic spinal neurons but drops to 35% during development. This correlates with a more negative threshold for action potentials and higher incidence of spontaneous calcium elevations in young neurons.	
HVA and LVA calcium channels	chick and mouse spinal cord	The number of motoneurones expressing LVA calcium channels declines during early development whereas expression of HVA current increases. Appearance of HVA current correlates with death of 50% of motoneurons.	Mynlieff et al. DevBiol142:407-11 (1992) McCobb et al. Neuron 2:1633-43 (1989)

additional functional differences between calcium channels result from the modulation of channel characteristics by phosphorylation and G-proteins (Hescheler & Schultz, 1993; Dolphin, 1995).

Ion channels during development are different from adult forms

Considering this big potential for complexity it must be assumed that differences evolved to fulfil specialised functions in the cell. Consistent with the notion that ion channels have different functions in an embryonic and an adult organism is the fact that the exact composition of ion channels changes during development. For instance certain isoforms of subunits of $GABA_A$ channels or neuronal nicotinic acetylcholine receptors are predominantly expressed during the embryonic phase (Margiotta & Gurantz, 1989; Wisden & Seeburg, 1992; Fritschy et al., 1994) and a similar temporal differential expression was observed for splice products of a calcium channel gene (CaCh2) in developing cardiac cells (Diebold et al., 1992). Although comparatively little is known about the functional significance of differential subunit composition during development, it was suggested that such structural differences in $GABA_A$ receptors are correlated with the change of the depolarising effect of GABA in developing neurons to the hyperpolarising action in mature nerve cells (Cherubini et al., 1991; Fritschy et al., 1994). An example which demonstrates that the regulation of the expression of specific calcium channel types can have marked effects on the development comes from *Xenopus* neurones in culture . As mentioned before, the increased expression of low voltage activated T-type calcium channels during a critical period is a requirement for spontaneous calcium oscillations and normal maturation of these neurones (Gu & Spitzer, 1993).

What are the aspects of developmental calcium channels that need to be studied to understand their function? The exact subunit composition of calcium channels is certainly a central question and can be studied with the methods of molecular biology. If markers or antibodies for specific developmental variations or subunits are available their subcellular and anatomical distribution can be investigated which can give important cues. Studies in adult rat brains for example have shown that different L channel $\alpha 1$ subunits (gene class C and D) are expressed mainly on the cell body and major dendrites implicating a function in general cellular signalling pathways, whereas the N channel $\alpha 1$ subunit (gene class B) is located mainly on synapses indicating a role in transmitter release (Westenbroek et al., 1992; Hell et al., 1993). Finally from the electrophysiological point it will be important to investigate the functional properties of developmental calcium channels such as voltage requirements, activation and inactivation kinetics. This information would allow conclusions about the circumstances when channels are activated, how large the calcium influx would be and consequently which developmental processes could be activated.

1.4 Significance of this study

In the work presented here I tried to investigate several aspects of the role of calcium as a second messenger in nerve cell development. The following section will briefly outline the approaches I took for this study and summarise the most important new findings.

In the first part of this work the mouse neuroblastoma cell line N1E-115 was used. These cells, when induced to differentiate, assume the

morphology of developing neurones and extend neurites with large growth cones (Kimhi et al., 1976). The large size of their growth cones makes these cells extremely suitable for the technically complicated imaging and patch clamp experiments performed here. The underlying question for chapter 3 and partly for chapter 4 was how calcium signals transmitted by voltage dependent L-type calcium channels are spatially organised in growth cones. Localised modulation of calcium changes has been proposed to underlie the steering or directional outgrowth of growth cones by neurotransmitter gradients, voltage signals or cell adhesion molecules (Silver et al., 1990; Williams et al., 1992; Doherty et al., 1993; Zheng et al., 1994). N1E-115 neuroblastoma cells are a particularly suitable model for the study of local calcium signals because depolarisation causes calcium to rise in a number of spatially restricted hotspots, triggering a localised advance (Silver et al., 1990). To facilitate analysis I restricted the experiments in this thesis to the simple club shaped growth cones which are characteristically found on advancing neurites (Silver et al., 1989; Soekarno et al., 1993). In chapter 3 I used the calcium indicator dye Fluo3 to image calcium changes in growth cones associated with activation of L-type calcium channels. Depolarisation caused calcium to increase in a number of hotspots and the average calcium rise was highest at the distal leading tip with a continuous falling gradient towards proximal growth cone regions. Agents that disrupt calcium induced calcium release did not affect these calcium dynamics, ruling out a local release of calcium from internal stores as the source of hotspots or the gradient. In chapter 4 I used the cell attached patch recording technique to show that L type calcium channels are present at a higher density at the distal tip of the growth cone. These results demonstrate that in growth cones depolarisation induced calcium gradients are a direct consequence of the distribution of single L-type calcium channels.

In the rest of chapter 4, I examined the single channel characteristics of L and T type channels on N1E-115 neuroblastoma growth cones. This is the first detailed investigation of single channel properties of calcium channels found on mammalian growth cones. Apart from Lipscombe et al. (1988), who reported that single channel conductances of L and N-type channels were the same in growth cones and cell bodies of frog sympathetic neurones, there have been no other investigations into the single channel properties of calcium channels on vertebrate growth cones and only one other study on any growth cone (Cohan et al., 1985; on the mollusc *Helisoma*). I report here single channel conductances, mean open times, inactivation timecourses and open probabilities for T and L-type channels. I also observed subconductance states of L channels, which is the first report of them on neuronal cell membranes in situ, although they were described on a pituitary cell line (Kunze & Ritchie, 1990).

The starting point for experiments in chapter 6 was the calcium optimum hypothesis for neurite outgrowth proposed by Kater's group (Mattson & Kater, 1987). This model, as mentioned earlier, predicts that outgrowth is optimal at a narrow range of intracellular calcium but is impaired by excursions of $[Ca^{2+}]_i$ below or above a set point. I tested whether this model applied to N1E-115 cell by clamping $[Ca^{2+}]_i$ to a wide range of different concentrations below and above the normal levels and then evaluating outgrowth parameters. In contrast to other cells tested such as rat dorsal root ganglion cells and cerebellar granule cells (Al-Mohanna et al., 1992; Zimprich et al., 1994) neuroblastoma cells showed no bell shaped dependence, but exhibited rather an optimal outgrowth at the lowest calcium levels achievable. Although this does not fit Kater's model easily it certainly confirms that the efficacy of neurite outgrowth is strongly dependent on $[Ca^{2+}]_i$.

Although culture systems allow greater experimental access, conditions are necessarily simplified as developing nerve cells are not exposed to many influences of their original environment. It is, therefore, difficult to judge which of the many potential roles of calcium reported in culture are also relevant under normal physiological conditions. However, only very few studies have made calcium measurements *in situ*, in part because of the great experimental difficulties involved. The aim of the work presented in chapter 7 was therefore, to establish a system for *in vivo* monitoring of calcium changes in developing nerve cells of life zebrafish embryos. In short: The calcium indicator dye calcium-green dextran was injected into one of the blastomere cells of a few hour old still unformed embryo. As this injected cell divided, the dye was passed on to a clone of daughter cells which by chance included nerve cells among the progeny. As the embryo is almost transparent at the time the nervous system forms, it was possible to monitor these developing neurones under a confocal microscope. In some developing spinal motoneurones, I observed spontaneous calcium transients which are reminiscent of calcium waves observed by a number of investigators in vitro (Gu et al., 1994; Williams & Cohan, 1994; Gomez et al., 1995; Gu & Spitzer, 1995).

CHAPTER 2

METHODS

SECTION A: EXPERIMENTS ON N1E-115 NEUROBLASTOMA CELLS

2A.1 CELL CULTURE

General culture conditions

N1E-115 Neuroblastoma cells were maintained in Dulbecco's modification of Eagle's medium (DMEM) buffered with 1.21 g/litre $NaHCO_3$ and supplemented with 10% foetal calf serum in an atmosphere of 5% CO_2 at 33°C. Cells were harvested from cell culture bottles by gentle rinsing and replated onto polylysine coated cell culture dishes (Bachofer, Germany). 2% dimethylsulphoxide (DMSO) was added to the growth medium to promote differentiation (Kimhi et al., 1976). Cells were left in this differentiation medium for 3 to 7 days by which time many cells had grown neurites with prominent growth cones.

Manipulating intracellular calcium in differentiating neuroblastoma cells

For experiments studying the effect of different intracellular calcium concentration ($[Ca^{2+}]_i$) on neurite outgrowth I manipulated $[Ca^{2+}]_i$ indirectly by varying the calcium concentration in the differentiation medium ($[Ca^{2+}]_o$). $[Ca^{2+}]_o$ was increased by addition of $CaCl_2$, or was reduced by chelation of some of the 1.9 mM total calcium by adding 1,2-bis(o-

aminophenoxy)-ethane-N,N,N',N'-tetraacetatic acid (BAPTA) (Molecular Probes). The vast majority of BAPTA molecules will each bind one calcium ion, so that media containing 1 and 1.5 mM BAPTA will contain 0.9 and 0.4 mM free $[Ca^{2+}]_o$ respectively, while media containing 2 mM BAPTA will have free $[Ca^{2+}]_o$ of around 1μM. The selectivity of BAPTA for calcium over magnesium is such that free magnesium should not change significantly (Tsien, 1980). However, to guard against artefacts due to variation of extracellular divalent cation concentration, I also added 20 mM magnesium chloride to the differentiation medium in some dishes to give a total extracellular magnesium concentration of 21 mM. In a different set of experiments $[Ca^{2+}]_i$ was raised by adding up to 1 μM of the calcium ionophore A23187 (Calbiochem) to the bathing medium. Cells were left for three days to differentiate under these conditions before the extent of neurite outgrowth was measured.

Measuring neurite outgrowth

I tried to assess two aspects of neurite outgrowth, initiation of new neurites and length of established neurites. For neurite initiation, I measured the fraction of all cells with at least one neurite longer than the diameter of the cell body. This parameter varied from experiment to experiment, maybe due to differences in the confluency and feeding state of the cultures. I therefore normalised data from any particular experiment such that the value in the control medium (calcium concentration not altered) became 1.

Immunostaining cells for tubulin and actin

To study the cytoskeletal organisation of neurites grown in different calcium concentrations I double labelled cells for tubulin and actin as

follows; all agents in phosphate buffered saline (PBS). Cells were fixed in 4% formalin for 20 min, permeabilized in 0.5% Triton X-100 for 5 min, labelled with a rat anti-α tubulin antibody (Amersham; diluted 1:50) for 30 min and then exposed to FITC-conjugated Fab_2 fragments of rabbit anti rat IgG (Amersham, dilution 1:100). Cells were then directly stained for actin with rhodamine labelled phalloidin (dilution 1:10; Molecular Probes). Between steps dishes were thoroughly washed with PBS. Photographs were taken on a fluorescent microscope in Dr Rhona Mirsky's lab.

2A.2 THE EPIFLUORESCENCE MICROSCOPE AND THE DIGITAL IMAGING SYSTEM

The digital imaging system consisted of an inverted microscope with an ultraviolet light source, a highly sensitive camera and a computer system capable of digitising video signals from the camera and manipulating data for analysis.

The epifluorescence microscope

For experiments in chapter 3 to 5 I used a Zeiss IM microscope with either a 40x or 100x glycerol immersion objective (Neofluor UV-F, Nikon). Both objectives had a numerical aperture of 1.3. Light in the UV and visible range was generated in a 150W high pressure xenon arc lamp (Wotan, Germany) and passed through a heat filter. When using the ratiometric dye Fura-2 a 350 or 380 nm narrow band filter was rotated into the UV path using a computer controlled stepper motor. Filtered light was then reflected by a dichroic mirror (400nm longpass) and directed to the specimen

through the objective. Light emitted from the specimen was again collected by the same objective and passed through the dichroic mirror and a broad band filter of centre wavelength 510 nm before directed either to the ocular or the video camera.

For experiments with the calcium indicator dye Fluo-3 light from the arc lamp was directed through a UV block filter and a 485 nm narrow band filter before being reflected by a 500 long pass dichroic mirror. Emitted light passed through a broad band filter of centre wavelength 535 nm. (All filters were bought from Omega Optical) The video camera used (extended ISIS-M, Photonic Sciences, UK) was an intensified CCD camera with a higher signal to noise ratio in the blue-green part of the spectrum.

Other parts of the imaging system

For experiments with Fura-2 AM the video signal was digitised and stored in 256 grey scale levels by a Gould FD 5000 image processor. Subsequent image manipulation was carried out by the image processor controlled by programs written by Angela G. Lamb and run on a DEC Microvax computer. For experiments on growth cones using Fluo-3 I used a Personal Computer based image processing system, consisting of a video adaptor, a Fidelity 100 Frame Grabber Board (Data Translation, MA), in a 486 DX 66 MHz PC with 16 MB random access memory and 230 MB hard disk memory. Images from the camera were digitised as an array of 768 x 576 pixels using a program written by Kevin Boone. After the experiment data were stored on a 1 GB optical disk. Image analysis was performed using a program called Global Lab Image (Data Translation) and a program written by Kevin Boone.

2A.3 MEASURING CALCIUM WITH FURA-2 AM

For measurements of $[Ca^{2+}]_i$ in neuroblastoma cells in chapter 6 the ratiometric calcium indicator dye Fura-2 AM was used.:

Loading cells with Fura-2 AM

The acetoxymethyl ester of Fura-2 (Fura-2 AM, Molecular Probes) is the membrane permeant form of the dye and converted by cell esterases to a highly impermeant form. It therefore remains trapped inside the cytosolic compartment. 2 mM of Fura-2 AM was added to the bathing medium and the dishes incubated at room temperature for 25 minutes in an atmosphere of 5% CO_2. Cells were then rinsed with the same medium but without Fura-2 AM and incubated at 33^o for 20 minutes before being placed on the stage of the Zeiss IM fluorescence microscope for measurement of $[Ca^{2+}]_i$ as outlined below.

Properties of Fura-2

The calcium indicator dye Fura-2, developed by Grynkiewicz et al. (1985), has a broad excitation spectrum ranging from below 300 nm to above 400 nm and an optimal emission at a wavelength of 510 nm. On binding calcium ions there is a change in the excitation spectrum in such a way that there will be more emission during 350 nm excitation, and at the same time less emission during 380 nm excitation. Although the absolute emission intensity at each of these wavelengths (I_{350} and I_{380}) is dependent on the concentration of the dye, this is not true for the ratio of I_{350}/I_{380} which is only dependent of the calcium concentration. Fura-2 is therefore also called a dual excitation ratiometric dye. The $[Ca^{2+}]_i$ can be associated with

the ratio of I_{350}/I_{380} (R) according to the following formula (Grynkiewicz et al., 1985):

$$(1) \quad [Ca^{2+}] = K_{1/2} \cdot \{[R-R_{min}] / [R_{max}-R]\}$$

Rmin is the minimum ratio when no calcium is bound; Rmax the maximum ratio when the dye is saturated. $K_{1/2}$ is a function of K_d, the dissociation constant. (K_d equals the calcium concentration where 50% of the dye is saturated):

$$(2) \quad K_{1/2} = K_d \cdot [I_{380free} / I_{380bound}]$$

$I_{380free}$ is the intensity at 380 nm excitation at zero calcium and $I_{380bound}$ the intensity at 380 nm when the dye is saturated with calcium.

Calibration of the Fura-2 signal

The values for R_{max}, R_{min} and $K_{1/2}$ depend on the optics of the microscope and other factors and need to be known for the calculation of $[Ca^{2+}]$ from R, the ration of I_{350} /I_{380}. For the calibration of these parameters on my Zeiss imaging setup (100x Nikon objective, room temperature) I employed the following approach.

Fura-2 solutions (10 mM) in a range of buffers with known calcium concentrations (Molecular Probes) were drawn up into microslides, cuvettes with 50 µm path length (Camlab, UK) and placed on the stage of the microscope. Fluorescence intensities at 350 nM and 380 nm were measured and background subtracted. Ratios of I_{350} /I_{380}.were calculated and plotted against the calcium concentration (Figure 2.1). $K_{1/2}$ R_{max} and R_{min} could be evaluated from the best curve fit through these points. As the Kd of Fura-2 at 20°C is 236 nM as compared to 285 nM at 37°C $K_{1/2}$ had to be adjusted accordingly (Groden et al., 1991). The final values were Rmin = 0.389, Rmax = 4.5 and $k_{1/2}$ (37°C)= 189 nM. To evaluate $[Ca^{2+}]_i$ in

Figure 2.1

Fura-2 calibration curve for the Zeiss imaging setup (room temperature, 20 x objective). The ratios of background subtracted fluorescence intensities at 350 and 380 nM of a 10 mM Fura-2 solution in microslides were plotted against the calcium concentration (Filled circles). The straight line is the best curve fit through these points using formula (1): $[Ca^{2+}] = K_{1/2} \cdot \{[R-R_{min}] / [R_{max}-R]\}$. The values obtained for these variables (Rmin = 0.389, Rmax = 4.5, k1/2 (adjusted for 37C) = 189nM) were then used to calculate intracellular calcium concentrations in Fura-2 AM loaded cells. The calcium concentration is plotted on a logarithmic scale after the breaklines.

Figure 2.1

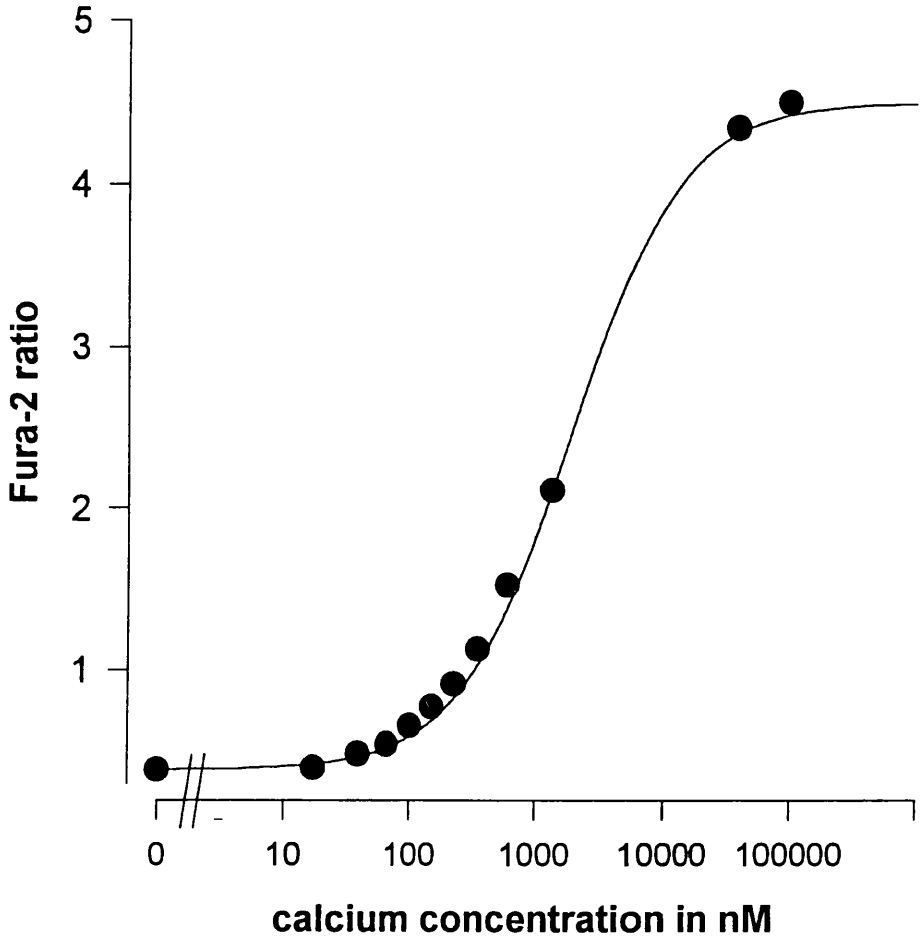
5
4
3
2
1
Fura-2 ratio
0
10
100
1000
10000
100000
calcium concentration in nM

Fura-2 AM loaded cells, the ratio of emission intensities at excitation at 350 nm and 380 nm was then measured and $[Ca^{2+}]_i$ calculated according to formula (1).

2A. 4 WHOLE CELL PATCH CLAMPING AND MEASURING CALCIUM WITH FLUO-3

For imaging experiments of calcium influx into growth cones in chapter 3, I used the patch clamp technique in the whole cell mode. This technique offered the advantages that the calcium indicator dye, Fluo-3, could be introduced into the cells in sufficient quantities to visualise the growth cones and at the same time allowed control over the membrane voltage.

Whole cell recording setup and solutions

For these experiments neuroblastoma cells were rinsed 4 to 7 days after plating with the following "whole cell bath medium":

120 mM	NaCl
10 mM	CsCl
5.5 mM	KCl
1.0 mM	$MgCl_2$
1.8 mM	$CaCl_2$
20 mM	TEA (tetraethylammonium chloride)
20 mM	TRIS (hydroxymethyl-aminomethane)
25 mM	glucose
1 μM	TTX; pH adjusted to 7.3

Patch pipettes were pulled on a L/M-3P-A pipette puller (List Medical, Germany) from thick walled borosilicate capillaries with inserted microfilaments (GC150F-10, 1.5 mm outer diameter, 0.86 mm inner diameter Clarke Electromedical) to give resistances of 5-8 MΩ. The following solutions were used to backfill the pipettes. In imaging experiments the "whole cell pipette solution A" contained:

135 mM	CsCl
25 mM	TEA
7.5 mM	HEPES (N-[2-hydroxyethyl]piperazine-N'-[2-ethanesulfonic acid])
1.0 mM	$MgCl_2$
5.0 mM	MgATP
10 mM	Fluo-3 pH adjusted to 7.0

In experiments where I determined the characteristics of the whole cell calcium currents, the 10 mM Fluo-3 was replaced with 10 mM EGTA and 1 mM $CaCl_2$ was added ("whole cell pipette solution B"). In some the experiments 5 μM of the dihydropyridine antagonist nifedipine (Calbiochem) was added to the bath .

A pipette, backfilled with either of the above solutions, was then connected to the headstage of an Axopatch 200 patch clamp amplifier (Axon Instruments) and positioned near the cell using a water filled hydraulic micromanipulator (Narashige, Japan). After offsetting the pipette current the pipette was sealed onto the cell body and on formation of a gigaseal the membrane patch at the tip ruptured by light suction. The cell was voltage clamped at -50 mV.

Depolarisation and image acquisition

About 10 min after rupture of the patch, sufficient Fluo-3 had diffused into the growth cone to allow easy visualisation in the imaging setup. The

growth cone was moved into the centre of the camera view, and the camera gain adjusted so that it was high enough for the growth cone to be clearly visible above the background noise, but low enough so that on Fluo-3 fluorescence increase the camera would not saturate. The holding voltage was then changed to -40 mV and after one minute the cell was depolarised to +10 mV for one second. The depolarisation protocol was controlled by Clampex, a program in the pClamp software (Axon Instruments), on a Personal Computer connected to the patch clamp amplifier via a digital-analog converter (TL-1/Labmaster, Axon Instruments). The voltage protocol in imaging experiments was designed to specifically open L type calcium channels, as T type calcium channels are inactivated at a holding potential of -40 mV (Silver et al., 1990). Cell currents were filtered at 1000 Hz digitised and saved on the computer for later analysis. Slightly before the cell was actually depolarised a signal was sent to the imaging computer to start image acquisition at a rate of 120 ms (in earlier experiments 240 ms) per image so that 4 images (earlier exp. 3) were acquired as controls before the cell was depolarised and 8 images during the depolarisation (Figure 3.4). Images were background subtracted and divided through the average of the control images. The resulting ratio was thus a measure of the fractional or relative fluorescence increase compared to before the depolarisation. For analysis of the spatial pattern, the fluorescence increase in every growth cone was averaged in sections of 5 µM from the tip, so that the fluorescence increase within 5 µM of the tip could be compared with more proximal regions (Inset in figure 3.7).

Inhibiting Calcium induced calcium release

To investigate the contribution of internal calcium stores to the overall fluorescence, increase in growth cones two depolarisations were

performed. The first run was intended as an internal control to get a value for the fluorescence rise in each growth cone. Immediately afterwards cells were exposed either to a bathing solution that contained inhibitors of internal calcium stores - 200 µM ryanodine (Calbiochem) or 40 µM dantrolene (Sigma) - or for control purposes left in the same solution. To change solutions without disrupting the delicate seal, I used a diamond shaped perfusion chamber (RC-26, Warner Instruments, CT). (Before the experiment this chamber had been sealed onto the dish with silicon grease). 210 sec after the first run the cell was again depolarised. Fluorescence changes during the second depolarisation were normalised to the 480 ms value of the first depolarisation. The normalised fluorescence increases in the control, ryanodine and dantrolene groups were then compared with each other.

2A.5 SINGLE CHANNEL PATCH CLAMPING

To recording single channel currents, I used the voltage clamp technique in the cell attached mode (Hamill et al., 1981).

The setup

The centrepiece of the cell attached patch clamp setup was the Axopatch 200 patch clamp amplifier with a CV 201 headstage (Axon Instruments). The headstage with an HL-1 pipette holder (Axon instruments) was mounted on the Zeiss IM microscope which was equipped with the 100x Nikon objective. For fine positioning of the pipettes a low drift water filled hydraulic manipulator (Narashige) was used. A silver wire in the pipette

holder with Ag/AgCl coating at the tip made contact with the pipette solution and a Ag/AgCl pellet served as an indifferent electrode in the bath. A TL-1 Labmasterboard was interfaced between the patch clamp amplifier and a 286 Personal Computer. This allowed digital to analog conversion of complicated voltage protocols to control the amplifier with the computer and it permitted instantaneous analog to digital conversion, so that the recordings could be digitally stored and further analysed on the computer. The software used for these purposes was the pClamp series (Axon Instruments). To achieve low noise recordings suitable for detecting single channel events smaller than 1 pA several factors were important. The amplifier itself was able to operate at very low noise levels of below 0.1 pA RMS (root mean square or standard deviation of the baseline noise current) at a bandwidth of 5 kHz. It achieved this low noise performance by using a capacitive feedback technique. The entire preparation (microscope, headstage, manipulator etc.) was shielded in a Faraday cage and all objects within the cage grounded via a central copper bar. To reduce noise from stray capacitance - from the pipette to the ground - I used thick walled pipettes pulled from borosilicate glass capillaries with an inner filament (GC150F-10, 1.5 mm outer diameter, 0.86 mm inner diameter, Clarke Electromedical) to resistances of 8 - 13 MΩ on a L/M-3P-A pipette puller (List Medical, Germany). Pipettes were kept as short as possible (~3 cm) which also improved mechanical stability. As most of the stray capacitance arises across the pipette wall where the pipette is in contact with the bath solution it is desirable to prevent water from creeping up the pipette wall. A thin hydrophobic film of silicone was therefore applied to the surface of the pipette by dipping it into sigmacote, a silicon-in-heptane solution (Sigma). To reduce stray capacitance further the depth of the bath solution was also kept to a minimum (~2-3 mm).

Solutions

Pipettes were backfilled with the following "single channel pipette solution"

110 mM	BaCl,
1 µM	TTX:
10 mM	HEPES; pH 7.3

Neuroblastoma cells 3 to 7 days after plating were rinsed and bathed in a "single channel bath solution" (Kobrinsky et al., 1994):

70 mM	NaCl
70 mM	KCl
1 mM	$MgCl_2$
10 mM	EGTA
10 mM	HEPES; pH 7.3

Where indicated 5 µM of the dihydropyridine (DHP) agonist BAYK 8644 (± racemate, Calbiochem) was added to the bath to increase the open probability of L-type channels. In some experiments 5 µM of the DHP antagonist nifedipine (Calbiochem) was used to suppress L channel current.

In the cell attached configuration the resting voltage of the cell is not known. To overcome this problem the high concentration of potassium ions in the bath was intended to depolarise the cell to a constant voltage near 0 mV which could then serve as a reference point. I measured the resting voltage in this depolarising bath solution in 11 cells. Pipettes were filled with the whole cell pipette solution B in these experiments. Cells were current clamped after establishing a whole cell recording configuration and the membrane voltage measured within a few seconds that is, before the caesium ions in the pipette had diffused out, blocking potassium channels. The average voltage recorded in these cells was -5.1 ± 1.9 mV. In the single channel experiments presented in chapter 4 I state patch voltages

as bath relative to pipette, thus the true membrane voltage is about 5 mV more negative

Formation of a high resistance seal

A pipette was positioned near the cell and the pipette current offset to zero. While moving the pipette to the desired location on the cell or growth cone I applied slight positive pressure to clear the tip from impurities that might affect the quality of the seal. On touching the cell surface I sucked slightly to pull the membrane patch onto the pipette tip. Usually this resulted within a few seconds in a very high resistance seal in excess of 20 GΩ. The membrane patch was then clamped at a voltage of -40 mV for several seconds before recording began. Currents were filtered at 1000 Hz and digitised at a sampling rate of 6.6 kHz. To ensure that the patch had remained cell attached during the whole recording I ruptured the patch after finishing the experiment. When the patch had been truly cell attached I was able to record a large capacity transient, typical of the whole cell configuration. This test excluded the rare cases of inside-out patches that had been pulled away from the cell due to a slight drift of the manipulator.

Analysis parameters

For the detection of single channel openings I used the 50 percent threshold crossing method (Colquhoun, 1987). A threshold was set halfway between the full opening and the shut level and a transition was considered to have occurred whenever this threshold was crossed. Using a 1 kHz filter I achieved on average baseline noise levels of less than 0.08 pA rms (largely determined by the quality of the seal) and as the threshold levels lay at around 0.6 pA I should only have detected less than one (only

very short) false threshold crossing event per 100 seconds of recording (Colquhoun, 1987). On the other hand filtering currents has the effect that very short true channel openings will not reach the threshold. In these experiments a 4-pole low pass Bessel filter was used with 1000 Hz as the -3 dB frequency. The 90% rise time of this filter was 0.35/1000 Hz or approximately 350 µsec. As the duration of an event needs to be roughly 1.3 of the rise time to be measured reliably, the resolution was therefore limited to around 500 µs. To measure amplitudes of openings correctly, the opening duration must be at least twice the rise time. I therefore excluded all events that were shorter than 1 ms for evaluating current amplitudes. For the construction of open time histograms an eventlist was created from the original current record. Channel open times were then binned into bins of 0.5 ms binwidth (Figure 4.6). Fitting of exponentials to obtain the "open-time time-constants" was performed after omitting the first bin from 0 to 0.5 ms. For arithmetic mean open times the arithmetic average of all openings (including those shorter of 0.5 ms) was calculated. For single channel conductance measurements the amplitude of channel openings to several test potentials was measured and then plotted against the voltage. A straight line was fitted through these points. The slope of this line equalled the single channel conductance. From the same graph the reversal potential could be determined as the point where the fitted line crossed the voltage axis.

One channel patches

Most single channel parameters could be determined from patches that contained more than one channel. However, estimation of the open probability of a single channel requires the identification of patches containing only one channel. Nine patches seemed to qualify. The average

recording time in these patches was 44 seconds (minimum 7, maximum 188 seconds) at +10 mV. In these patches only one channel ever opened at one time. I refer to these as "possible one channel patches". For each patch I calculated the probability that the records would have been obtained if two channels were in the patch according to the following consideration. The assumption is that there are two independently opening channels in the patch. What is the probability of obtaining a record in which each of the two channels opens only when the other one is closed? If A is the channel that has opened most recently or is still open B is the other one. There are N openings in the record. How many of these openings would one expect to be of the B channel? Slightly more than 50%, because B is available for opening all the time but A only $(1-P_o)$ of the time. In fact one would expect $N/(2-P_o)$ closed to open transitions of the B channel. The probability that the B channel opens during a time interval when no channel is open is $(1-P_o)$, which is the fraction of the time when the A channel is shut. The probability that all $N/(2-P_o)$ openings of the B channel occurred in this time interval is therefore: $(1-P_o)^{[N/(2-P_o)]}$. Patches for which the probability was low were unlikely to contain more than one channel. In two of the nine possible one channels patches this probability was less than 0.05, equivalent to a 5% confidence that there was only one channel. These two patches are referred to as "probable one channel patches".

Patch area

Pipettes used in these experiments were pulled from thick walled borosilicate capillaries to resistances of 8-13 MΩ. Such pipettes have been found to be very reproducible in terms of their tip geometry with tip opening areas in the range of 0.6 to 1.2 μm^2 (Sakman & Neher, 1983). A widely

used method to determine accurately the inner diameter of pipette tips is to measure the "bubbling pressure (P_b)", the pressure necessary to expel bubbles of air through the pipette tip into a methanol solution (Martin & Cook, 1990). When pressure applied to the pipette is large enough to overcome the surface tension of the air-methanol surface, bubbles will leave the tip. The most important variable influence on the bubble pressure is the tip diameter (d).

(3) $P_b = 4\sigma / d$

σ is the surface tension (for methanol at 20°C it is 22.61 dynes/cm). To measure Pb, I connected a 50 cc syringe to the pipette, pushed the plunger and observed the syringe volume (Bubble number or B) when bubbles emerged into the methanol solution. From this volume Pb could be calculated:

(4) $P_b = [(50/B)-1] \cdot Pa$ (atmospheric pressure =1013250 dynes/cm^2)

By reforming equation (3) d could be determined. For thick walled pipettes of 8-13 MΩ, tip opening diameters were calculated to be in the range of 0.76 to 0.92 μm. As very good seals formed usually without much suction and tip cones are almost parallel in thick walled pipettes patch areas were estimated to be similar to the tip opening area at somewhere between 0.5 and 1 μm^2.

SECTION B: EXPERIMENTS ON ZEBRAFISH

2B.1 ZEBRAFISH EMBRYOS

The zebrafish, *Danio rerio*, is a freshwater species native to India (Meyer et al., 1993; Westerfield, 1994). Adult Fish 2 to 4 cm in length were bought from a local aquarium shop (Tachbrook Tropicals, UK). 25 fish - males and females mixed - were kept in a 45 l tank in deionised water with added seasalts (60 mg/l). Half the water was exchanged 3 to 4 times a week. In addition an internal sponge filter with a capacity of 180l/h (Eheim, Germany) was used to keep the water clean. The temperature was kept between 28° and 30°C and an airpump (Interpet, Japan) continuously oxygenated the water. Aquaria were held on a 14 hour light and 10 hour dark cycle and covered in a box during dark cycles to keep out ambient light. When embryos were needed fish were fed 3 times a day with flake food, frozen tubifex worms or brine shrimps. During rest periods when no embryos were collected fish were only fed once a day.

Collection of embryos

Zebrafish produce embryos every morning shortly after sunrise. Immediately after switching on the light a glass container (20cm x 10cm), filled with marbles, was put into the tank. Soon, fish exhibited typical breeding behaviour. Females layed eggs mainly over the marble container, and males swimming closely behind fertilised them. Eggs dropped between the marbles and thus escaped from being eaten. After 30 minutes I carefully removed the marble container from the tank and filtered the water to collect the 1 mm big eggs. On average it was possible to gain more than

100 eggs, 2 to 3 times a week. Eggs not used for experiments were returned to the tank. Eggs were then washed in embryo medium and kept at a temperature of 26 to 28°C. All further manipulation of the embryos were carried out in embryo medium unless stated otherwise. Embryo medium (Westerfield, 1994) was made up of:

13. 7 mM	NaCl
1.3 mM	$CaCl_2$
1 mM	$MgSO_4$
0.54 mM	KCl
25.2 µM	Na_2HPO_4
44.1 µM	K_2HPO_4

a few crystals of methylene blue were added to colour the solution light blue and the pH adjusted to 7.2 with NaOH.

Dechorionation of eggs

For experiments on developing embryos, it was necessary to free eggs from the chorion, the transparent but resistant eggshell. For this purpose embryos were placed on a small petridish with a 1% agar bottom, under a preparation microscope (magnification 30x, Vickers Instruments, UK). Using two sharp forceps, I gently tore the chorion apart until the egg fell out. Embryos could then be transferred with a fire polished Pasteur pipette to the injection dish on the microscope stage .

2B.2 Injecting embryos with calcium-green dextran

The Injection setup and solutions

The microscope used was an upright Labophot 2 (Nikon Japan) with a Plan 10 x objective (NA 0.3 and a long working distance). The microscope was fitted with a 100 W UV lamp for epifluorescence and a fluorescein filter set. A Faraday cage was built around the microscope. The pressure injection setup included an NL 102 DC Pre-Amplifier (Neurolog) and an NL 102G headstage for current injection and recording of the pipette voltage. Connected to the amplifier via a TL-1 digital-analog converter (Axon Instruments) was a 286 computer running pClamp software (Axon instruments) that served as an oscilloscope. Pipettes were drawn from thin walled borosilicate glass (GC150TF-10, outer diameter 1.5 mm, inner diameter 1.17 mm, Clark Electromedical) on a vertical pipette puller (David Kopf Instruments, CA) to give resistances in the range of 100 MΩ. They were introduced in a home made pipette holder, suitable for pressure injection, and mounted on a micromanipulator (Narashige) on the microscope stage. Pressure from a compressed air cylinder could be regulated with a standard control pressure valve and turned on and off with a footswitch operated solenoid valve. Pipettes were backfilled with ~0.2 µl of a 20 mM calcium-green dextran (MW 10 000, Molecular Probes) solution in 130 KCl. To avoid blocking up pipette tips during injection, dyes were filtered using Ultrafree-MC filter units for microcentrifuge tubes (pore size 0.22 µm, Millipore). As soon as the dye - drawn along the inner filament - had filled the tip the rest of the pipette was filled with 130 KCl. A silver wire coated with a layer of silver chloride connected the pipette solution to the headstage and a Ag/AgCl pellet served as an indifferent electrode in the bath.

The injection technique

20 to 25 dechorionated embryos were transferred to the injection petridish coated with a layer of Sylgaard at the bottom (this provided a non sticky surface) and lined up along a groove. The pipette was moved near the embryos and the pipette current zeroed. At this stage I adjusted the air pressure to the minimum setting that still permitted dye ejection, usually below 2 bar. The pipette tip was then positioned on the surface so that a dimple appeared and a short hyperpolarising current of up to 20 nA applied. This resulted in the penetration of the pipette through the cell membrane. which was confirmed by the recording of a negative resting voltage of the inside of the blastomere (around -70 mV). Under visual control 1 to 3 short puffs of the green fluorescing dye were injected into the cell until the outline of the cell became clearly discernible. The pipette was then quickly retracted. Shortly after the injection, and also 15 min later, the cell was observed to determine whether the injected cell had survived, and the dye had remained intracellularly.

Development after injection

Each successfully injected embryo was transferred to a separate compartment (1 cm diameter) of a multiwell culture dish with an agar coated bottom. Embryos were kept separately because those that did not survive caused the death of all other embryos in the same well. Embryos were kept in embryo medium with added antibiotics (100 000U Penicillin/l, 0.25 mg amphotericin/l and 100 mg streptomycin/l, all Sigma), pH 7.2, at a temperature of 26 to 28°C until the developmental stage desired. Zebrafish embryos develop normally between 25 and 33°C However, the speed of development is dependent on the temperature. Embryos were therefore staged using a standardised morphological staging series and the age then

converted to the standard development time which is hours post fertilisation at 28.5°C (hpf) (Westerfield, 1994). All times of development in this study are given as hpf although the real time passed after fertilisation may have been longer. Generally embryos were investigated between 16 hpf, just before the first nerve cells develop processes and 24 hpf.

2B.3 THE CONFOCAL MICROSCOPE

A confocal laser scanning microscope (CLSM, Leica, Germany) was used because of its higher resolution and better signal to noise ratio compared with conventional imaging systems. It achieves this by rejecting fluorescence from below or above the focal plane. This feature was important in experiments where the fluorescence from single cells lying in the three dimensional structure of the spinal cord was monitored. Light emitted from cells below or above the optical section did not interfere with the recording from the cell of interest. A beam of 488 nm wavelength from an argon ion laser was passed through a pinhole, directed through a short wavelength pass (<510 nm) dichroic mirror and a Nikon 20x objective (NA 0.75) of the inverted microscope to the specimen. Emitted light from the specimen entered again the objective, was deflected by the dichroic miror and then guided through an adjustable pinhole. Light not from the focal plane was rejected by the pinhole. Light was finally filtered (515 nm longpass) and detected by a photomultiplier tube. By a rapid scanning motion of the laser an image in the x y plane was built up. The signal from the photomultiplier tube was transmitted to a VME computer system with a Motorola 68020 microprocessor and a total of 8 MB RAM. Acquired Images

were then stored on optical discs. The Leica CLSM software was used to control most parameters on the confocal microscope and for image analysis. Before specimens were scanned in the confocal mode, they were viewed in a conventional epifluorescence light using a fluorescein filter set.

2B.4 CELL DISSOCIATION EXPERIMENTS

For these experiments calcium-green dextran was injected into embryos up to the 8 cell stage (1¼ hpf). At this time there are still intercellular connections between the cells so that the dye when injected into one cell soon labelled the whole embryo. At around 16 hpf embryos were transferred into a petridish with calcium free cell dissociation medium, washed several times under sterile conditions in a laminar flow cabinet, and left for 15 min at room temperature. Cell dissociation medium:

116 mM	NaCl
2.9 mM	KCl
5 mM	HEPES,
2 mM	tricaine (Sigma)
2 mM	EGTA pH 7.2

A sterile coverslip was dropped onto the embryos and moved around to dissociate embryos. The suspension was transferred to a centrifuge tube and spun at 300G for 7 min, the supernatant removed, and the pellet resuspended in "growth medium" consisting of:

L-15 Medium Leibovitz (containing 300 mg/l L-Glutamine), (Sigma)	
100 000U/l	penicillin, (Sigma)
0.25 mg/l	amphotericin, (Sigma)
100 mg/l	streptomycin, (Sigma)
3%	foetal calf serum (Advanced Protein Products. UK).

Cells were again centrifuged and resuspended in fresh growth medium before being plated on polylysine (2 µm/ml) coated Petriperm dishes (Bachofer, Germany) and incubated at 28.5°C. Two to four hours later dishes were transferred to the stage of the confocal microscope. By this time nerve cells -labelled as all other cells in the preparation with calcium-green dextran - were clearly identifiable as cells expressing neurites and growth cones. A labelled nerve cell was brought into the centre of the view and the fluorescence intensity monitored using the 100x Nikon objective (glycerol, NA 1.3) by scanning every 320 ms. After acquiring 30 control images I depolarised the cell with a solution containing 130 mM KCl, 2 mM $CaCl_2$ and 5 mM HEPES and 10% dilution of the growth medium. To exchange the solutions I used a diamond shaped perfusion chamber (RC-26, Warner Instruments, CT) sealed onto the dish with silicon grease. For analysis, images were background subtracted and ratioed through an average of the control images.

2B.5 Monitoring calcium in vivo

Zebrafish embryos from 16 to 24 hpf were anaesthetised in a solution of embryo medium and 2 mM tricaine (Sigma), pH 7.2, and then embedded in a Petriperm dish in 1% agar just above the gelling temperature of 30°C (Sigma). While the agar was still fluid embryos were oriented so that the spinal cord was on its side and horizontal. The agar hardened and provided a stable matrix, which prevented embryos from floating around during observations. Dishes were then placed on the stage of the confocal microscope and viewed with the 20x Nikon objective under blue light from a

fluorescein filter set. Calcium-green labelled cells emitted green fluorescing light. A suitable nerve cell was chosen for observation and monitored usually for 30 min by scanning several confocal sections below, through and above the cell. This was necessary because if one scanned only one section through the cell, one could not rule out movement artefacts such as might occur if cell migration or gross movements of the embryo caused the more brightly labelled nucleus to move into the plane of focus. By inspecting all optical sections such mistakes were however ruled out. To determine how far optical sections should be apart in order not to miss too much light from the cell between optical planes but at the same time using a minimum of illumination I measured the confocality of the setup (Figure 2.2). To do this the dichroic mirror was replaced with a neutral beam splitter to use the confocal microscope in a light reflectance mode. A thick glass slide was put on the stage and the light reflected by one of the surfaces detected by the photomultiplier. With the adjustable pinhole fully open (position 255), I then measured the reflected light intensities at various z positions. Three microns below or above the plane of focus of the surface still 90 percent of the reflected light was detected (dotted line in Fig. 2.2). In scanning experiments of cells a distance of 3 µm between focal planes was then usually chosen as a compromise setting that avoided unnecessary excitation but still gave an accurate reading of the entire thickness of the cell. In experiments where a faster detection rate was necessary, such as monitoring fluorescence changes in contracting muscle cells, I focused on the brightest optical section of the cell and only scanned at this focal plane. Any movement of the cell could therefore only result in a fall of the fluorescence intensity.

Figure 2.2

Confocality of the Leica, CLSM. The histogram illustrates the effective thickness of optical sections with fully open pinholes.The reflectance mode of the CLSM was used. The distance of the focal plane at various z positions from the reflecting surface of a glass slide is plotted against the reflected light intensities (normalised to the value at 0 µm). (Filled circles) The full line was fitted by the computer through the points. Dotted lines indicate that at a distance of three microns from the reflecting plane 90 percent of the light is still detected.

Figure 2.2

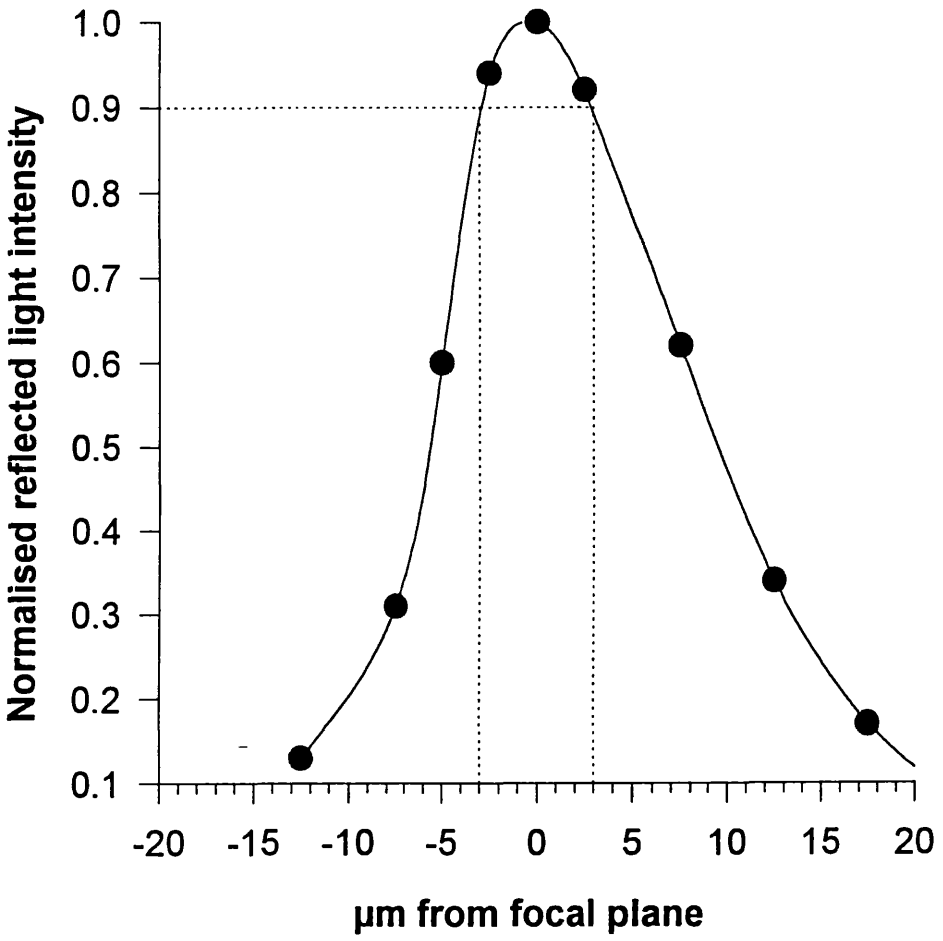
Normalised reflected light intensity
1.0
0.9
0.8
0.7
0.6
0.5
0.4
0.3
0.2
0.1
-20
-15
-10
-5
0
5
10
15
20
µm from focal plane

CHAPTER 3

IMAGING CALCIUM INFLUX

IN NEUROBLASTOMA GROWTH CONES

This, and part of the next chapter, presents my results on the spatial organisation of calcium signals in growth cones associated with depolarisation of the membrane. In this chapter I will first outline the findings from imaging experiments, studying the influx of calcium ions through L type calcium channels. Using the patch clamp technique in the cell attached mode, I then describe in chapter 4 the underlying distribution of individual L type channels on the growth cone membrane and also describe their single channel characteristics.

Growth cones of the N1E-115 mouse neuroblastoma cell line exhibit a wide range of morphologies. To facilitate comparison between imaging and membrane patch measurements, this study was restricted to growth cones of a particularly simple shape. I only used non-branching growth cones in which the leading edge could be unequivocally identified, hereafter I shall call them club shaped (Figure 3.1). Growth cones of this simple form are motile for a significant proportion of the time, and advance usually straight forward along the line of the neurite and do not branch (Silver et al., 1989; Soekarno et al., 1993).

In the following imaging experiments I will show that the voltage protocol, used to depolarise neuroblastoma cells, specifically activates an L type calcium current. The associated calcium influx, detected with Fluo-3, showed a clear distal to proximal gradient in club shaped growth cones and was partly concentrated in hotspots, localised areas of higher calcium.

Figure 3.1

Club shaped growth cones: A) and B) Growth cones of this simple shape were selected for experiments in chapter 3 and 4. For these figures neurones were fixed in 4% formaline and observed by differential interference contrast photomicrography. The cell body is out of the field of view to the left. Filopodia especially at the tip of these growth cones are clearly visible. The growth cone in (B) exhibits a "fan-structure" along the neurite shaft (Bolsover et al., 1992).

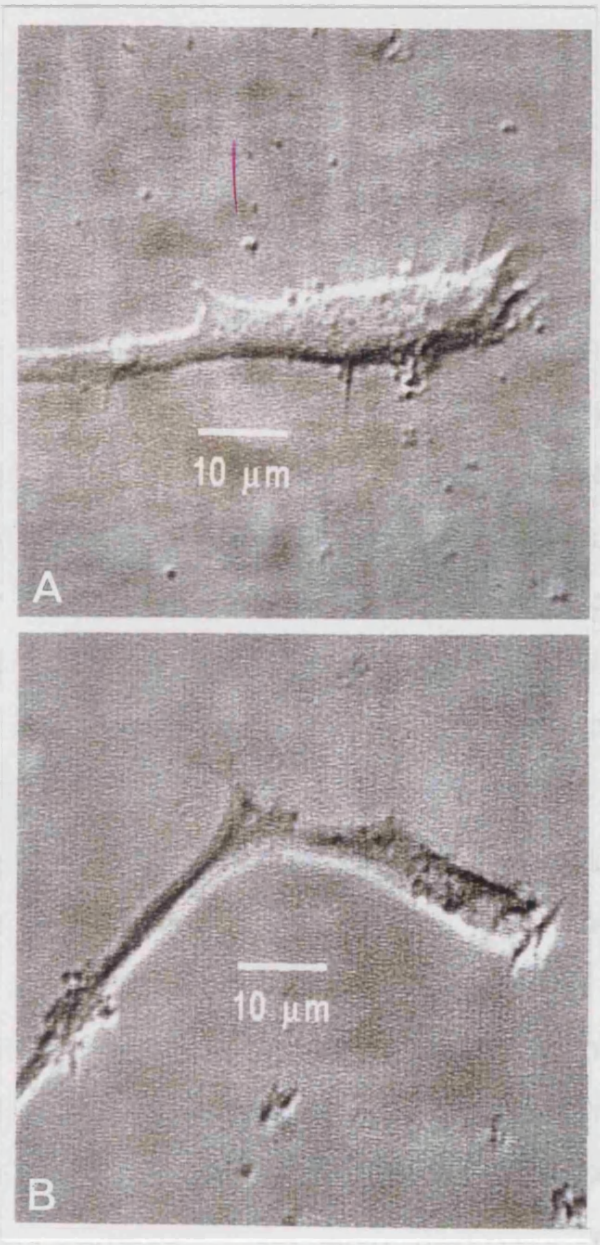
10 µm
A
10 µm
B

Finally, it is demonstrated that there is no contribution from internal calcium stores to this calcium increase.

3.1 THE HVA CALCIUM CURRENT IN NEUROBLASTOMA CELLS

Neuroblastoma cells were described to express two types of calcium currents: a low voltage activated (LVA) type I (or T type) current, and a high voltage activate (HVA) type II (or L type current) (Narahashi et al., 1987; Silver et al., 1990). As cell lines can change their characteristics, I performed control experiments to confirm the nature of the whole cell calcium currents in my batch of N1E-115 neuroblastoma cells. In the following experiments I used the patch clamp technique in the whole cell variation to establish the characteristics of HVA calcium current.

Cells were clamped at a voltage of -40 mV. At this potential LVA calcium current are inactivated (Silver et al., 1990; and own observation). If cells were depolarised to various test potentials an inward current, carried by calcium ions, set in at a relatively high depolarising test voltage of -25 mV. It reached a peak at around +10 mV and finally reversed at around 45 mV. Figure 3.2 illustrates this in a plot of the current voltage relationship for a representative cell. This current activated quickly but hardly inactivated even during long depolarisations of up to 1 sec (Figure 3.3 and 3.4). On repolarisation it showed tail currents. Sensitivity to dihydropyridines is the defining criterion for L type calcium channels (Hess et al., 1984). To test therefore the pharmacological sensitivity I added 5 µM of the dihydropyridine (DHP) antagonist nifedipine to the bath in 5 experiments where I had recorded this HVA current. Figure 3.3 shows the averaged

Figure 3.2

Current voltage (IV) relation for the L-type (type II) current in a representative neuroblastoma cell. The cell was voltage clamped at -40 mV and depolarised to various test potentials ranging from -50 mV to +55 mV. The test potential is plotted against the amplitude of the current which was measured 50 ms after the depolarisation. This plot demonstrates that at a holding potential of -40 mV only a high voltage activated calcium current is elicited that sets in at -25 mV and shows a maximum amplitude at +10 mV. This inward current reversed to become an outward current at around +45 mV. These features are characteristic for the L type calcium current. The pipette contained pipette solution B. Sodium channels were blocked with 1 µM TTX in the bath. Potassium channels were inhibited with 20 mM TEA in the bath and 25 mM TEA plus 135 mM CsCl in the pipette.

Figure 3.2

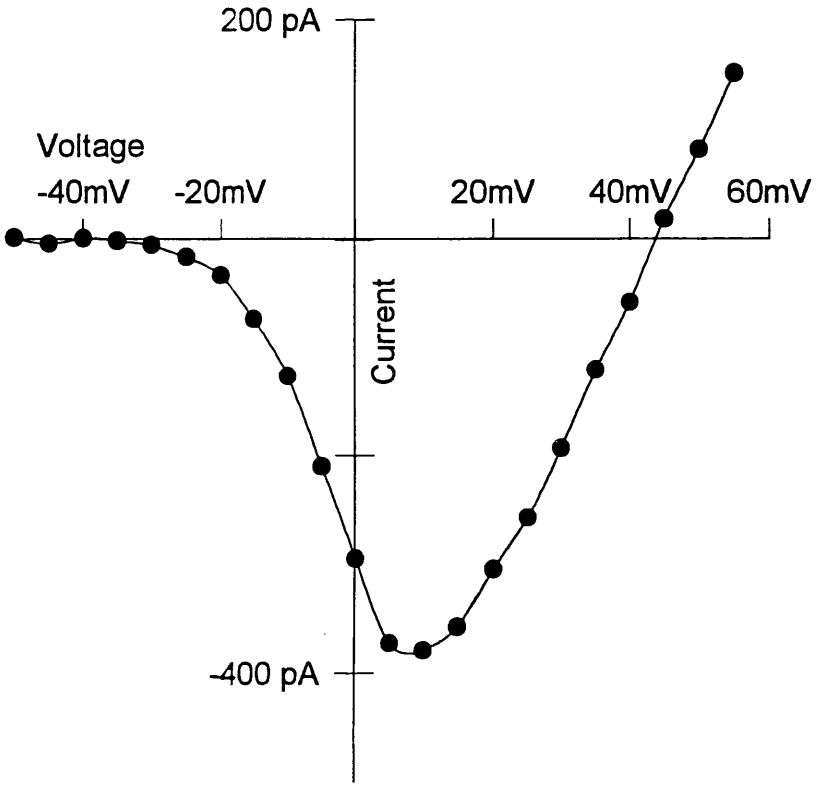

Figure 3.3

Nifedipine blocks L type current: The HVA current in neuroblastoma cells is completely inhibited by 5 μM of the dihydropyridine (DHP) antagonist nifedipine. Data are averages from 5 experiments. As the voltage protocol (top) shows cells were held at -40 mV and then depolarised to +10 mV. The lower current trace (without nifedipine) illustrates the slow inactivation kinetics. Upper current trace was recorded from the same cells shortly after addition of nifedipine to the bath. This sensitivity to DHPs identifies the L type calcium current.

Figure 3.3

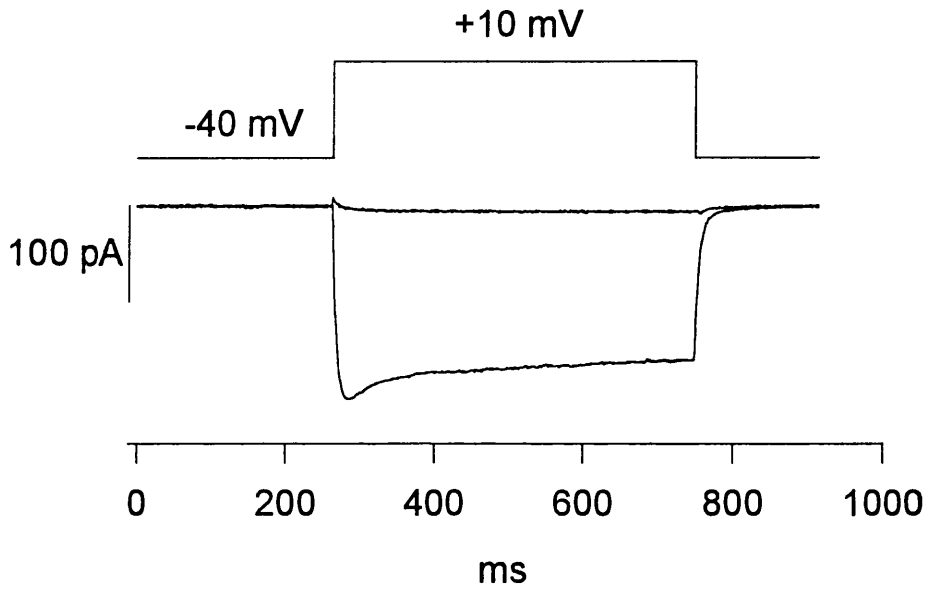

current traces before and after application of nifedipine. In all 5 cases the current was completely suppressed.

In conclusion, there can be little doubt that the present current is indeed an L type calcium current as pharmacological, voltage and kinetic characteristics are in good agreement with other authors (Nowycky et al., 1985; Narahashi et al., 1987; Silver et al., 1990; Kasai & Neher, 1992).

3.2 PATTERN OF CALCIUM INFLUX

To study the spatial pattern of calcium influx, caused by the activation of L type calcium channels on growth cones, neuroblastoma cells had to be loaded with a calcium indicator dye. For this purpose the whole cell voltage clamp pipette, used to depolarise the cell, also contained 10 mM of the penta-potassium salt of Fluo-3 (MW 854). About 10 min after rupture of the membrane patch, that is after "going whole cell", enough of the dye had diffused out into the growth cone to image its fluorescence. At that time an L type calcium current was elicited, by stepping the membrane voltage from the holding potential of -40 mV to +10 mV for 1 sec (Figure 3.4). Due to binding of calcium ions to Fluo-3 molecules, the fluorescence over the cell rapidly increased. The vertical bars on the x-axis of Figure 3.4 indicate when, in relation to the voltage changes, fluorescence images of the growth cones were acquired. Figure 3.5 illustrates one experiment in which the time course of the average fluorescence increase over 17 growth cones during the first 480 ms after depolarisation was monitored. The fluorescence intensities are expressed as ratios to the control values of just before the depolarisation. Due to the continued influx of calcium ions - L

channels hardly inactivated - the fluorescence rose monotonically over time.

Fluo-3 fluorescence did not increase homogeneously over the whole growth cone but rose in spatially localised hotspots. This is illustrated in two examples in pseudocolour images of the ratioed fluorescence increase. Warm colours indicate higher calcium levels (Figure 3.6). In a series of 15 club shaped growth cones I studied the distribution of these hotspots. My subjective definition for hotspots was a region between 5 and 10 µm in diameter that showed a larger calcium increase than its surroundings. I observed between one and three hotspots per growth cone, 5 growth cones with one hotspot, 7 with two hotspots and three growth cones with three hotspots. Most of these hotspots occurred nearer to the distal end, in fact all 15 growth cones had a hotspot at the tip (Figure 3.6). In an attempt to quantify this subjective observation, I averaged the relative fluorescence increase in 5 µm wide sections along the growth cone from the distal tip to more proximal regions, as sketched in the inset of Figure 3.7. The histogram demonstrates that in agreement with the initial conclusion the fluorescence increase was indeed greater at the tip. At 240 ms after the depolarisation fluorescence increase was 2.4 fold at the tip but declined monotonically towards more proximal regions. The results are not normalised and a large fraction of the individual variability (± sem) reflects growth cone to growth cone differences in calcium current amplitude. However, if this variability was removed by a paired t-test the differences between the tip and all other more proximal sections were clearly significant ($p<0.05$ for 5-10 µm and $p<0.01$ for all others).

Figure 3.4

Voltage protocol and image acquisition in imaging experiments. Pipettes were filled with the whole cell pipette solution A which contained 10 mM Fluo-3 instead of EGTA. Cells were held at -40 mV. About 10 min after rupturing the patch they were depolarised to +10 mV for 1 second. The trace below the voltage protocol is a representative example of an L type calcium current recorded during such an experiment. The vertical bars on the time axis indicate when fluorescence images of the growth cone were acquired as in experiments seen in Fig. 3.5 and 3.8. The sampling rate in the experiment in Fig. 3.7 was slower, only 240 ms per image.

Figure 3.4

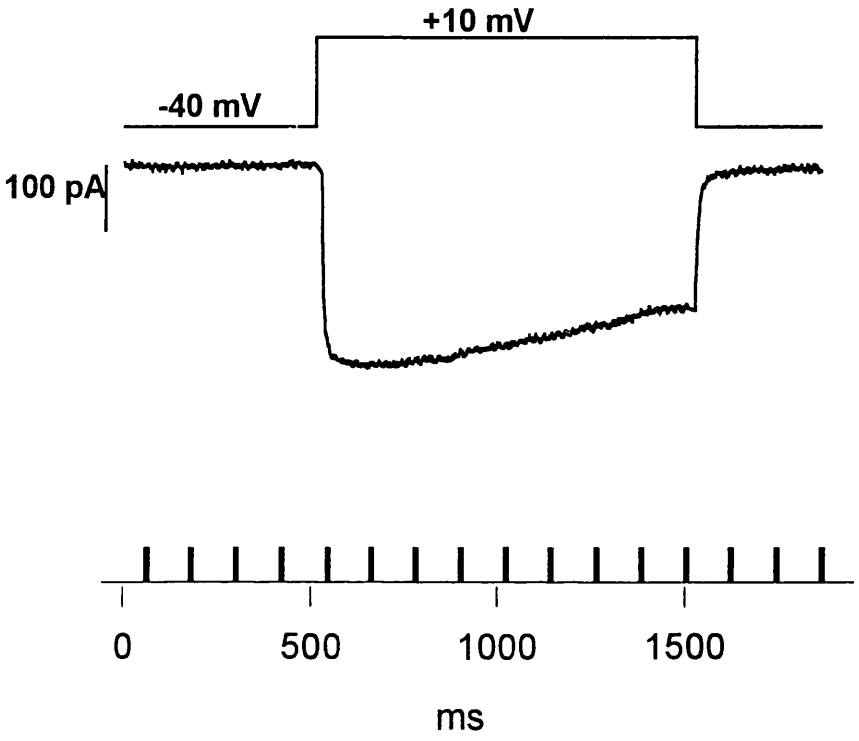

Figure 3.5

Timecourse of the Fluo-3 fluorescence increase over the entire growth cone. Cells were depolarised at 0 ms as shown in the protocol in Figure 3.4. Images were background subtracted and divided through an average of the four control frames, acquired just before depolarisation (1 means no fluorescence change). Filled circles are means (± sem) from 17 experiments. Fluorescence intensities still rose after 480 ms, but in most cases this saturated the camera gain so that true intensity values could not be measured.

Figure 3.5

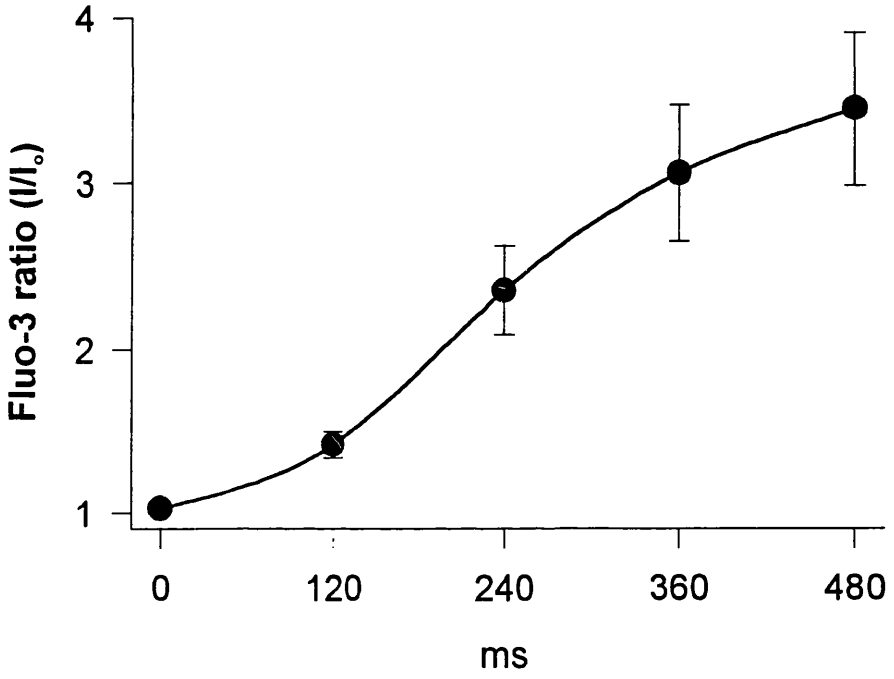

Figure 3.6

Hotspots at the tip of growth cones: A) and B) Cells were depolarised according to the protocol in Figure 3.4. The relative Fluo-3 fluorescence increase (I/I_0) is depicted on a pseudocolour scale as seen in (C). Warm Colours represent higher calcium values. These two growth cones demonstrate hotspots, localised areas of fluorescence increase. Hotspots occured near to the tip of growth cones. Images were acquired 120 ms after depolarisation in (A) and 240 ms in (B).

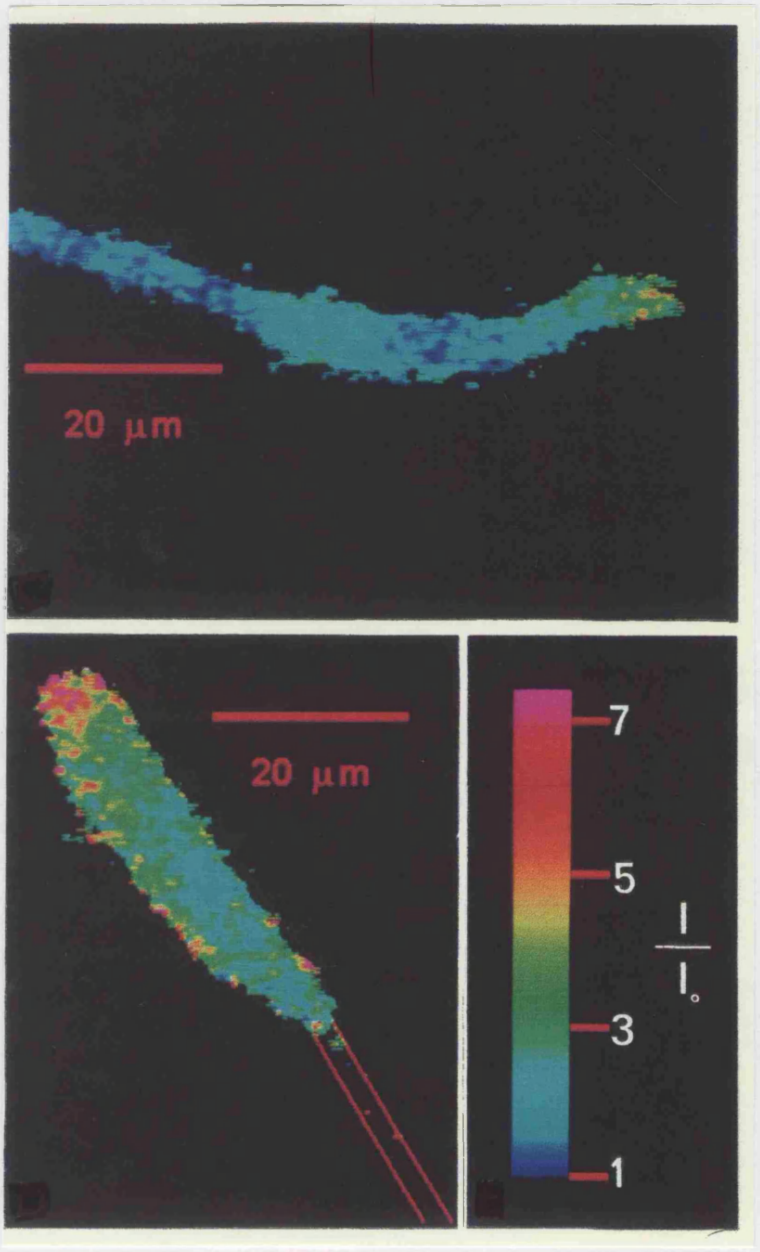
A
20 µm
B
20 µm
7
5
3
1
I
I°
C

Figure 3.7

A distal to proximal gradient of calcium rise: Images were aquired 240 ms after depolarisation. Histogram shows the relative fluorescence increase averaged form 15 experiments (mean ± sem) versus the distance from the tip. Each coloumn represents the average fluorescence change in a 5 µm wide section of the growth cone as indicated by the inset. Result are not normalised. The large errorbars are a result of growth cone to growth cone differences in calcium current amplitudes. These variabilities between growth cones were removed by a paired t-test, results of which are shown as asterisks. *:significantly differrent from the 0-5 µm value, $p<0.05$ **:$p<0.01$

Figure 3.7

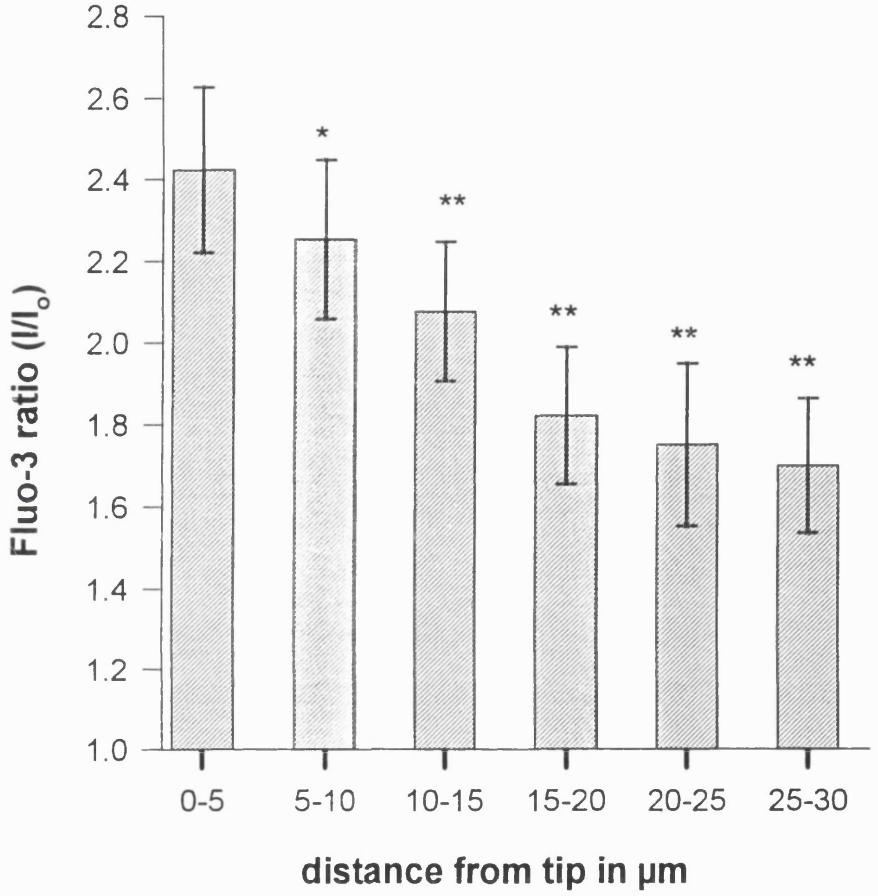
2.8
2.6
2.4
2.2
2.0
1.8
1.6
1.4
1.2
1.0
Fluo-3 ratio (I/I$_o$)
*
**
**
**
**
0-5
5-10
10-15
15-20
20-25
25-30
distance from tip in µm

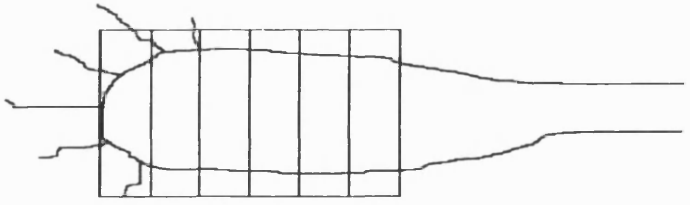

3.3 INTERNAL CALCIUM STORES

The above experiment demonstrated that activation of L type calcium current caused a significant rise of intracellular calcium in growth cones. It did however not clarify whether or not calcium induced calcium release (CICR) contributed to the rise in intracellular calcium. CICR is a phenomenon whereby a rise in cytosolic calcium causes release from intracellular calcium stores in a positive feedback mechanism (Berridge, 1993; Simpson et al., 1995). CICR is blocked by drugs such as ryanodine and dantrolene. A dantrolene sensitive release, for instance, has been proposed as the cause of large $[Ca^{2+}]_i$ increases triggered in growth cones of rat dorsal root ganglion neurones by the inhibitory cell surface protein NI-35 (Bandtlow et al., 1993). In order to investigate whether CICR contributes to the observed calcium dynamics in neuroblastoma growth cones I blocked release from intracellular organelles. Cells were bathed in either dantrolene (40 µM) or ryanodine (200 µM) for 210 sec before cells were depolarised. The fluorescence increase was then compared to controls where no drug was added (Figure 3.8). Neither drug affected the amount of calcium increase in growth cones. Moreover the pattern of calcium increases in individual growth cones before and after adding drugs was identical. These experiments confirm that the depolarisation induced calcium increase in neuroblastoma growth cones is caused by calcium flux through voltage operated calcium channels and calcium induced calcium release plays no role.

Figure 3.8

Neither dantrolene nor ryanodine affect calcium dynamics at the growth cone.: Growth cones were depolarized twice. The second depolarization was performed 210 seconds after the first. Fluorescence ratioes (I/I_0) during the second depolarization were then normalized to the 480msec value of the first depolarization and are plotted here. Circle: no change of bathing solution between first and second depolarization, n=5. Diamond: 200 µM ryanodine added 210 seconds before second depolarization, n=5. Square: 40 µM sodium dantrolene added 210 seconds before second depolarization, n=7. Because of calcium current rundown, and the increase of calcium buffering power as more Fluo-3 diffused into the growth cone, the fluorescence change during the second depolarization was smaller than in the first. This is why the normalized change is in all cases less than 100%.

Figure 3.8

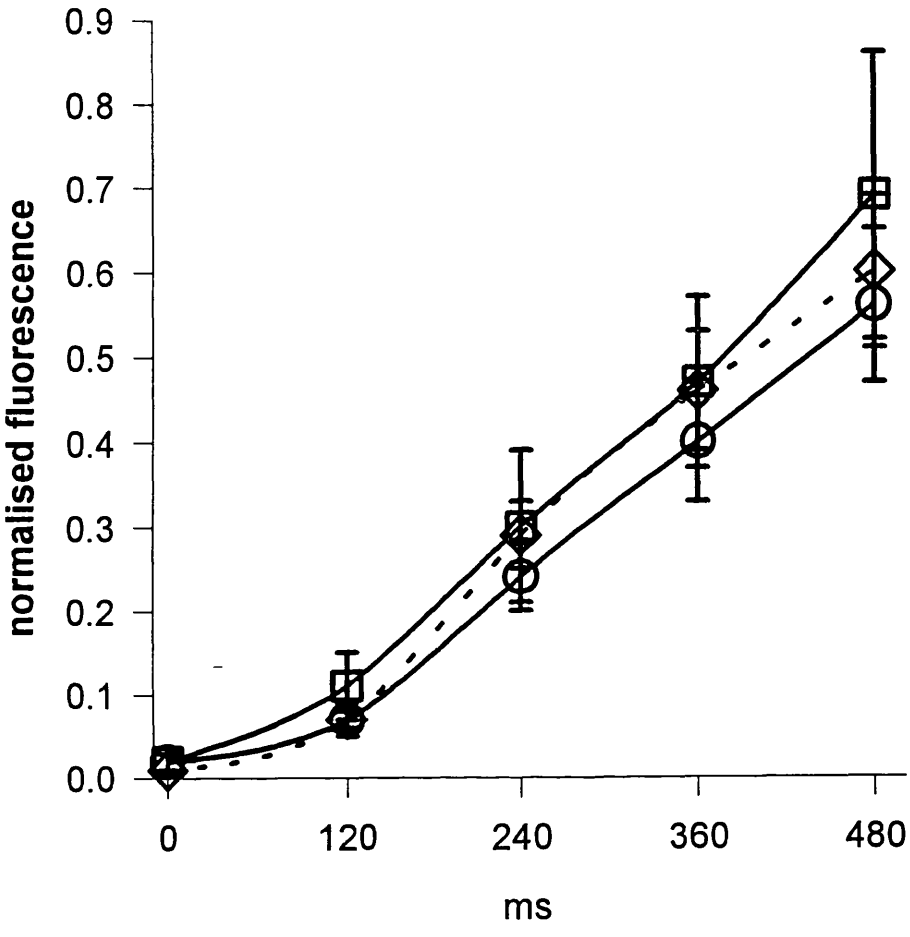
normalised fluorescence
0.0
0.1
0.2
0.3
0.4
0.5
0.6
0.7
0.8
0.9
0
120
240
360
480
ms

CHAPTER 4

CALCIUM CHANNELS

ON NEUROBLASTOMA GROWTH CONES

This chapter reports results from experiments on calcium channels using the single channel technique in the cell attached mode. First, I will present in detail the single channel properties of T and L type calcium channels, the two calcium channel types found on neuroblastoma growth cones. I will then show that the pattern of calcium influx, as described in chapter 3, can be accounted for by the distribution of individual L channels on the growth cone membrane. In an appendix to chapter 4 data are presented that favour a fractal model as explanation for the distribution of L channel open times.

4.1 SINGLE CHANNEL PROPERTIES

4.1.1. T TYPE CALCIUM CHANNELS

The first channel type was characterised by a low single channel conductance of 7.5 pS and a requirement for a relatively negative holding potential. On the basis of these and the following findings, I was able to identify them as T type calcium channels (Nowycky et al., 1985; Fox et al., 1987; Fisher et al., 1990; Shuba et al., 1991). I observed these channels in 14 out of 21 patches on growth cones, and on 21 out of 24 patches on cell somas. The relative frequencies of channels on growth cones and cell

bodies was not significantly different (Fisher's exact test, Altman, 1991). Channel behaviour was identical at the two locations and the following values are for the complete dataset. T channels were characterised by short bursts of low amplitude openings, clustered at the beginning of depolarisations from -90 mV to $\geq$ -50 mV (Figure 4.1). In contrast, depolarisations from -40 mV elicited hardly any openings, consistent with an almost complete steady state inactivation of T channels at this voltage. (Narahashi et al., 1987). This effect is most apparent if single channel traces from patches held at the respective holding voltages, but depolarised to the same test voltages, are summed, and the current amplitudes compared (Figure 4.2). From a plot of single channel current amplitudes against depolarisation voltages, I could calculate, averaged from 12 experiments, the single channel conductance which was 7.5 (±0.36) pS, and extrapolate the reversal potential to -50 mV (Figure 4.3). During the course of a 200 ms depolarisation channels inactivated rapidly. The decay of the ensemble current (as seen in Figure 4.2) was well fit by a single exponential with a time constant of 32 ± 3 ms at -50 mV (3 patches). The arithmetic mean open time at 0 mV was 1.68 ± 0.25 ms (7 patches). In 16 patches I observed T channel openings in the presence of 5 µM of the dihydropyridine antagonist nifedipine indicating that these channels are - unlike the L type current (see below and chapter 3) - not sensitive to DHPs. These results extend the findings of Shuba et al. (1991) and demonstrate that T type channels are present on N1E-115 cell growth cones, as predicted from fluorescence measurements (Silver er al., 1990).

Figure 4.1

T channel openings. Single channel current traces from a patch on a growth cone. Downward deflections represent inward current channel openings. Holding potential was -90 mV. Shown are the recordings during depolarising test pulses (starting at 0 ms) as indicated to -60 mV, -50 mV, -45 mV and -35 mV. Note openings at a relatively negative potential of -50 mV. Channel openings occur early during the depolarisation and are of low amplitude of below 1 pA. Capacitance currents were not subtracted and are responsible for the rapidly changing baseline at the start of the third and fourth traces.

Figure 4.1

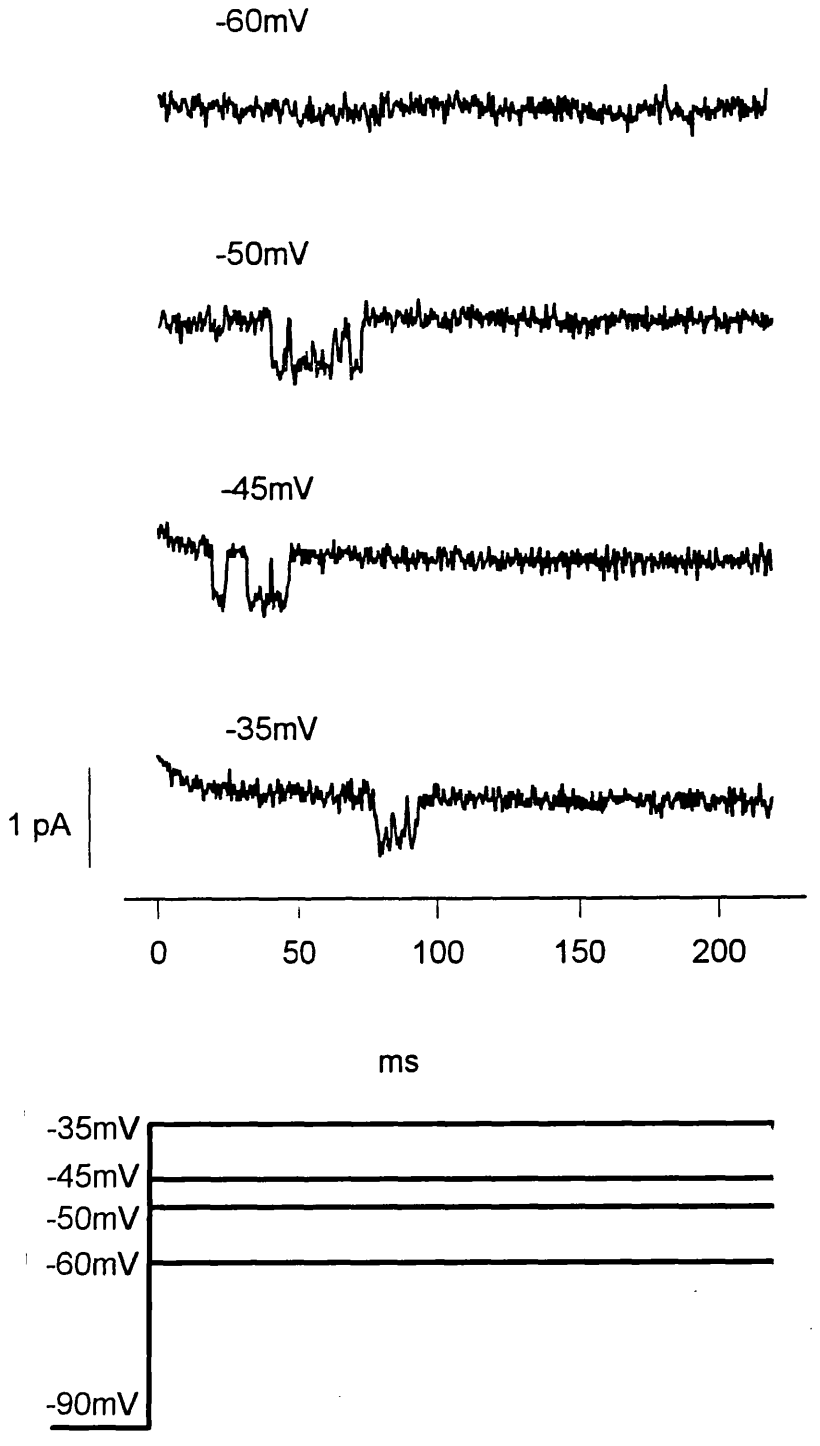
-60mV
-50mV
-45mV
-35mV
1 pA
0
50
100
150
200
ms
-35mV
-45mV
-50mV
-60mV
-90mV

Figure 4.2

Steady state inactivation of T channels at -40 mV. Summed single channels traces from a growth cone patch in the presence of 5μM nifedipine. The patch was either held at -40 mV or at -90 mV and depolarised to 0 mV. From -90 mV, but not from -40 mV, many channel openings were seen producing a rapidly inactivating ensemble current. Below are shown individual traces from holding voltages of -90mV (left) or -40mV (right). From a holding voltage of -40 mV openings (such as in the 4th trace from above) were only seen infrequently.

Figure 4.2

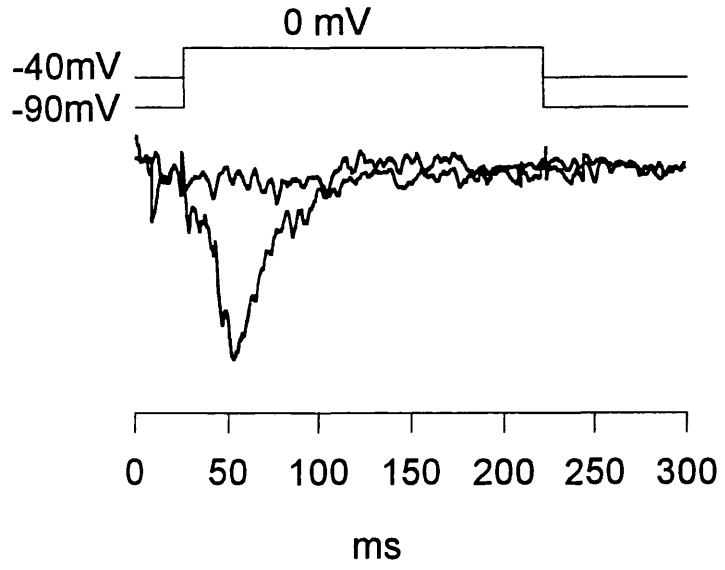
0 mV
-40mV
-90mV
0
50
100
150
200
250
300
ms

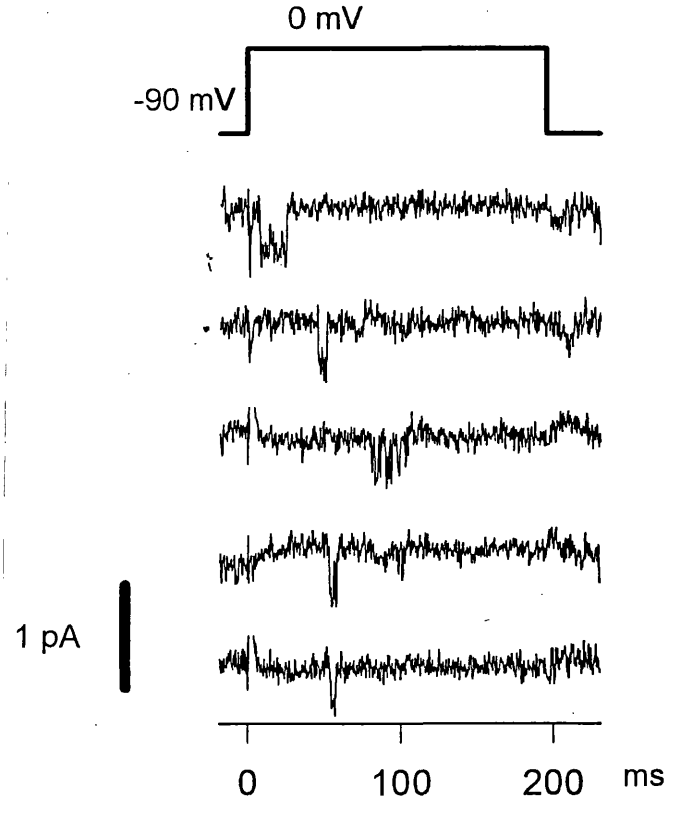
0 mV
-90 mV
1 pA
0
100
200
ms

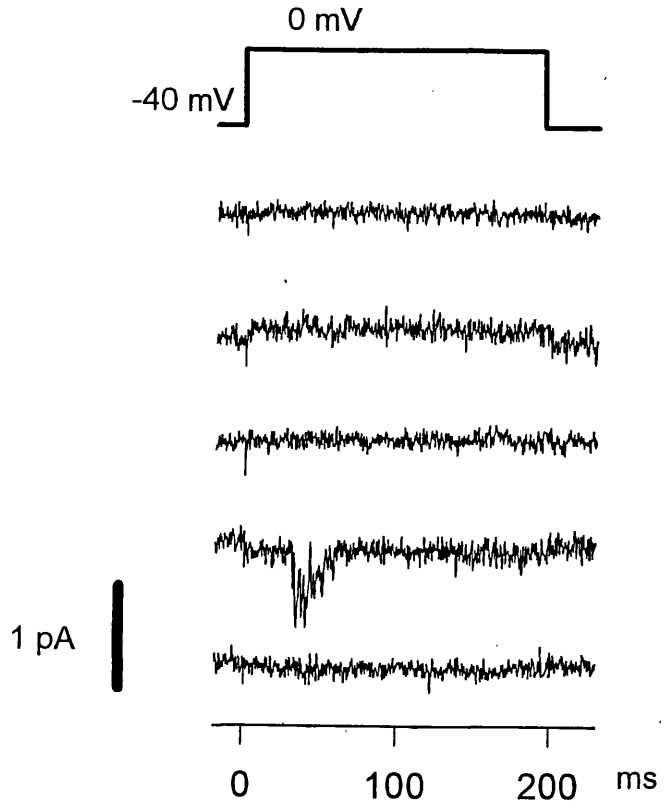
0 mV
-40 mV
1 pA
0
100
200
ms

Figure 4.3

T channel conductance: Plot of unitary T channels currents versus test potential. The slope of the line, 7.5 pS, is an estimate of the single channel conductance. The extrapolated reversal potential is +51 mV. Averaged data of 12 patches. Where error bars (SEM's) are not seen they are smaller than the symbols.

Below are examples of individual current traces from which the current amplitudes at various test voltages were measured. 5 μM of the dihydropyridine antagonist nifedipine were present in the bath. Patches were held at -90 mV and then depolarised to the indicated test voltages. Capacitance transients were not subtracted and are responsible for the rapidly changing baseline

Figure 4.3

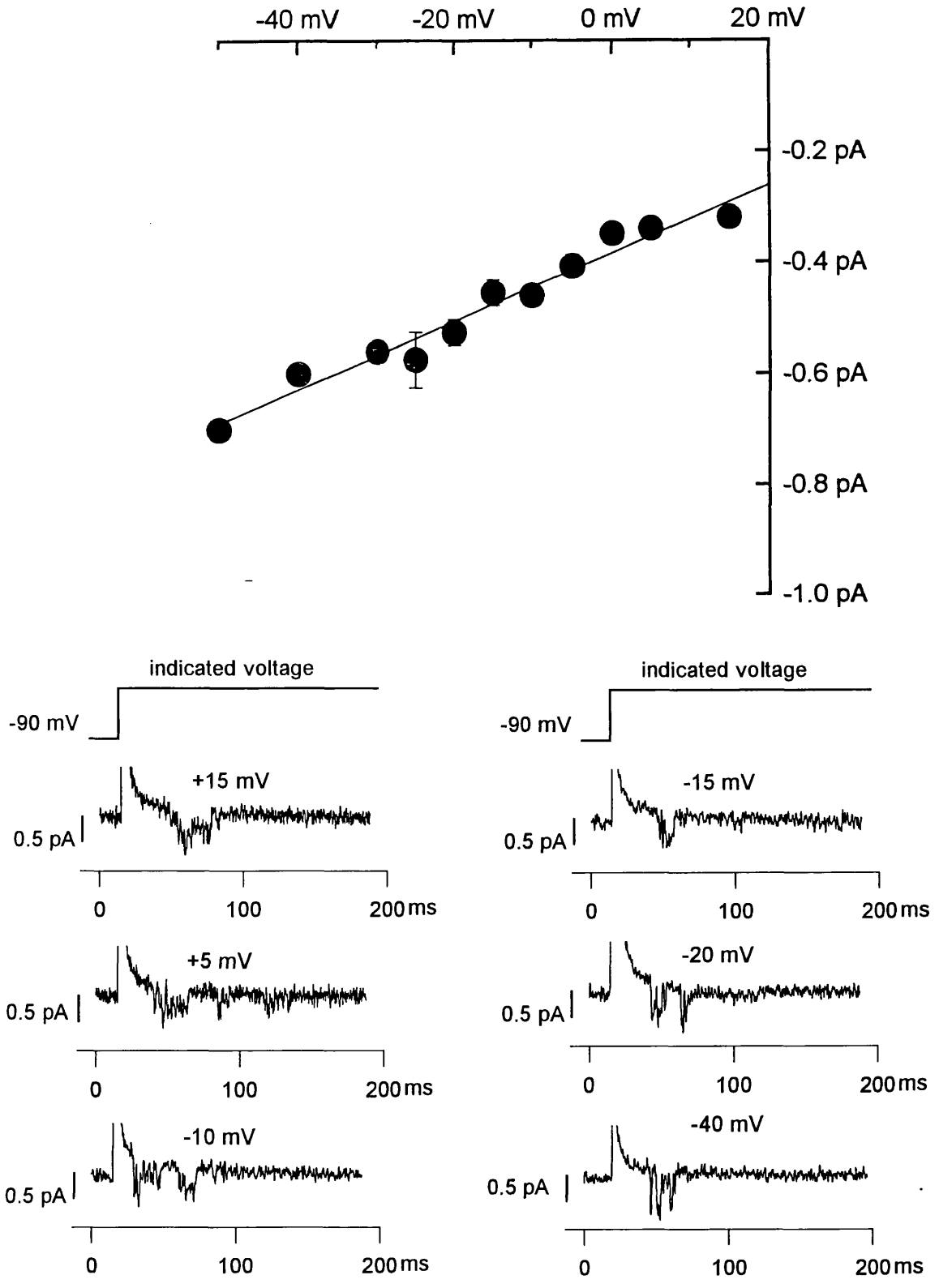
-40 mV
-20 mV
0 mV
20 mV
-0.2 pA
-0.4 pA
-0.6 pA
-0.8 pA
-1.0 pA
indicated voltage
-90 mV
+15 mV
0.5 pA
0
100
200 ms
+5 mV
-10 mV
indicated voltage
-90 mV
-15 mV
-20 mV
-40 mV

4.1.2 L TYPE CALCIUM CHANNELS

The second inward current channel type was clearly different from T channels as it was still available from a holding potential of -40 mV, and the current amplitudes were larger. The top trace in Figure 4.4 shows an examples of these channel openings. However, the open probability was extremely low and individual openings were too short to be resolved fully. Thus, although these openings were suggestive of L type calcium channels, more definitive descriptions were not possible. The identifying characteristic of L type channels is their sensitivity to dihydropyridines. I therefore added the DHP agonist BAYK 8644 (5 μM) to ten patches that showed either these low open probability channels or no openings at all. In all these patches I observed the appearance of many, well resolved channel openings of up to 100 ms during depolarisation from -40 mV to ≥ -20 mV (Figure 4.4). In one experiment the addition of 5 μM of the DHP antagonist nifedipine completely blocked such openings. On the basis of their dihydropyridine sensitivity and their single channel conductance of 25 pS (see below), I could identify these channels as L type calcium channels. The frequency with which these currents appeared, in randomly placed patches on the cell body or the growth cone, were similar (19 of 39 patches at the cell body, 37 of 79 at the growth cone, not different by Fisher's exact test). I could find no differences in the properties of channels from the cell body or the growth cone, and the following values are for the complete dataset. For these experiments the dihydropyridine agonist BAYK 8644 was always used to maximise open probability. Figure 4.5 illustrates an experiment in which the membrane voltage was ramped from +60 mV to -10 mV, while one L channel was open most of the time. As this trace was leak subtracted, the slope of the line fitted through all open points is the

single channel conductance (24.6 pS). The extrapolated reversal potential in this patch was +61 mV. In 12 cells the average single channel conductance and reversal voltage - estimated from single channel current amplitudes in voltage step experiments (as seen in Figure 4.4) - were 24.8± 0.8 pA and +56± 3 mV. The open time histogram of this channels of one representative patch is shown in Figure 4.6. It shows the frequency of open time durations binned into 0.5 ms intervals. It was reasonably well fit by two exponentials (ignoring the first bin between 0 and 0.5 ms). Averaged from 4 patches the time constants were 1.7 (± 0.2) ms and 12.0 (± 1.8) ms, with amplitudes of 85 (± 2)% and 15 (± 2)% at t=0. The arithmetic mean of all channel openings (not binned), the "mean open time", was 6.7 (± 0.9) ms (n=4). Inactivation was slow and incomplete over 200 ms as the ensemble current in Figure 4.7 demonstrates. This is a characteristic feature of L type channels carrying barium ions (Nowycky et al., 1985). After repolarisation to -40 mV the channels showed delayed closing (deactivation). This produced a tail current in the sum of single channels traces in Figure 4.7. To assess the single channel open probability (P_o) of L channels at +10 mV in the presence of 5 µM BAYK8644 I considered patches that were likely to contain only one L channel. (See Methods for explanation of possible and probable one channel patches). In two probable one channel patches P_o was 0.024 and 0.013. The mean P_o in nine possible one channel patches was 0.011 ± 0.003.

Figure 4.4

L channel openings. Single channel traces (without the DHP agonist BAYK 8644, top trace) and in the presence of 5 μM BAYK 8644. Downward deflections represent inward current openings. Patches were held at -40 mV and depolarised at 0 ms to the indicated potentials. Without BAYK 8644 only very short mainly unresolved openings were seen. In the presence of BAYK 8644 long L channel opening were observed at test potentials of -20 mV and more positive.

Figure 4.4

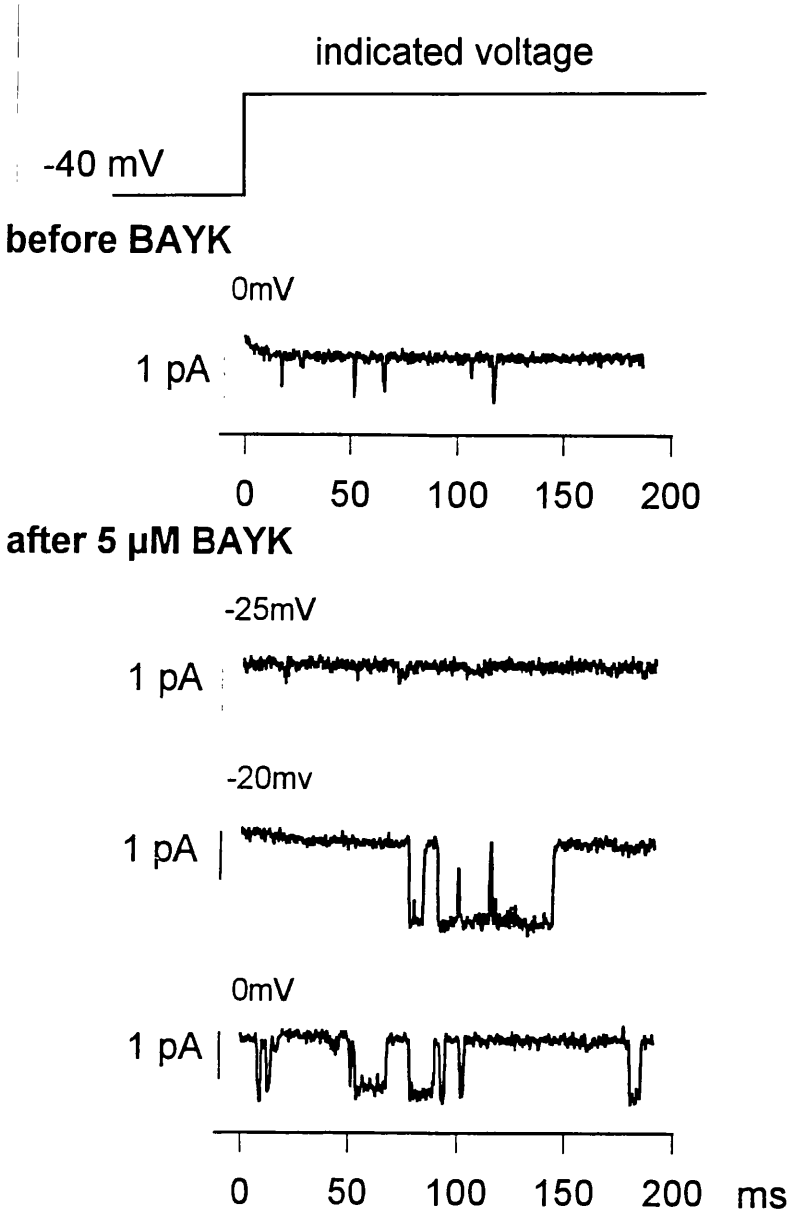
indicated voltage
-40 mV
before BAYK
0mV
1 pA
0
50
100
150
200
after 5 µM BAYK
-25mV
1 pA
-20mv
1 pA
0mV
1 pA
0
50
100
150
200
ms

Figure 4.5

L channel conductance: This patch was held at a voltage of -40 mV, then - as shown in the voltage protocol - depolarised to +60mV and continuously ramped back to the holding voltage of -40 mV. In the trace shown one L channel was open most of the time during this depolarisation. The current amplitude of the channel increased as the voltage became more negative. The straight line is a fit through all current readings while the channel was open. As this trace was leak subtracted the slope of this line in the current voltage diagram (24.6 pS) is a direct estimate of the single channel conductance. 5 µM BAYK8644 was present in the bath.

Figure 4.5

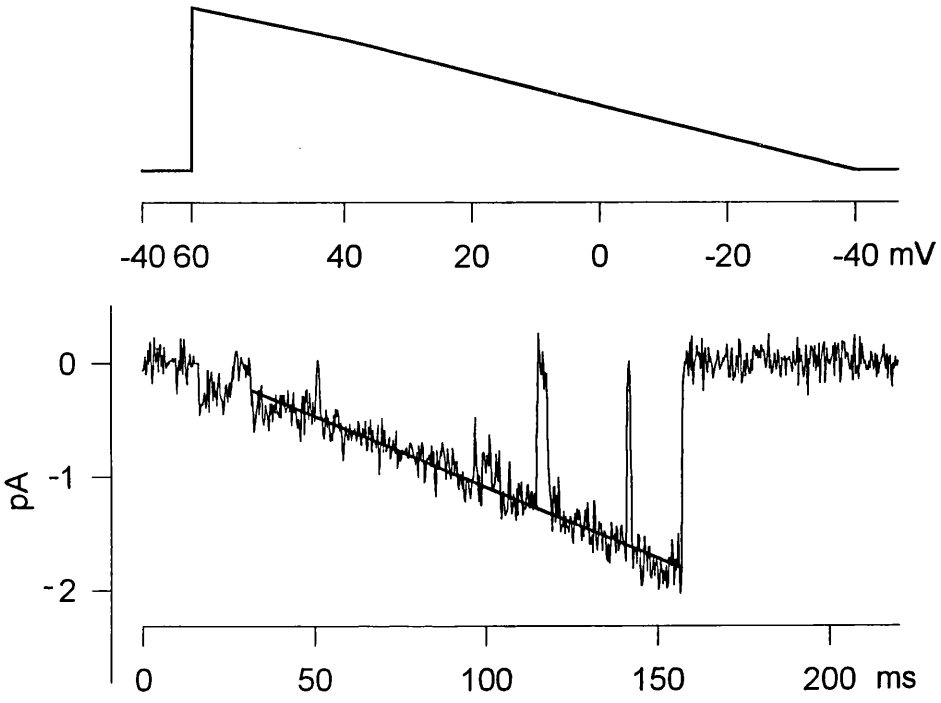

Figure 4.6

L channel open time histogram. The patch was held at -40 mV and depolarised to +10 mV in the presence of BAYK 8644. The open time durations were binned into 0.5 ms intervals. The frequency distribution was fit with two exponentials (continuous line). Time constants of 1.26 ms and 12.59 ms gave a reasonable fit.

Figure 4.6

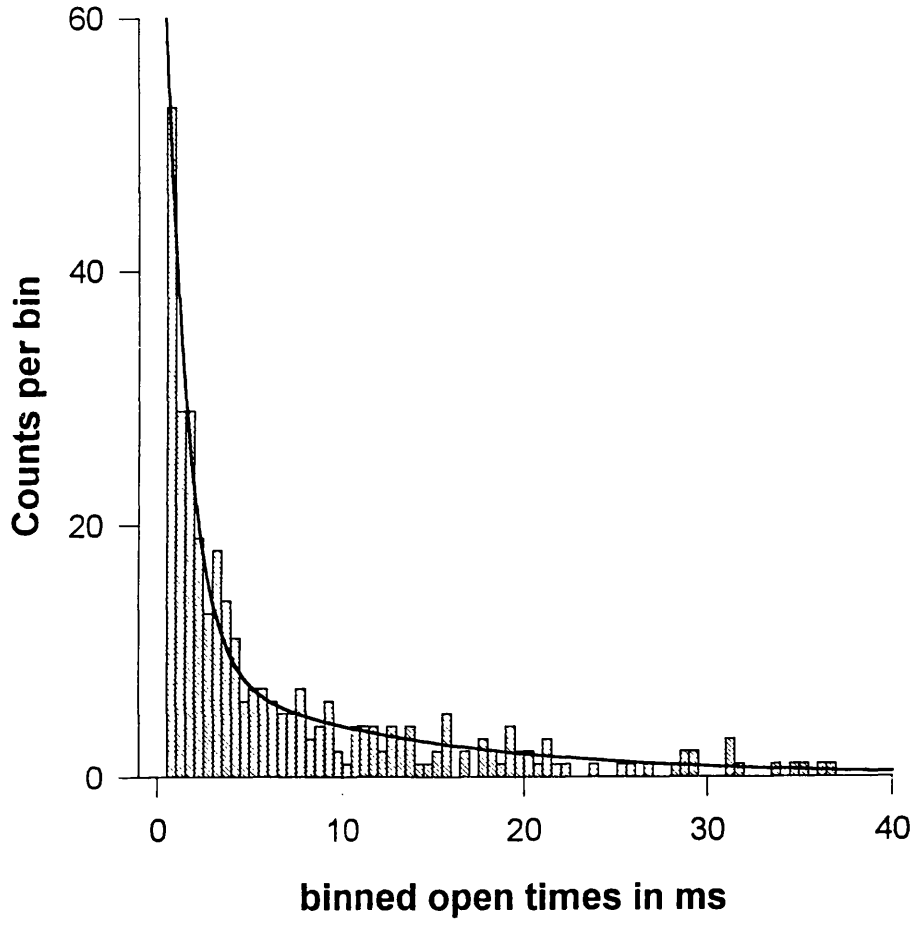

Figure 4.7

L channel inactivation Sum of 59 individual traces showing L channel activity from one patch in the presence of 5 μM BAYK 8644. The patch was held at -40 mV and depolarised to +10 mV. The sum current inactivated slowly during this 200 ms depolarisation. After repolarisation a large and long lasting tail current persisted for more than 100 ms. These are typical L channel characteristics.

Below are shown examples of individual traces. Leak current and capacitance transients were subtracted. This patch contained at least 4 L type channels as judged by simultaneous openings (top trace, left column). In those traces where a channel continued to be open after repolarisation to -40 mV (trace 1 and 2 left column, trace 1 and 3 right column) the single channel current amplitude increased due to the higher electrical driving force for the charge carrying Barium ions. This produced the tail current in the ensemble current above.

Figure 4.7

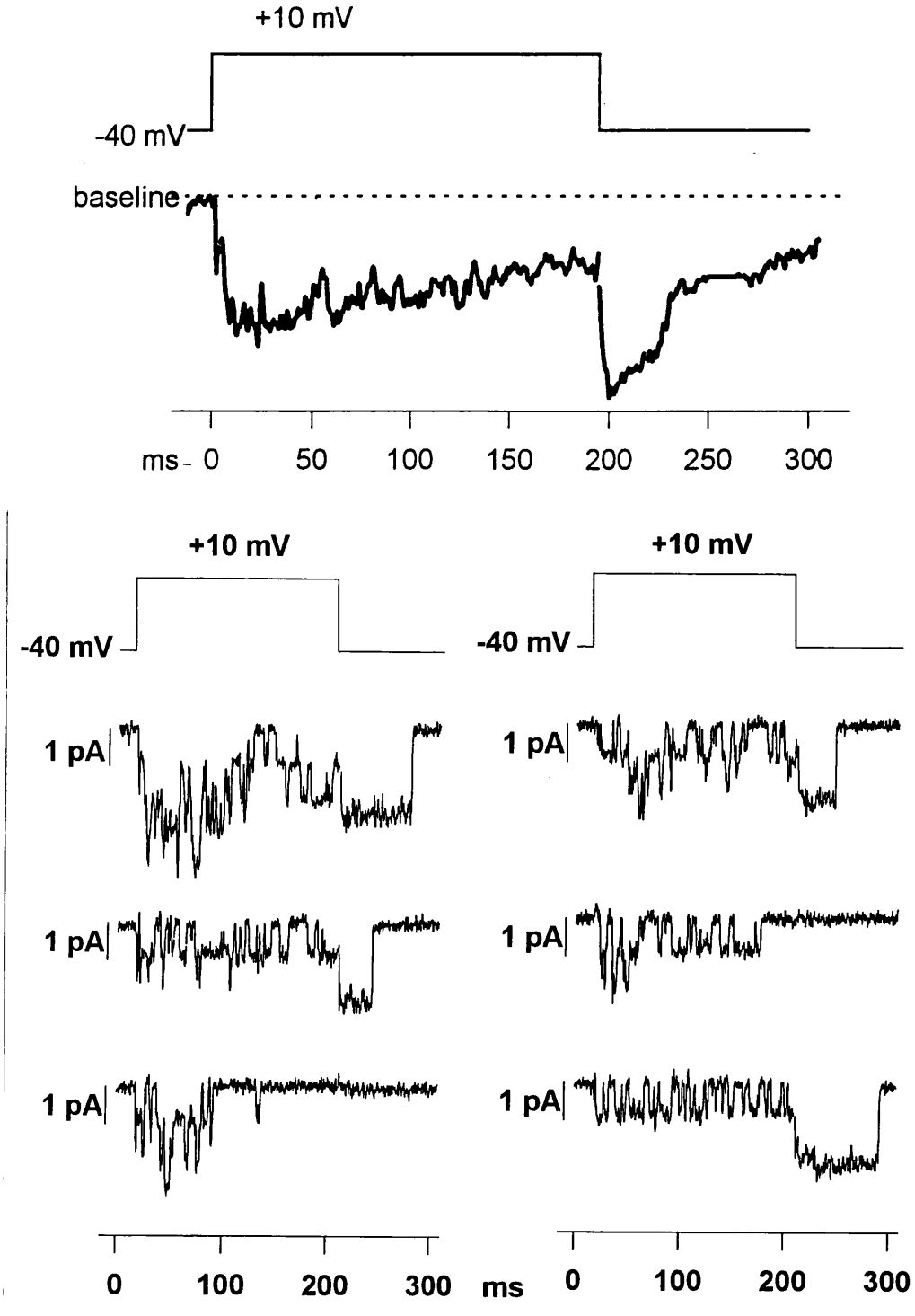
+10 mV
-40 mV
baseline
ms 0 50 100 150 200 250 300
+10 mV
-40 mV
1 pA
1 pA
1 pA
0 100 200 300 ms
+10 mV
-40 mV
1 pA
1 pA
1 pA
0 100 200 300

L channel subconductance states of 12 pS

In 80% of recordings from patches containing L channels the 25 pS openings were interspersed with openings of lower amplitude (Figure 4.8a). Figure 4.8b shows the all-points amplitude histogram for the patch of Figure 4a. The peak at 0 pA is noise and that at 1.1 pA represents full L type openings of 26 pS. The shoulder at 0.45 pA is produced by the lower amplitude openings. Unlike T channel openings, this type of low amplitude event was recorded upon depolarisation from -40 mV and was detectable only in the presence of BAYK 8644 implying that, like standard L currents, they were potentiated by this dihydropyridine. In one experiment they were subsequently blocked by 5 μM nifedipine. The channels producing these currents had voltage dependencies of activation and steady state inactivation indistinguishable from those of true L channels, however, the single channel conductance was lower at 12.1 ± 0.5 pS, n=4 patches. These currents had the same extrapolated reversal potential as L currents (+54 ± 2 mV, n=4). For two reasons I believe these events are openings of L channels to subconductance states. First, all patches displaying these events also contained true L channels, revealed by openings of 25 pS conductance. Second, on several occasions I observed a direct transition from a 25 pS opening to a lower conductance opening. The arrows in Figure 4.9 mark 5 such transitions that are most easily explained as transitions from a fully open L channel to a subconductance state.

Figure 4.8

a) A third single channel event of ~12 pS. In 80% of patches with L currents additional smaller openings were seen. (recorded in the presence of 5 µM BAYK 8644 holding voltage -40mV and depolarised to +10 mV). The opening in the middle is of typical L type. The other two represent openings of a channel that, like L channels, is not inactivated by a holding voltage of -40 mV but has a lower conductance. **b**) All points amplitude histogram of the same patch. The continuous lines are an unconstrained PSTAT (pClamp) fit. The peak at 0 pA is baseline noise and that at 1.1 pA represents full L type openings of 26 pS. The hump at 0.45 pA is produced by the lower amplitude openings.

c) Current Voltage diagram for this small conductance channel. Patches (n=4) were held at -40 mV and depolarised to various potentials. Current amplitudes were measured and are plotted here against the test voltage. (Values are means and sems). The slope of this relationship is a measure of the single channel conductance. It was 12.1 ± 0.5 pS.

Figure 4.8

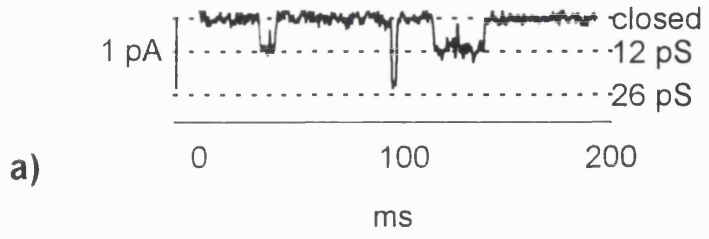

a)

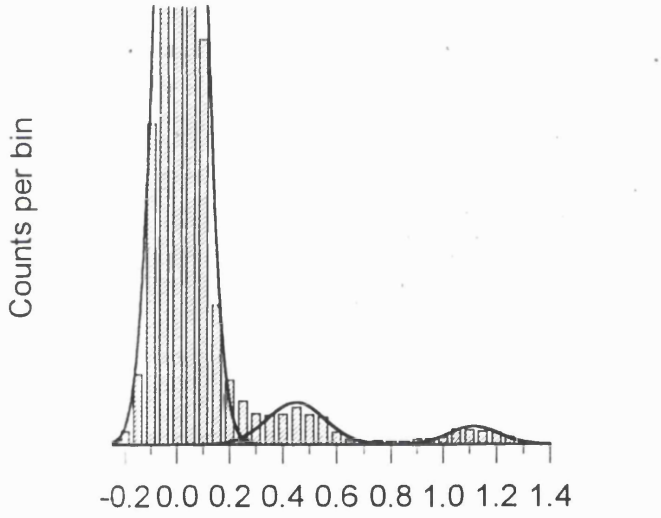

b)

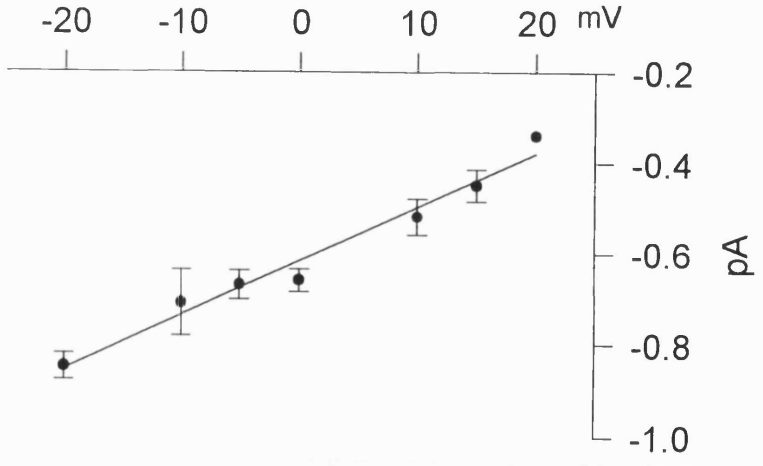

c)

Figure 4.9

Direct transitions between small openings and classical L channels. Traces from one patch that contained apart from small amplitude openings at least two classical L channels judging by two simultaneous openings at 25 pS (not shown). Recorded in the presence of 5 μM BAYK8644. Patch was held at -40 mV and depolarised at 0 ms to the indicated test potentials. Arrows indicate direct transitions between large L openings and smaller currents with no intervening closure. The best explanation for these transitions is a direct switch to a subconductance state. In a total of 120 ms no outward current opening were seen in the patch. This fact practically excludes the possibility that "transitions" were classical L channels with an outward current opening superimposed.

Figure 4.9

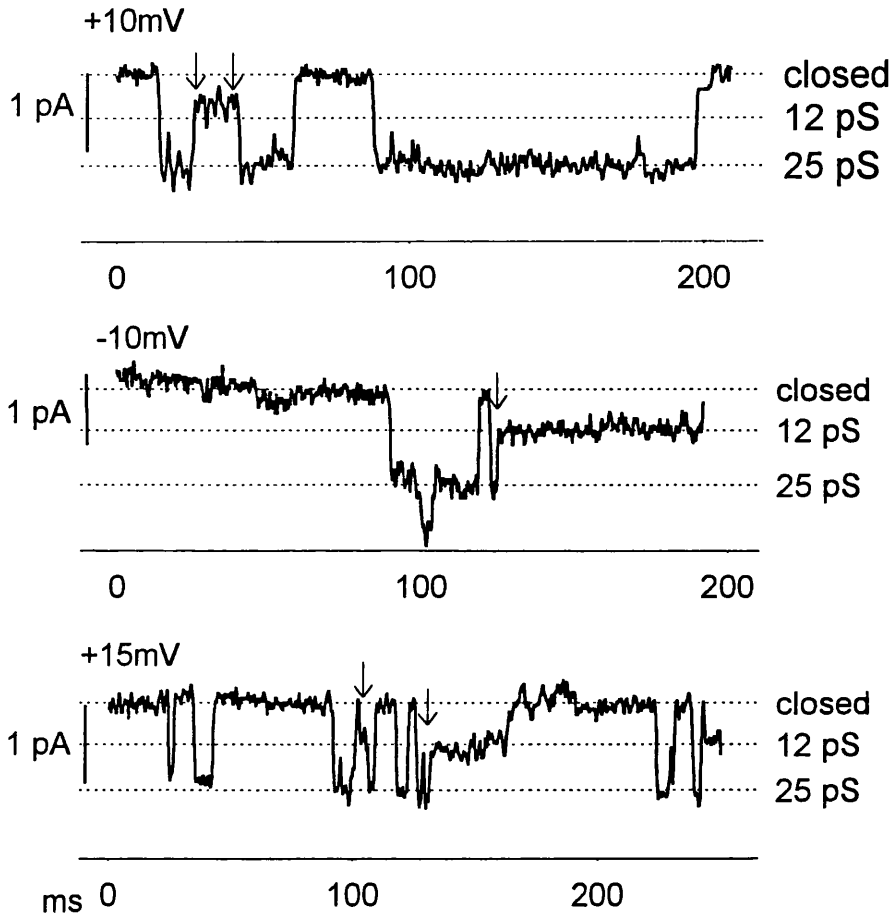
+10mV
1 pA
closed
12 pS
25 pS
0
100
200
-10mV
1 pA
closed
12 pS
25 pS
0
100
200
+15mV
1 pA
closed
12 pS
25 pS
ms 0
100
200

4.2 DISTRIBUTION OF L CHANNELS ON GROWTH CONES

Imaging of the calcium influx into growth cones after L channel activation revealed that calcium rises in a characteristic pattern. There are spatially localised hotspots and a distal to proximal gradient. In the following experiments I tested whether this pattern was reflected by an appropriate distribution of L channel activity on the growth cone membrane using again the patch clamp technique in the cell attached mode. To maximise L channel open probability, these experiments were performed in the presence of 5 µM of BAYK 8644, the holding potential was -40 mV, and cells were depolarised to +10 mV. An example for a patch with a high channel activity is shown in Figure 4.10. Individual 25 pS openings were always clear, allowing the channels to be unequivocally identified as L type. One problem especially in patches with many channels was, that it is not directly possible to determine the number of channels (N) or their open probability (P_o) (see below). However, $N \cdot P_o$, the product of the number of channels in a patch and their open probability could be measured easily. This value is the average number of channels open at any one time and can be used to compare L channel activity between patches.

L channels activity is not randomly distributed, but higher at the tip

The mean N•Po in randomly placed patches over the whole growth cone was 0.061. The spread of values was, however, large. The continuous line in Figure 4.11 shows the cumulative distribution of N•Po of this experiment. 27 of 60 patches contained no channel activity (during recordings of 60 sec), and the largest value was 0.63. Looking at these data, it appeared that channel activity is not spread evenly over the membrane but

concentrated in clusters. To subject this distribution to a statistical test, I assumed that Po (= 0.011) is the same in all patches, and as explained below there are reasons to believe that. Taking a mean channel number of 5.56 I then compared the distribution from the experiment of 60 patches with a random or Poisson distribution (dashed line in Figure 4.11). To record nearly 50% (27/60) zero channel patches would be an extremely unlikely occurrence, if channels followed a Poisson distribution ($p<0.001$, χ^2 test; making the null hypothesis, that channels are distributed without any spatial organisation, very unlikely). I then investigated whether there was a distal to proximal gradient of channel activity on these club shaped growth cones. To do this I compared recordings from patches at the distal tip (within 4 µM of the tip) or more proximally (11 to 22 µm from the tip). N•Po from 36 patches at the tip of the growth cone was 0.0916 ± 0.027. This value was significantly greater than N•Po from 24 more proximal patches (0.0154 ± 0.0067) ($p<0.01$, t-test) (Figure 4.12). Thus the larger calcium current flows through the membrane at the tip, where $[Ca^{2+}]_i$ changes in imaging experiments were largest.

Is the higher N•Po at the tip due to more channels or a higher Po?

Theoretically, a larger N•Po could be caused by a higher channel number or an increase in the single channel open probability. How is it possible to differentiate between these two possibilities? The simplest way of estimating the channel number in a patch is to observe the number of simultaneous openings. Figure 4.10 shows a patch with a high N•Po of 0.503, but a maximum number of only 4 simultaneous openings. Although this approach clearly gives the minimum number of channels it is not suitable in estimating the total number, when Po is small and N high, as it becomes increasingly unlikely that all channels will open at the same time.

Figure 4.10

Individual traces from a growth cone patch that showed a high current. The maximum number of L channels simultaneously open was 4. Over a total of 12 seconds at +10 mV the average number of open channels at any one time (N•Po) was 0.53. The patch was held at -40 mV and depolarised to +10 mV starting at 0 ms in the presence of 5 μM BAYK8644.

Figure 4.10

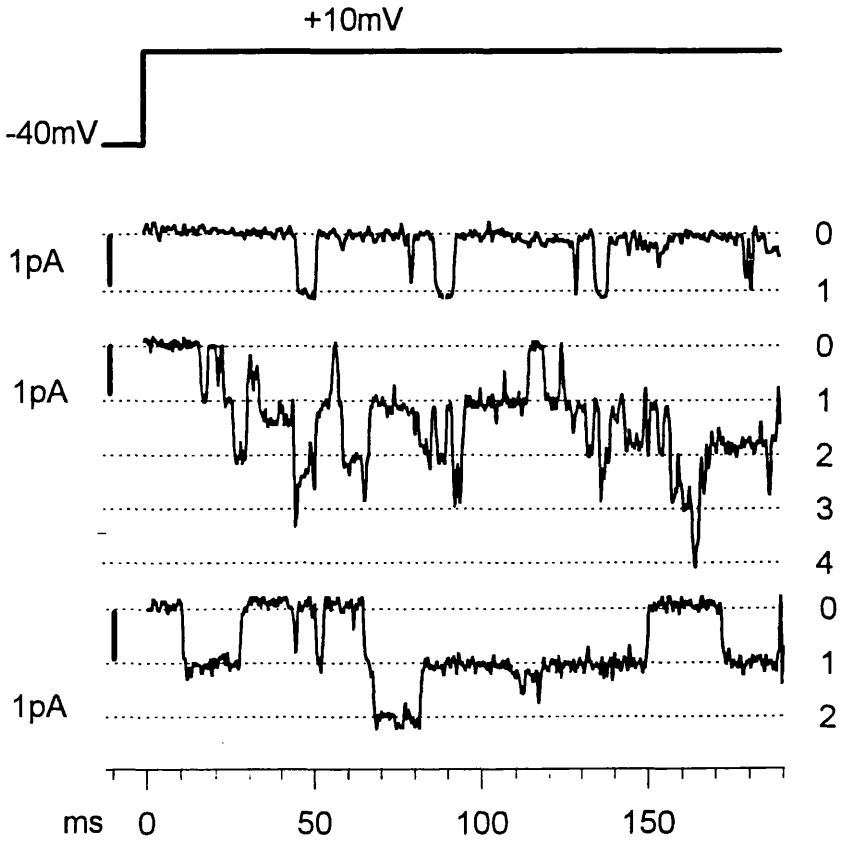

Figure 4.11

Cumulative distribution of N•Po values of 60 growth cone patches. (Continuous curve). Patches showed a wide range of L channel current values (N•Po). 27 patches had no L channels while N•Po in the most active patch was 0.63. Dashed line: Cumulative frequenct distribution predicted from a Poisson distribution of mean 5.56 channels per patch, each with a Po of 0.011. In order to perform a simple significance test, I considered the measured number of zero-channel patches: 27 in 60. Such a sample would be extremely unlikely if only 0.4% of all possible patches had no channels, as predicted by the Poisson distribution ($p<0.001$, χ^2 test.) This indicates that L channels are organised in clusters.

Figure 4.11

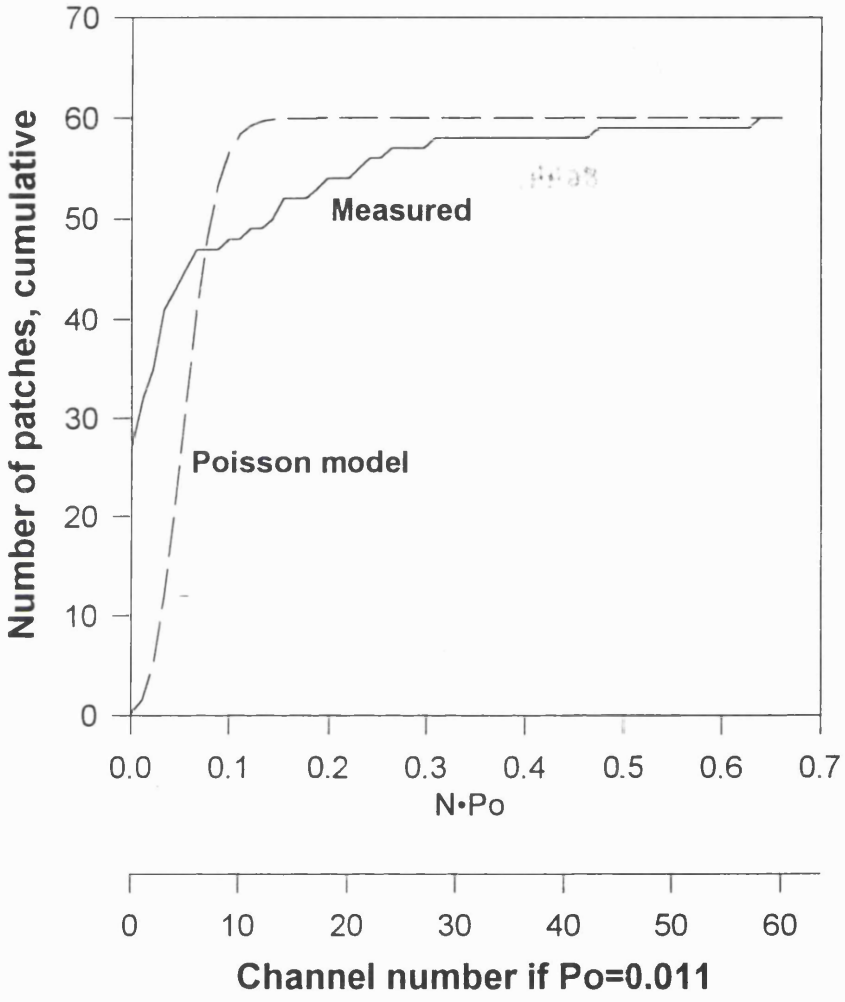
Number of patches, cumulative
70
60
50
40
30
20
10
0
Measured
Poisson model
0.0
0.1
0.2
0.3
0.4
0.5
0.6
0.7
N•Po
0
10
20
30
40
50
60
Channel number if Po=0.011

Figure 4.12

Patches from the distal tip have a markedly higher L channel current than more proximal patches. Left hand bar: Mean N•Po for 36 patches located within 4 µm within the the distal tip was 0.0916 ± 0.027. Right hand bar: Mean N•Po for 24 patches located 11 to 22 µm from the distal tip was 0.0154 ± 0.0067. The difference between these values was significant ($p<0.01$, t-test). All measurements were done at +10 mV in the presence of 5 µM BAYK.8644.

Figure 4.12

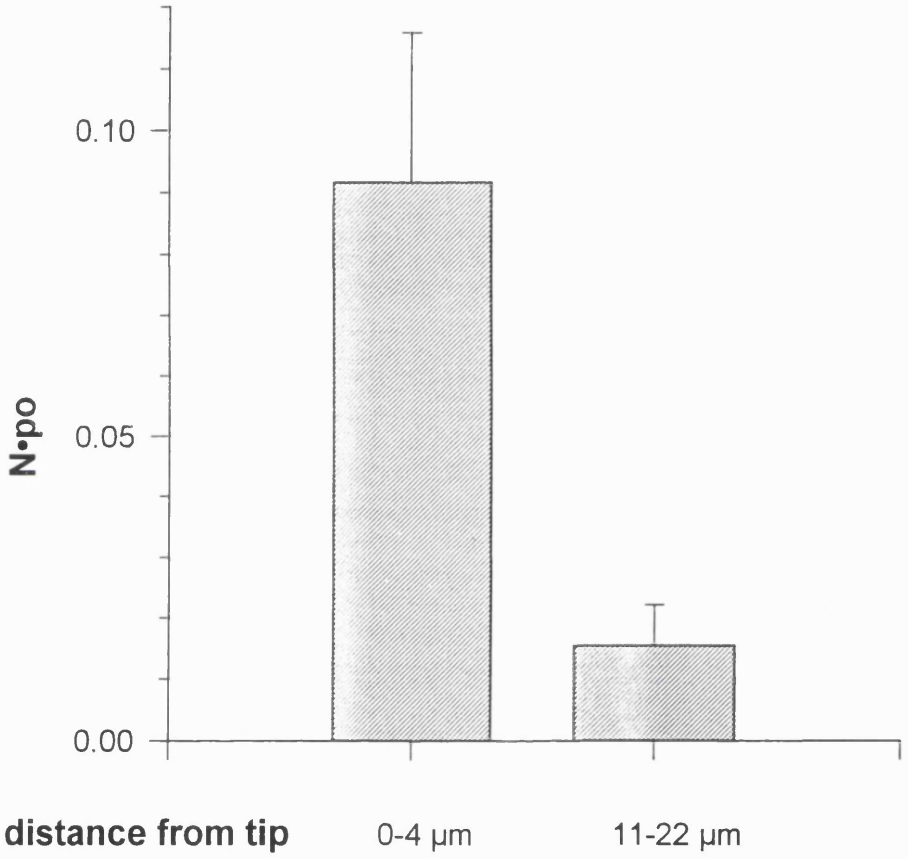

To test the reliability of this method for L channels, I summed 98 consecutive 290 ms episodes of a patch that contained one L channel (Po = 0.01). This sum trace was therefore equivalent to a model patch of 98 channels, each with a Po of 0.01 and a total N•Po of 0.98, yet it only showed a maximum of three simultaneous openings. Given the possibility that Po remains low in patches with a high N•Po, this method is therefore not a reliable indicator of the true channels number. Another commonly used statistical method to estimate the number of channels in multi-channel patches is the Maximum Likelihood Estimate (MLE) (Horn, 1991). This test assumes that channel openings are independent from each other and that the numbers of channels that open simultaneously at any one time are binomially distributed. This means in a patch with N channels the probability of recording at random 0, 1 , 2 channels, ... k channels ... or all N channels open at the same time can be evaluated by using the formula of the binomial distribution:

$$(N!/[k!(N-k)!]\ )\ Po^{N}\ (1-Po\ )^{N-k}$$

In a recording with unknown N but an observed maximum of m simultaneous openings, one can tabulate the frequency of samples where 0,1,2....k.... or m channels were open and, according to the above formula, calculate the probability that the recorded distribution would have been observed if m, m+1, m+2 .... channels had been in the patch. The probability curve should reach its maximum at N. However, the drawback of this test is that it can become problematic if Po is small (Horn, 1991). When I applied the MLE test to the model 98 channel patch it predicted that only 5 channels were present, a clear error.

Despite the failure of the statistical tests to give a clear answer, it seems unlikely that the higher current at the tip resulted from a locally high Po for the following reasons:

1) Five possible one channel patches (see Methods for definition) from the tip showed a Po of 0.010 ± 0.004, not different from the Po in the four possible one channel patches from the proximal growth cone (0.011 ± 0.005). In addition both probable one channels patches were from the tip and gave normal Po values (0.011 and 0.024). (Figure 4.13). The finding that N•Po is larger at the tip therefore indicates that N is on average higher, that is the density of L type calcium channels is higher at the tip.

2) Another indication comes from the distribution of patches without any channels. At the tip 13 of 36 that is 36% of patches contained no channels whereas 14 of 24 or 58% of patches at proximal regions showed no channel activity. Although the p value from a χ^2 test was between 10% and 5% the result is consistent with the view that the channel density is higher at the tip.

Figure 4.13

The single channel open probability of L channels was very similar in patches at the tip and in more proximal patches. (At depolarisations to +10 mV) This indicates that higher N•Po in some patches is due to higher channel numbers. Circles are Po of individual L channels from possible or probable one channel patches within 4 µm of the tip (left hand column) or 11-22 µm away from the tip (right hand column). Horizontal bars indicate the average values and sem's: tip: 0.010 ± 0.004 (n=5); proximal: 0.011± 0.005 (n=4).

Figure 4.13

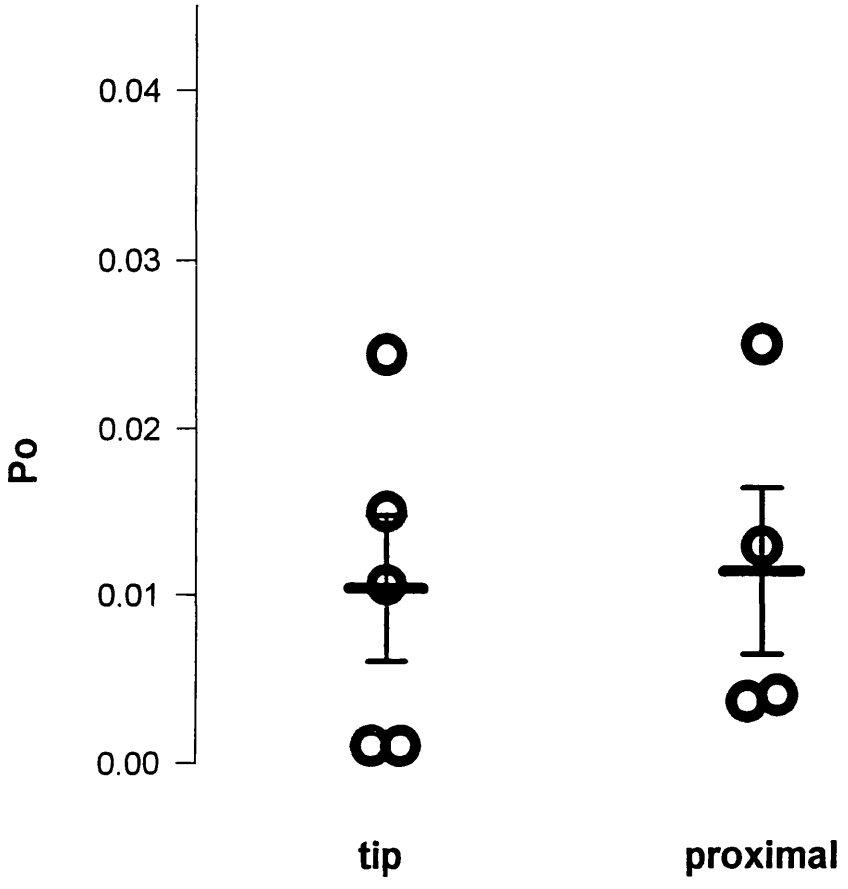

APPENDIX TO CHAPTER 4:

THE FRACTAL MODEL OF CHANNEL KINETICS

Introduction

The patch clamp technique allows the detection of open and closed states of ion channels but it is not possible to differentiate between conformational states that the channel protein might assume during either the open or the closed condition. However, the distribution of open or closed time durations can be used to extract information about such electrically indistinguishable states. The generally used Markov model of channel behaviour assumes that there is a small number of discrete conformational states in which a channel protein could be (Colquhoun, 1983). The transition probability - that is the probability that the protein will leave this conformational state - is described by a single exponential decay with a fixed time constant. The Markov model predicts that if there are n conformational states (within the open or closed state) the open or closed time distribution will be the sum of n exponential decays. This means that the number of rate constants will mirror the number of conformational states of the protein. However, the kinetics of some channels are only inadequately described by such a model. For instance, the number of exponentials that are needed to best fit the closed time distribution of inwardly rectifying potassium channels or calcium activated potassium channels is dependent on the sampling rate (Liebovitch & Sullivan, 1987; French & Stockbridge, 1988). That is with a better temporal time resolution of the recording an unexpectedly higher number of very short closings can be resolved and to account for them new shorter time constants have to be added to fit the closed time distribution curve. In fact this observation

continued as far as technical limitations allowed to increase the time resolution.

Liebovitch et al. (1987) proposed a new model of channel kinetics which is based on Mandelbrot's concept of fractal geometry. The underlying assumption to the fractal model of channel kinetics is that the channel protein can exist in a very large number or even in a continuum of conformational states rather than in a few discrete ones. The hypothesis is that the energy barriers that separate these states and accordingly the transition rates for leaving them will show a very wide continuous distribution ranging from picosecond events such as rotation around bonds to longer events lasting minutes such as ligand binding and protein unfolding. In the analysis of channel records only those rate constants will be picked up that fall within the range of the timescale employed. In Liebovitch's model the effective kinetic rate constant of leaving the open or closed state is not a constant but dependent on - that is a regular and predictable function of - the time scale. This is the essential idea of fractal geometry that a measured value can be dependent on the measuring scale in a regular mathematical relationship. Benoit Mandelbrot illustrated this originally by showing that the length of the coastline of Britain is not a meaningful value (Mandelbrot, 1967). As the measurement is done on maps with a finer scale more details are resolved and the length of the coastline becomes longer. However he also showed that this increase in length was not unpredictable but linearly proportional to a power of the scale in the form of:

$$\text{length} = (\text{constant}) \cdot (\text{scale})^{(\text{Eucledian dimension} - d)} .$$

The Eucledian or topological dimension for a line is 1. The constant d is a measure for the convolutedness of the coastline and closely linked to the concept of dimension. For a straight line the length does not vary with the

precision of the measurement and d equals 1. A convoluted line has in a certain respect a higher dimension than a straight line because it fills a two dimensional space more than the straight line. The exponential d - the fractal dimension - expresses this idea. For a convoluted line it becomes a non integer value between 1 and 2 (in the case of the west coast of Britain 1.25). In recent years a large number of processes were discovered to exhibit fractal behaviour. A few examples are the perimeters of clouds, intensity of earthquakes, the branching pattern of ferns and other plants, the branching pattern of the bronchial tree or of vessels in the retina (Goldberger et al., 1990; Daxer, 1993).

According to the fractal model of channel kinetics the effective kinetic rate constant for leaving the open or closed state is given by:

$$k_{eff\ (t_{eff})} = A \cdot t_{eff}^{\ (1-d)}$$

The term t_{eff} is the effective timescale and A is a constant. In the exponential the figure 1 is the value for the topological dimension because the process takes place in the one dimensional space of time and d is the fractal dimension of channel opening or closing. One way to test whether a channel follows Markov or fractal kinetics is to plot the rate constants that can be appropriately assessed at certain time scales against these time scales in a double logarithmic plot. A channel with a two state Markov behaviour will show two distinct plateaus in regions where the timescales match the rate constants for the two discrete Markov states. (Figure 4.14a). If the channel however exhibits fractal behaviour the plot will show no plateaus but be linear with the slope of (1-d).

L channel open times do not show fixed transition rates

I analysed the kinetic behaviour of L-type channels in three patches (Two from growth cones and one from the cell body). Patches were held at

-40 mV and depolarised to +10 mV. These experiments were performed in the presence of 5 µM BayK 8644. Original data were sampled at a frequency of 1 kHz. Judging from infrequent simultaneous openings there were at least two channels in all patches. It was therefore not possible to measure closed times and the analysis was restricted to channel openings. To construct diagrams of kinetic rate constants against time scales, I followed the procedure described by Liebovitch et al. (1987). Open time durations were binned in either 0.5, 1, 2, 4, 8, 16 or 32 ms intervals and frequency histograms constructed. In each diagram the binwidth determined the effective timescale. Only the second to the fifth bin were used to fit single exponential curves. (The first and the higher bins had to be excluded because they included events that were much shorter or longer than the effective timescale). The rate constant for leaving the open state was then evaluated by taking the inverse of the time constants of the fitted exponentials. These data were plotted on a double logarithmic scale (Figure 4.14b). As can be seen, the rate constants in all three experiments were then linearly dependent on the effective timescales without showing plateaus. The slopes of fitted lines were -0.52, -0.5123 and -0.65; The correlation coefficients were 0.97, 0.99 and 0.93. To compare these results with a two state Markov model, I simulated an open time histogram using two time constants of 1.7 ms and 12 ms, the values I report in section 4.1.2. As for the real patches, I binned the data as above and fitted single exponentials. In contrast to the three real patches, the double logarithmic plot clearly shows two plateaus corresponding to the time constants. (Figure 4.14a). These data indicate that L channel open times over the timescale investigated - 0.5 to 32 ms - do not show discrete Markov behaviour.

Figure 4.14

Markov and fractal behaviour of L channel openings. Both diagrams are double logarithmic plots of the open time rate constants versus the effective timescale. Rate constants were evaluated by plotting a single exponential curve from the second to fifth bin of an open time distribution (such as figure 5.6). The binwidth determined the effective timescale. **a)**: This plot was constructed from a simulated open time distribution which was created using two time constants of 1.7ms and 12.0 ms In agreement with a two state Markov model this plot shows two plateaus in the range of the timeconstants used. **b)**: Plots from three "real" L channel patches show no such plateaus. In contrast there is a linear dependence of the rate constants on the effective timescales over the whole range investigated. The slopes of fitted lines were -0.52, -0.5123 and -0.65. Correl ation coefficients were 0.97, 0.99 and 0.93.

Figure 4.14

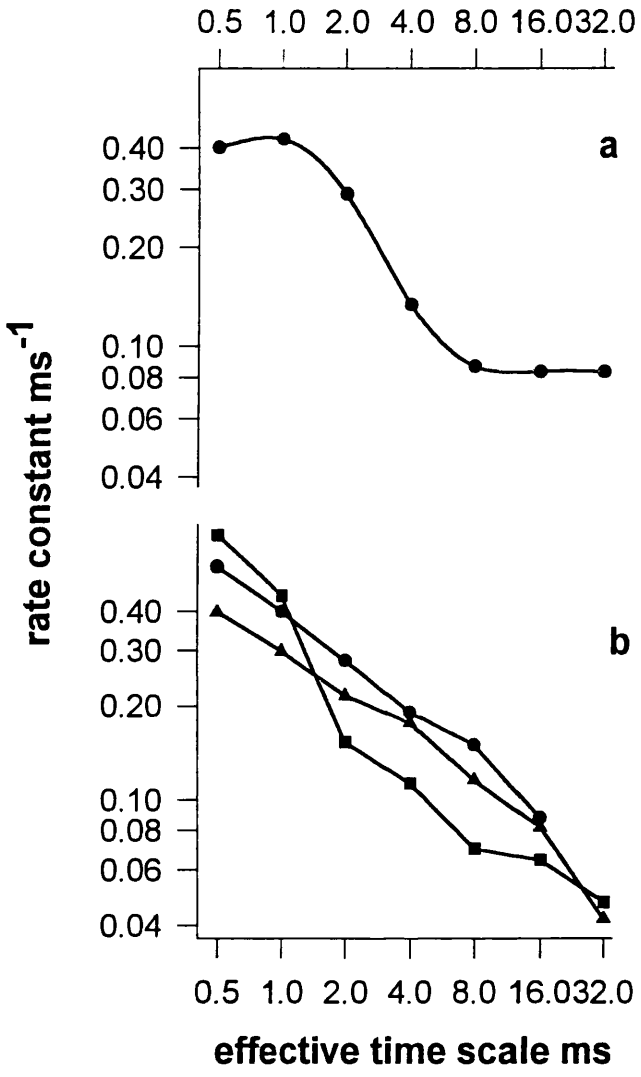
0.5 1.0 2.0 4.0 8.0 16.032.0
0.40
0.30
0.20
0.10
0.08
0.06
0.04
a
b
rate constant ms-1
effective time scale ms

Discussion of the fractal model

Figure 4.6 shows that the open time distribution with binning intervals of 0.5 ms can be reasonably well fit with two exponentials. In 4 experiments the average of these time constants were 1.7 ± 0.2 ms and 12.0 ± 1.8 ms. This is in good agreement with values other investigators report of L channels (Hess et al., 1984; Wang et al., 1993) but different from other authors (Ono & Fozzard, 1992). Hess et al. (1984) attributed the existence of these two time constants to two different gating states the open L channel could assume. A short lasting mode 1 opening with a high transition rate and a longer lasting mode 2 opening that was found to be promoted by dihydropyridine agonists. These "conventional" open time distributions for L channels are performed using binwidth of around 0.5 ms. Although the two exponentials describe the decay of the open time curve reasonably well for practical purposes, I noticed that the values of the timeconstants varied a lot when different binwidths (eg 0.5 ms versus 1 ms) were used.

When I fitted one exponential at a wider range of timescales to the bins in the range of the timescales a more complicated picture emerged. If the kinetics followed a true two state Markov model one would expect two plateaus in a double logarithmic plot of time scale versus time constants as simulated in Figure 4.14a. However in three patches investigated I observed a linear relationship. This means that there were not two discrete transition rates but apparently a different one at each timescale. The fractal model fits these data better then a two state Markov model. Thus the corresponding physiological explanation that the protein can exist in a continuum of states, is a better model of the real protein than the conventional model in which the protein exists in a small number of discrete states.

CHAPTER 5

DISCUSSION OF CALCIUM CHANNELS ON GROWTH CONES AND THEIR DISTRIBUTION

5.1 IDENTIFICATION AND PROPERTIES OF CALCIUM CHANNELS ON GROWTH CONES

In the present study of cell attached recordings from N1E-115 neuroblastoma cells I found T and L type calcium channels on patches of growth cone membranes. The same two channel types have recently been demonstrated in single channel recordings from the cell body of these cells which confirmed indications from whole cell voltage clamp experiments that N1E-115 cells express both T and L type calcium channels (Narahashi et al., 1987; Shuba et al., 1991; Herman et al., 1993). My findings are also in line with the view that calcium channels are expressed on growth cones of developing neurons (Streit & Lux, 1989; Gottmann & Lux, 1990; Silver et al., 1990; Reber & Reuter, 1991; Vigers & Pfenninger, 1991; Przywara et al., 1993) and represent the first characterisation of calcium channels on a single channel level in mammalian growth cones. As Lipscombe et al. (1988) who studied the single channel conductance of HVA channels of frog sympathetic neurons on the cell body and on the growth cones I could also find no obvious difference in the channel properties betweeen these two locations. Although one study using a whole cell voltage clamping technique, spatially restricted to either the cell body or the growth cone, reported a faster inactivation of the HVA calcium current in growth cones of PC12 cells (Streit & Lux, 1989), the current carried by barium ions through

single L channels in my experiments shows, in contrast, equal slow inactivation at both locations.

All T channel characteristics investigated here, the low inactivation threshold, the single channel conductance of 7.5 pS and the rapid inactivation are very similar to reports by Shuba et al. (1991) who studied T channels on the cell body of N1E-115 cells and also very similar to findings from other neuronal cells (Nowycky et al., 1985; Fox et al., 1987; Fisher et al., 1990) which underlines the view that the T channel group is very homogenous.

L type calcium channels in this study were identified by their sensitivity to dihydropyridines. I describe a number of their single channel properties here, such as a single channel conductance of 25 pS, a high voltage requirement for activation, open time constants and the slow inactivation kinetics. These results extend the findings of Herman et al. (1993) who studied L channels on patches of the cell body of N1E-115 cells. Moreover, these characteristics are similar to those found for L channels in many other preparations and match the classical neuronal or cardiac L type channel description (Hess et al., 1984; Fox et al., 1987; Plummer et al., 1989; Fisher et al., 1990; McCarthy & TanPiengco, 1992; Morton et al., 1992; Forti & Pietrobon, 1993; Wang et al., 1993; Griffith et al., 1994). Some recently described variations of L channels in cerebellar granule cells which were characterised by their increased tendency to open at negative potentials after a predepolarisation could not be observed in N1E-115 cells (Forti & Pietrobon, 1993).

However two unusal observations deserve special mention. The value for the mean single channel open probability even in the presence of 5 µM of the dihydropyridine agonist BAYK 8644 was very low at 0.011+0.003. Although low this is not outside the range found in other preparations

(Plummer et al., 1989; Ono & Fozzard, 1992; Forti & Pietrobon, 1993; Wang et al., 1993). However, most other authors put the single channel open probability in the presence of dihydropyridine agonists higher at between 0.1 and 0.2 (Fox et al., 1987; Morton et al., 1992; Griffith et al., 1994). Which factors determine the open probabilities of L channels? Modulation of the C terminal tail of the α_1-subunit, possibly by phosphorylation, seems to be one mechanism that controls the open probability. (Wei et al., 1994) Another possibility that explains variability in Po is the expression of different isoforms that constitutively vary in that property. For instance, Forti et al., (1993) describe two L channel isoforms, both expressed in the same cerebellar granule cells, that differ considerably in their Po. It is not clear whether such differences in Po have a significance in the regulation of calcium signalling during development. However, one interesting observation in this context is that in many neurons the high voltage activated calcium current increases with time during development (McCobb et al., 1989; Mynlieff & Beam, 1992). The neuroblastoma cells in this study have not completed their electrophysiological maturation (Cosgrove & Cobbett, 1991), it might therefore be an interesting question whether a low Po is a specific feature of developing neurons and whether it increases with further maturation.

The second unusual observation was the frequent occurence of L channel subconductance states. These were openings of lower amplitude that were indistinguishable from full L channel openings in every respect apart from the lower conductance of around 12 pS. The detection of several direct transitions between the 25pS and the 12 pS open states, without intervening closings, leave no doubt that the lower openings are indeed L channel subconductance states. As far as I am aware, there have been no other similar observations of L channel subconductance states in native

membranes on intact cells apart from one report in a pituitary cell line (Kunze & Ritchie, 1990). Interestingly subconductance states are regularly seen in reconstitution experiments at a time when L channels are inserted and assemble in the artificial membrane (Hymel et al., 1988). Such experiments would therefore suggest that subconductance states are a phenomenon of newly expressed channels or of channels in transformed cell lines, both conditions in which maybe the correct subunit composition has not been established fully .

Finally, it can not be excluded that some techniqual artefacts are responsible for both the low open probability and the occurence of subconductance states. For example, sucking of the membrane in the patch pipette could break connections between the channels and the cytoskeleton. Such a disconnection causes inactivation in molluscan neurons, and one could evoke a similar mechanism to explain the above phenomena (Johnson & Byerly, 1993).

5.2 CALCIUM CHANNELS ARE CLUSTERED AT THE TIP OF GROWTH CONES

In the investigation of the distribution of L type calcium channels I restricted the sample to unbranched, club shaped growth cones. Growth cones of such simple shape usually advance straight along the neurite axis and do not turn or send off branches as growth cones of more complex shape do (Silver et al., 1990; Soekarno et al., 1993). In such simple growth cones I noticed a tendency for L channels to show in their distribution a distinct pattern. Channels occured in clusters at the tip of growth cones to produce, on electrical activation, a distal to proximal gradient of cytosolic calcium

rise. Depolarisation caused calcium in growth cones to rise principally in spatially restricted hotspots. Silver et al., (1990) found these hotspots mainly at the base of newly extending processes from complex shaped growth cones, I found hotspots at the leading edge of clubshaped growth cones. Common to both studies is that hotspots were localised at sites of presumptive outgrowth. One possible source for large cytoplasmic calcium increases in most cells is the mechanism callled calcium induced calcium release (CICR) in which cytoplasmic calcium ions act in a positive feedback loop (Berridge, (1993; Simpson et al., 1995). Bandtlow et al. (1993) suggested that the large calcium rises that are associated with growth cone collapse in dorsal root ganglion cells stem mainly from a ryanodine receptor based CICR. Such a mechanism is however very unlikely to contribute to the calcium changes seen in my experiments as two potent blockers of CICR, dantrolene and ryanodine, did not affect the calcium dynamics in any way. This view is in line with results from Reber et al. (1991) who report that calcium stores are of minor importance in growth cones of PC12 cells.

In contrast, the distribution of individual calcium channels matches the pattern of cytosolic calcium rise very well. Near to the tip on average 8.3 channels were in a patch whereas further behind only 1.4 channels were found per patch. It is therefore a much more plausible explanation that the distal to proximal gradient of $[Ca^{2+}]_i$ is a direct result of the distribution of individual channels on the plasmalemma.

Functional significance of channel distribution.

Many studies have shown that developing and also regenerating neurons are electrically active. (Wall & Gutnick, 1974; Schilling et al., 1991; Gu et al., 1994; O'Donovan et al., 1994). As demonstrated here activation of

calcium channels, clustered at the tip, results in a calcium concentration gradient. Such a spatial regulation of calcium changes is ideally suited for differential signalling. Support for a significance on developmental processes, such as neurite elongation and guidance, comes from the fact that the highest calcium changes were seen at sites of future outgrowth, in my studies and also in observations by Silver et al. (1990) , Davenport et al. (1992) and Bedlack et al. (1992). Another possible function for channel clusters in developing neurons could consist in the role of calcium in transmitter release. It is well known that in presynaptic terminals of neurons calcium channels are clustered to produce large calcium changes around vesicles and two recent papers have directly demonstrated that such preysynaptic clusters give rise to local hotspots of cytosolic calcium (Issa & Hudspeth, 1994; Bokvist et al., 1995). My experiments present clear evidence that calcium channel clusters already occur in growth cones of developing neurons before they have made contact with postsynaptic membrane. The formation of clusters could be seen as a prepartion for the eventual transformation of a growth cone into a presynaptic terminal, alternatively, it would also be consistent with the finding that neurotransmitters are already released from outgrowing neurons, presumably to transmit signals into the enviroment (Sun & Poo, 1987; Przywara et al., 1993). The mechanisms that induce channel clustering are unknown although Froehner (1993) emphasised the role of extracellular matrix molecules secreted by the postsynaptic cells. The early formation of clusters before synaptogenesis indicates that mechanisms in the neuron itself are sufficient.

CHAPTER 6

THE EFFECT OF MAINTAINED CALCIUM CONCENTRATIONS ON NEURITE OUTGROWTH IN NEUROBLASTOMA CELLS

The experiments of the last chapters investigated mechanisms of how calcium ions enter the cytoplasm. The emphasis lay on spatial considerations of transient calcium signals. In contrast, this chapter is concerned with the influence of maintained calcium levels on the regulation of some calcium dependent process. Such steady state calcium changes are very likely to occur during nerve cell development for example due to changes in calcium buffering capacity (Hendrickson et al., 1991) or because of changes in the expression of calcium channels (Gu & Spitzer, 1993).

6.1 THE DEPENDENCY OF NEURITE OUTGROWTH ON $[Ca^{2+}]_i$

One process that has been suggested to depend on the intracellular calcium concentration $[Ca^{2+}]_i$ has been the expression and prolongation of neurites (Mattson & Kater, 1987). In the following experiments I tested whether this hypothesis applied to neuroblastoma cells by measuring parameters of neurite outgrowth at various cytosolic calcium concentrations that were maintained over the whole experimental period of several days. To quantify the effectiveness of neurite outgrowth, I measured two aspects of this process. The initiation of new neurites, as percentage of cells expressing neurites, and the length of the longest established neurite. To set $[Ca^{2+}]_i$ at a range of levels, I chose an indirect

approach, by altering the extracellular calcium concentration $[Ca^{2+}]_o$. I achieved an extracellular calcium concentration $[Ca^{2+}]_o$ ranging from 0.4 mM through the normal value of 1.9 mM to 41 mM by adding either up to 1.5 mM of the calcium chelator BAPTA or up to 40 mM additional calcium chloride to the culture medium. Such variations in $[Ca^{2+}]_o$ did not affect the adhesion of cells to the polylysine substrate. This observation is consistent with findings by Yavin & Yavin, (1974) that adhesion to polylysine does not require divalent cations. However, to rule out other possible unspecific effects due to low divalent cation concentrations, I performed some of the experiments in a high extracellular magnesium concentration of 21 mM. Also, alterations in $[Ca^{2+}]_o$ had no discernible effect on the morphological appearance of neurites and growth cones (Figure 6.1 a,d,g) Cells grown in either increased or decreased $[Ca^{2+}]_o$ showed a normal distribution of cytoskeletal proteins with tubulin in the neurite shaft (Figure 6.1 b,e,h,) and actin located at motile structures at the growth cones or along the neurites (Figure 6.1 c,f,i). Very low $[Ca^{2+}]_o$ however, induced by BAPTA concentrations in excess of 2 mM, caused a significant number of N1E-115 cells to die. Cultures with such a low calcium concentration were not used in further experiments.

Effects of $[Ca^{2+}]_o$ on $[Ca^{2+}]_i$

Neuroblastoma cells grown at various $[Ca^{2+}]_o$ were loaded with the calcium indicator dye Fura-2 AM, and the fluorescence signal measured over the whole cell body. Having performed the calibration experiments for Fura-2 in chapter 2 I could now transform the ratio I_{350}/I_{380} to a calcium concentration. When increasing $[Ca^{2+}]_o$, the concentrations of cytosolic calcium rose monotonically with increasing extracellular concentrations (Figure 6.2). The average intracellular levels achieved ranged from 35

Figure 6.1

Photomicrographs of N1E-115 cells grown in medium containing 0.4 mM free calcium (a,b,c), 1.9 mM free calcium (d,e,f) and 21.9 mM free calcium (g,h,i). **a,d,g**: phase contrast images of neurite-bearing cells. Calibration bar in a is 30 µm. **b,e,h**: tubulin immunofluorescence of the same regions. **c,f,i**: actin revealed by rhodamine-phalloidin fluorescence.

Neurite shafts, indicated by arrowheads, stained strongly for tubulin, indicating that these neurites have the microtubule lattice typical of extending neurites (Gordon-Weeks & Mansfield, 1992). Actin was confined to the tips of growth cones (indicated by asterisks) or to discrete fans (Bolsover et al., 1992) on the neurite shaft. I observed no consistent differences in morphology or cytoskeleton organization at different $[Ca^{2+}]_o$ in that fraction of cells that did extend neurites.

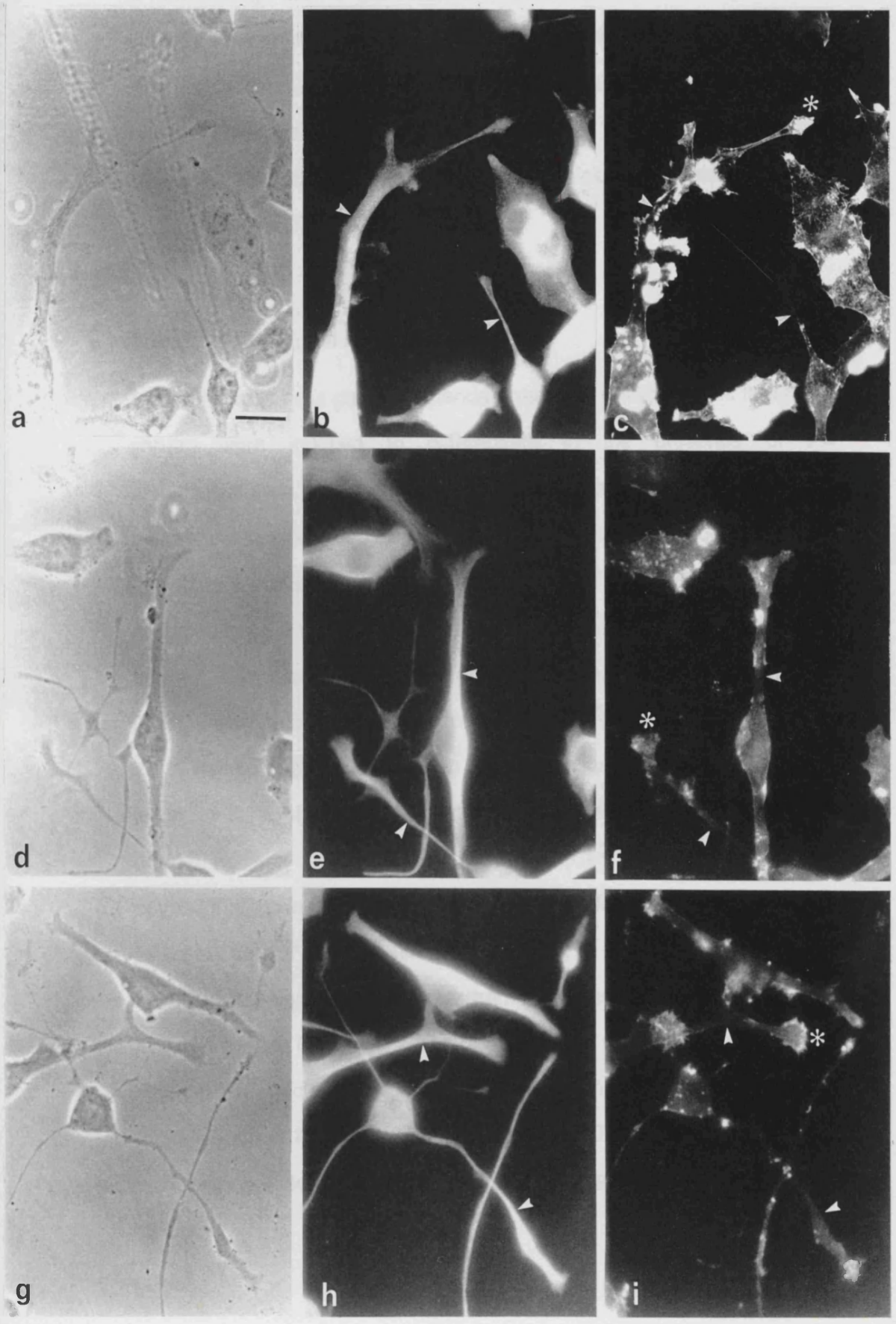
a
b
c
d
e
f
g
h
i

± 1 nM through the normal value of 108 ± 2 nM to 254 ± 4 nM. In those cultures where magnesium was added the cytosolic calcium concentration was slightly lower ranging from 21 ± 2 nM to 217 ± 20 nM (Figure 6.2). The fact that $[Ca^{2+}]_i$ is lower in the presence of Mg^{2+} is consistent with a well known blocking effect of magnesium ions on calcium channels (Fukushima & Hagiwara, 1985).

Effects of $[Ca^{2+}]_o$ on neurite outgrowth

Neuroblastoma cells plated in standard medium (DMEM +10% foetal calf serum) were induced to differentiate in the presence of 2% dimethylsulfoxide. Under these control conditions with time an increasing number of cells extended neurites. (6 ± 1% of cells at three days in culture and 16 ± 3% after 5 days). The percentage of cells with neurites was assumed to be a measure for neurite initiation. The percentage of neurite bearing cells, measured at three days in culture, was at its lowest when $[Ca^{2+}]_o$ was at 6.9 mM (corresponding to $[Ca^{2+}]_i$ of 132 ± 3 nM). The value was 56 ± 8% of the value in normal medium which was significantly lower, $p<0.1\%$) (Figure 6.3). When $[Ca^{2+}]_o$ was reduced through the normal value of 1.9 mM (corresponding to $[Ca^{2+}]_i$ of 108 ± 2 nM) and beyond that, an increasing number of cells were found to express neurites, so that at a $[Ca^{2+}]_o$ of 0.4 mM (corresponding to $[Ca^{2+}]_i$ of 35 ± 1 nM) the fraction was significantly higher than in normal medium (166 ± 18%, $p<0.1\%$) (Figure 6.3). When 20 mM magnesium was added to the culture medium the effects of low $[Ca^{2+}]_o$ on neurite initiation became dramatic (hollow symbols in Figure 6.3). At a $[Ca^{2+}]_o$ of 0.4 mM the percentage of cells with neurites was almost 7 times higher than in medium with normal calcium.

The above data show that the expression of neurites can be significantly enhanced if the calcium concentration of the bathing medium is reduced from the normal value. One result that came as a surprise, was that the fraction of cells with neurites can also be increased, when $[Ca^{2+}]_o$ was set above the 'low-point' of 6.9 mM. When cells were grown in a $[Ca^{2+}]_o$ of 21.9 mM the fraction of neurite bearing cells was more than 4 times higher than in the control medium. The values were significant for all points above 6.9 mM in media without added magnesium ($p<0.1\%$ except for 11.9 mM for which $p<1\%$, t-test).

Effects of $[Ca^{2+}]_o$ on neurite length

To investigate the effect of $[Ca^{2+}]_o$ on the growth rates of neurites once they have been initiated, I assessed the length of the longest neurite. In cultures with 21 mM magnesium the relationship between neurite length and calcium concentration was very similar to the relationship between neurite initiation and $[Ca^{2+}]_o$.(Figure 6.4).That is at 6.9 mM $[Ca^{2+}]_o$ neurites were shortest, and at both higher and lower calcium levels neurite length increased. However, in cultures without added magnesium any trend in the data was hidden in the noise (Figure 6.4 filled symbols)

Ionophores promote neurite outgrowth

The above experiments showed that changing the concentration of calcium ions in the bathing medium has pronounced effects on the development of neurites. It is likely that this effect was due to corresponding changes in the intracellular calcium concentration at least in conditions of low calcium levels, because Mg^{2+} guarded against unspecific effects of low divalent cations concentrations in extracellular

medium. To determine whether the surprising effects of $[Ca^{2+}]_o$ above 6.9 mM are also due to the increased intracellular calcium ion concentration or rather any unspecific consequence of the high extracellular calcium level, I tried to raise $[Ca^{2+}]_i$ more directly. In the following experiments I exposed cultures with normal $[Ca^{2+}]_o$ for three days to low levels of the calcium ionophore 4-Br-A23187 ranging from 50 nM to 1 µM. Neurite initiation was significantly enhanced in cultures with 0.1 to 0.5 µM of the ionophore compared to untreated control cultures (Figure 6.5a). There were, for instance, nearly 3 times as many cells with neurites when grown in the presence of 0.2 µM of the ionophore.

The increase in neurite length in low levels of the ionophore (0.1 µM) was not statistically significant.

(Figure 6.5b). Interestingly, when measuring Fura-2 AM ratios in cultures with the same low ionophore concentrations, the results showed that $[Ca^{2+}]_i$, averaged over the whole cell body, was not significantly different from control conditions (103 ± 20 nM). In contrast, higher levels of this ionophore (eg 17 µM) caused a large increase in $[Ca^{2+}]_i$ (data not shown) but such ionophore concentrations were not compatible with prolonged cell survival. Even though it is unclear why low levels of the ionophore failed to elevate $[Ca^{2+}]_i$ measurably over the whole cell, it could be that calcium only rose in a narrow shell under the cell membrane.

Figure 6.2

Cytosolic calcium concentration measured at the cell body using the ratiometric dye Fura-2 AM at various imposed $[Ca^{2+}]_o$. Filled circles represent experiments where extracellular magnesium was 1 mM and hollow diamonds show experiments where $MgCl_2$ was added to a total of 21 mM. Where error bars (± sem) do not appear they are smaller than the symbols employed. The experiment was performed three times, each point is the mean ± sem of at least 41 cells. The straight lines are best-fit regressions to the data after logarithmic transformation of $[Ca^{2+}]_o$ .The horizontal axis shows $[Ca^{2+}]_o$ on a logarithmic scale. This graph demonstrates that intracellular calcium rises monotonically with increasing extracellular levels.

Figure 6.2

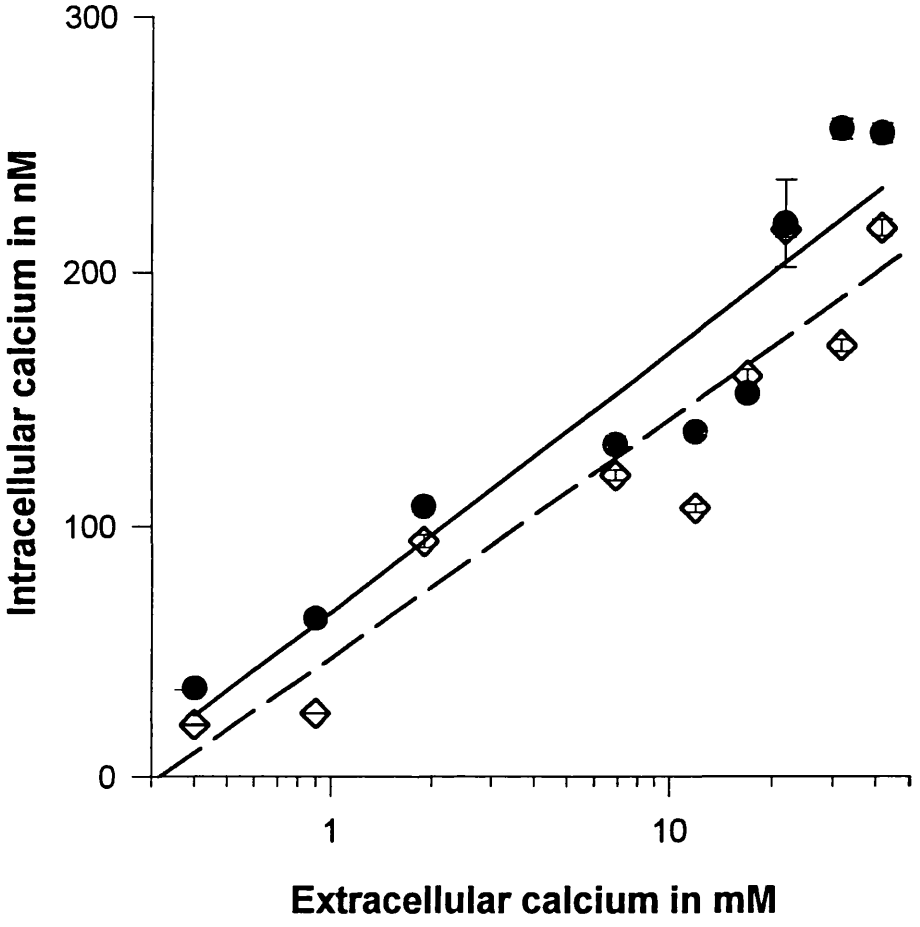
300
200
100
0
Intracellular calcium in nM
1
10
Extracellular calcium in mM

Figure 6.3

The effect of $[Ca2+]_o$ on the expression of neurites: The data presented here are averages from six experiments. In each experiment cells were grown under various $[Ca^{2+}]_o$. After three days in culture the fraction of cells with neurites longer than one cell diameter were counted. 100 to 500 cells were assessed per dish and in each calcium concentration group at least three dishes were counted per experiment. For each experiment the average value in each group was normalised such that the value in the control medium without added calcium became 1. This normalisation was necessary as the absolute percentage of neurite bearing cells varied between the six experiments (between 1 and 16 percent in the control medium). The points plotted in the graph are the mean ± sem of these 6 normalised values. Filled circles show experiments with 1 mM Mg^{2+} in the bath; hollow diamonds with 21 mM Mg^{2+}. Neurite initiation is promoted at low $[Ca^{2+}]_o$, but surprisingly also at $[Ca^{2+}]_o$.above 6.9 mM.

Figure 6.3

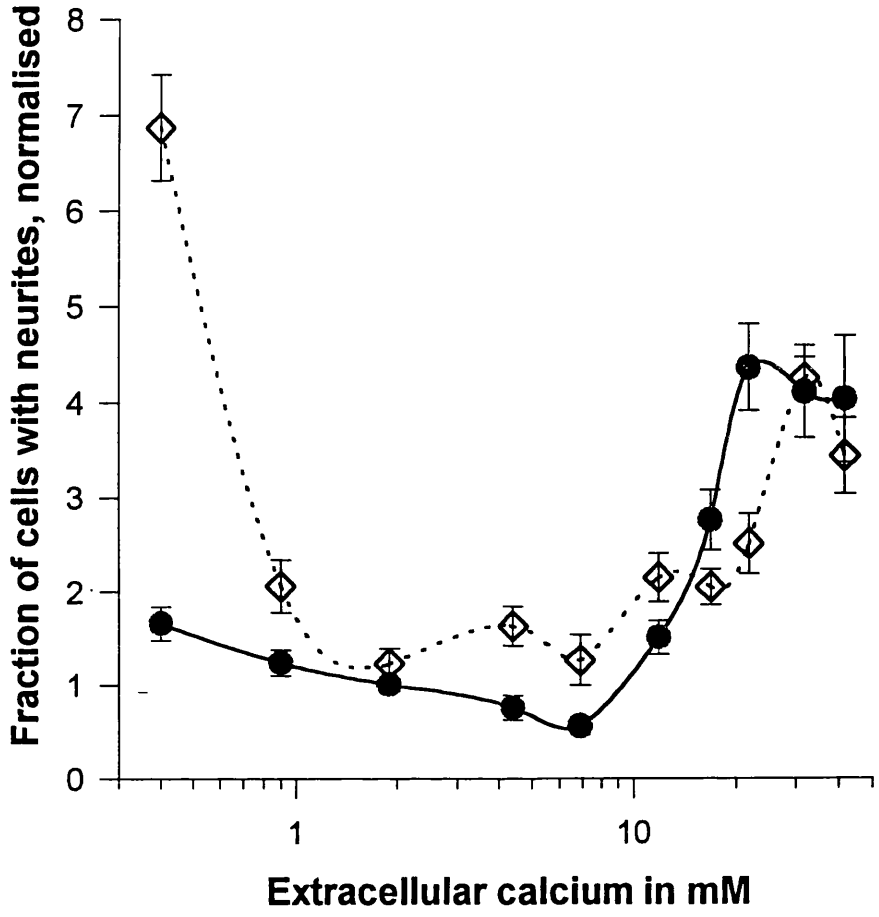
Fraction of cells with neurites, normalised
0
1
2
3
4
5
6
7
8
1
10
Extracellular calcium in mM

Figure 6.4

Length of the longest neurite at different $[Ca^{2+}]_o$ Filled circles represent experiments were extracellular magnesium was 1 mM and hollow diamonds show experiments where $MgCl_2$ was added to a total of 21mM. The experiment was performed six times, each point represents at least 32 (median 71) cells.

In cultures with 21 mM $MgCl_2$ neurite length was increased when $[Ca^{2+}]_o$ was below the normal value and but also when $[Ca^{2+}]_o$ was raised above 6.9 mM.

Figure 6.4

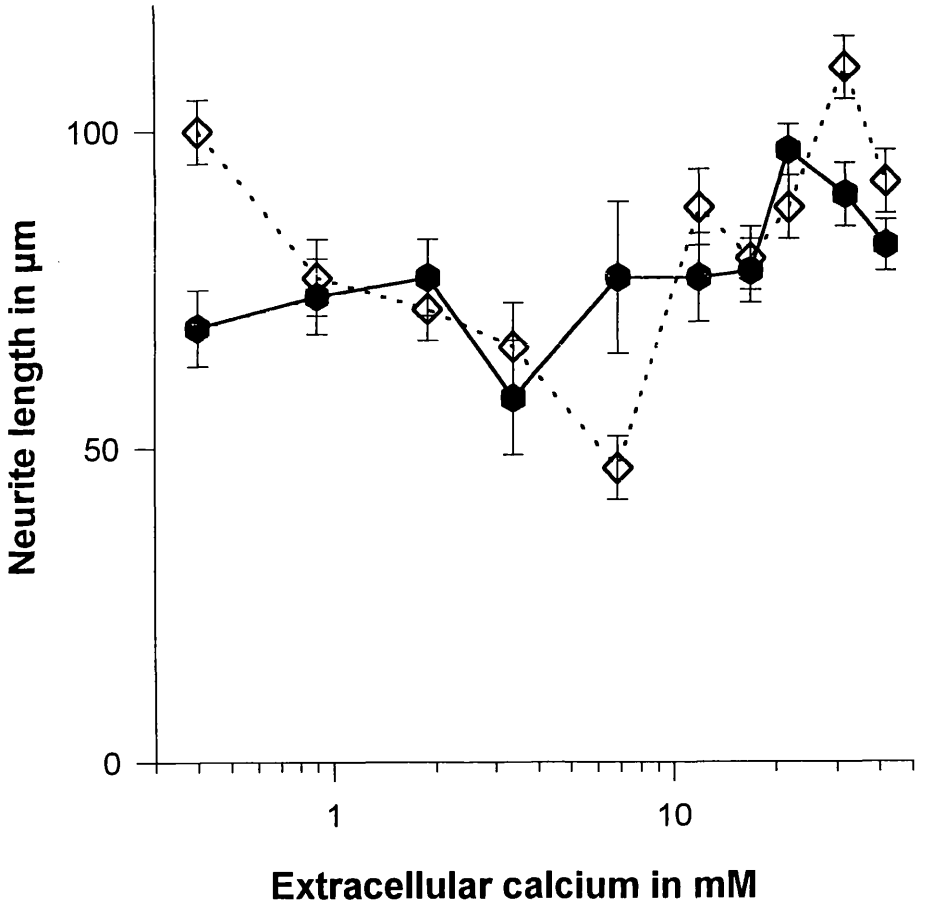
100
50
0
Neurite length in µm
1
10
Extracellular calcium in mM

Figure 6.5

Ionophore 4-Br-A23187 promotes neurite outgrowth in N1E-115 cells. **a)** The diagram shows the fraction of cells with neurites at different ionophore concentration. Data were collected and normalized as in Figure 6.3. Neurite initiation was significantly higher in cultures with 0.1 to 0.5 μM of the ionophore (vs control, ** $p<0.01$, * $p<0.05$, t-test) **b)**: length of the longest neurite vs ionophore concentration. Although not significant neurite length peaked at 0.1 μM of the ionophore.

Figure 6.5

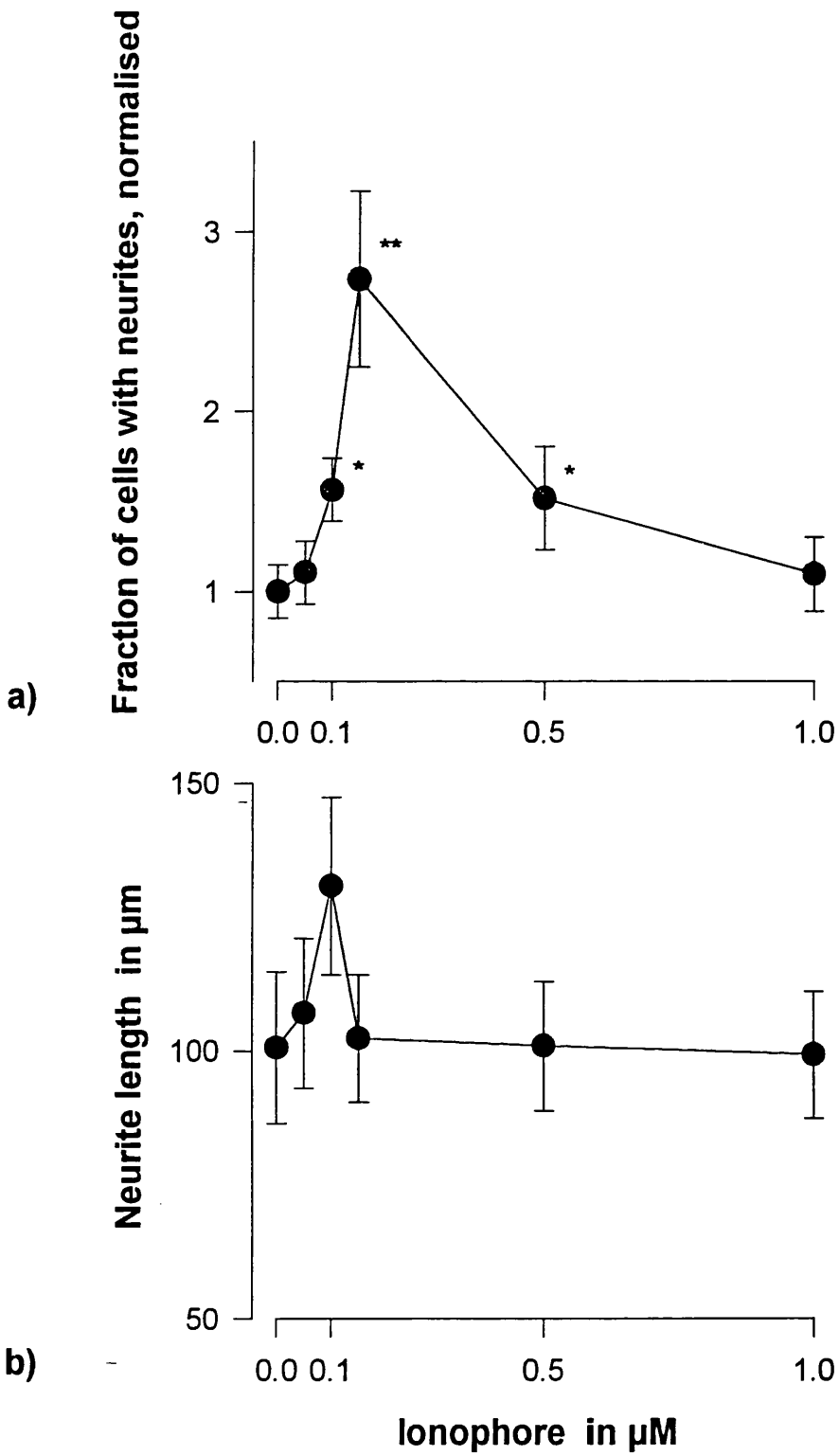
a)
Fraction of cells with neurites, normalised
3
2
1
**
*
*
0.0 0.1
0.5
1.0
b)
Neurite length in µm
150
100
50
0.0 0.1
0.5
1.0
Ionophore in µM

6.2 Discussion of results

Mattson and Kater (1987) suggested a model in which neurite outgrowth is regulated by influx of Ca^{2+} across the plasmalemma. According to this hypothesis neurite outgrowth is optimal in a narrow range of intracellular calcium concentrations. Excursions above or below a set point causes a reduction in neurite outgrowth. Such a bell-shaped dependence on $[Ca^{2+}]_i$ could be demonstrated in primary sensory neurones and cerebellar granule cells (Al-Mohanna et al., 1992; Zimprich et al., 1994). Both types of nerve cells showed a clear optimum of neurite initiation in the range of 35 to 45 nM of $[Ca^{2+}]_i$. In contrast to these neurones N1E-115 cells do not fit Mattson and Kater's model easily. In discussing the results I will consider neurite behaviour in low calcium (up to 6.9 mM $[Ca^{2+}]_o$) and high calcium separately. The $[Ca^{2+}]_o$ below 6.9 mM is similar to the range of calcium levels that was present in other neurite growth studies and data are therefore more directly comparable (Kater & Mills, 1991; Al-Mohanna et al., 1992). Moreover it seems likely that at low and high calcium levels different mechanisms operated.

Looking at the low calcium data first there was no bell shaped dependence of neurite outgrowth with an optimal set point. Rather neurite initiation was greatest at the lowest calcium level that could be achieved. This was even more apparent, when I added 20 mM $MgCl_2$ to reduce non-specific effects of a low divalent cation concentration. Although the effects of calcium on neurite length were less clear similar trends could be observed in the presence of 20 mM $MgCl_2$. Neurites were longest in the lowest possible $[Ca^{2+}]_o$ and shortest at 6.9 mM $[Ca^{2+}]_o$ (which is a calcium concentration well above the normal level). Regarding these results in the low calcium range the findings are consistent with calcium measurements in individual

N1E-115 growth cones which showed that growth cone advance only occurred at the lowest $[Ca^{2+}]_i$ and elevations of $[Ca^{2+}]_i$ were associated with an inhibition of neurite elongation (Silver et al., 1989). One might interpret these results in such a way that the machinery which modulates neurite outgrowth is aberrant in this transformed cell-line. One the other hand it is conceivable that in spite of the apparent 'non-bell shaped relationship' neurite growth in N1E-115 cells does follow Kater's model and is optimal at a true set point. But in contrast to dorsal root ganglion cells or cerebellar granule cells this set point would be not near the normal calcium level but well below at a $[Ca^{2+}]_i$ that is not compatible with cell survival in these particular culture conditions.

The observation that raising $[Ca^{2+}]_o$ above 6.9 mM also promoted increased neurite initiation and neurite length was an unexpected finding. A similar positive effect could be induced in normal extracellular calcium with low levels of the calcium ionophore 4-Br-A23187 present in the bathing medium. These molecules act as pores and cause a flux of calcium ions across the cell membrane, however it was not possible to measure a significant rise of $[Ca^{2+}]_i$ at the concentration of ionophores employed in this study. Still, the fact that ionophores stimulated neurite growth argues strongly against a nonspecific extracellular mechanism of unphysiological high $[Ca^{2+}]_o$ but in favour of the view that the effect was mediated by increased $[Ca^{2+}]_i$. A question that always has to be asked, especially when transformed cell lines are studied, is whether results are an unnatural property of a particular cell type or if they also apply to other cells. In support of the latter possibility, a similar growth promoting effect in high calcium was also observed in freshly dissociated rat cerebellar granule cells (Zimprich et al., 1994) and in another neuronal cell line (Reboulleau, 1986). In contrast to the outgrowth promoting effect of the

ionophore 4-Br-A23187 (0.1 - 0.5 µM) in my experiments Reboulleau reported no effect of calcium ionophores (5 - 40 µM) on neurite growth in rat neuroblastoma B50 cells, implying that $[Ca^{2+}]_o$ acted not by raising $[Ca^{2+}]_i$. Rather, he suggested that high $[Ca^{2+}]_o$ triggered neurite outgrowth by reducing the phosphatidylinositol turnover on the plasmalemma. In the light of my results a second possibility is that Reboulleau's ionophore concentrations were too high to allow him to observe increased neurite outgrowth.

In this chapter I was investigating the effect of maintained calcium levels. Experiments that cause such prolonged but constant alterations in the calcium concentration provide information on the permissive range of ongoing calcium dependent processes such as neurite outgrowth that takes place over many hours. In contrast to this, short lasting and spatially localised calcium changes associated with electrical activity will presumably only signal events such as a turn in the growth direction or a collapse of the growth cone. Which are the calcium sensitive processes in neurite outgrowth? Active outgrowth certainly requires the insertion of new membrane, a process that critically depends on presence of calcium ions (Burgoyne & Morgan, 1995). Disassembly and reassambly of microtubules and of actin filaments are further important steps in neurite elongation which are regulated by calcium (Bentley & O'Connor, 1994). Each of these processes has its own optimum concentration of calcium and the composite of all these calcium requirements will determine the permissive range of calcium for optimal neurite outgrowth. It is likely that the low calcium concentrations in the present experiments included the physiological permissive range for the processes of neurite outgrowth. Silver et al. (1989) showed that N1E-115 cells with spontaneously advancing neurites had a $[Ca^{2+}]_i$ of below 100 nM whereas retracting neurites exhibited $[Ca^{2+}]_i$ of around 200 nM. The fact that at 200 nM , the

range of the high calcium peak in my experiments, neurite outgrowth still occurred at all can probably be explained by the phenomenon of accommodation (Fields et al., 1993). Why neurite outgrowth was even promoted under high calcium conditions compared to control cultures is unclear but it could be speculated that an additional positive effect such as increased gene transcription set in.

CHAPER 7

CALCIUM DYNAMICS IN NEURONS OF LIVE ZEBRAFISH EMBRYOS.

7.1 INTRODUCTION

As outlined in the general introduction, experiments performed on isolated nerve cells in culture have led to the belief that calcium is a central second messenger in neuronal development. The surprising picture that emerged from such studies was that calcium can, as it seems, influence almost any process during nerve cell development. It is, however, a big step from simple culture conditions to the far more complex situation in a living embryo. The question mark that remains therefore, is which of the many reported effects of calcium are really relevant under normal physiological circumstances. Only very few studies have attempted to measure $[Ca^{2+}]_i$ in developing nerve cells in situ. Bentley et al. (1991) found calcium gradients in migrating pioneer grasshopper neurons. Yuste et al. (1992) studied the emergence of coloumnar units or domains in the developing rat neocortex and observed synchronised calcium changes in all cells of a domain. O'Donovan et al. (1994) imaged calcium changes in electrically coactive neurons in developing chick spinal cords, and finally Gu et al. (1994) investigated spontaneous calcium waves and spikes in developing neurons in amphibian spinal cord preparations. The reason, why there are only relatively few investigations, probably lies in the associated experimental difficulties. Some of the problems encountered are how to introduce a calcium indicator dye - without causing damage - into nerve cells that lie inaccessibly under the surface

or how to monitor fluorescence reliably through several layers of other cells.

The embryo of the zebrafish (*Danio rerio*) seems to offer a number of advantages that would make it particularly suited for the task of measuring calcium *in vivo*. Zebrafish are not only easy to maintain and produce large quantities of eggs but, most importantly, embryos are almost transparent. Therefore, developing neurons including growth cones can be easily visualised with Nomarski interference optics. The morphological development of the zebrafish nervous system has been extensively studied. In 18 to 20 hours old embryos the central nervous system is a simple system (Wilson et al., 1990; Kimmel, 1993). The spinal cord for instance contains per hemisegment only five classes of well characterised neurons (Bernhardt et al., 1990). The neuron class which has been most widely studied are the primary motoneurons (Eisen, 1991). In each segment ā rostral, a medial and a caudal primary motoneuron can always be identified and sometimes a variable primary is present (Eisen et al., 1986; Eisen et al., 1990). During their development they exhibit a sequence of events in a predictable and stereotypic manner. After axogenesis at 17-18 hours the growth cones grow on a characteristic path interrupted by pauses at guidepost stations and they show collapse and retraction of some branches that grew in the wrong direction. On the way collaterals contact specific muscle groups and form functioning synapses (Eisen et al., 1986; Myers et al., 1986). One of the motoneurons, the variable-primary (VaP), undergoes apoptosis in the majority of cases after having extended a neurite to the common guidepost station (Eisen et al., 1990). Given the favourable optical properties of embryonic zebrafish, I tried to develop an imaging technique suitable for monitoring calcium changes during in vivo nerve cell development, to begin to address the

question of whether any of the mentioned events are correlated or perhaps caused by changes in $[Ca^{2+}]_i$.

7.2 CALCIUM-GREEN LABELLING OF SPINAL NEURONS

The first task was to introduce a calcium censitive dye into nerve cells without disturbing the delicate development. To do this I adapted a technique which had been established for the study of cell fate mapping and lineage tracing in zebrafish embryos (Kimmel & Law, 1985). This method is based on the observation that a dye which is introduced into a blastomere cell is passed on to all daughter cells without being much diluted because cell size decreases during development. The calcium sensitive dye chosen was calcium-green dextran (MW 10 000). Dextrans are not metabolised in the cell, neither are they sequestered into organelles and are also too large to be pumped out of the cell. A further advantage of calcium-green was that at its excitation spectrum of 488 nM there is only neglegible autofluorescence from zebrafish cells. Its Kd for calcium lies around 400 nM. Figure 7.1 illustrates the injection technique and sketches key stages of the development from the fertilised egg to a 20 hpf old embryo with developing motoneurons. I injected dechorionated embryos at the 32 to 128 cell stage.(2-3 hpf) (Figure 7.1b) At this stage the central blastomere cells are no longer connected by cytoplasmic bridges. I pressure injected 20 mM calcium-green dextran from a high resistance pipette into the blastomere so that the cell was clearly fluorescing in 488 nm excitation but, when viewing with transmitted light, the amount of the orange coloured dye injected was not enough to stain

Figure 7.1

Key stage in early zebrafish development

a) The one cell stage: The fertilised egg separates into a granular yolk region (y) and a large blastomer cell. **b)** The 32 cell stage (1¾ hpf). Usually the blastomeres lie in 4x8 arrays. The central blastomeres have lost their connections to the yolk sac. Calcium green dextran injected into a central blastomere does therefore not leak into other cells. **c)** 70%epibole (~7hpf) During further development blastomere cells get smaller as they divide and migrate away from the animal pole to engulf the yolk cell. During this movement, called epiboly, involution takes place which results in the formation an epiblast and hypoblast germ layer. During epiboly and involution cells of one clone (labelled black) are widely scattered and contribute to both germ layers. **d)** Bud stage (10hpf) Epiboly has come to an end and cells are concentrated on the dorsal side. The neural keel forms and is rostrally thicker. Soon the first somites start to appear. **e)** 20 somite stage (19hpf) Brain vesicles and spinal cord have formed. The optic vesicles are clearly visible and the otic vesicles are just appearing. The V shaped myosepta have emerged from the somites. The yolk sack is still large and covered with epidermal cells. **f)** Detailed view of labelled motoneurons in the spinal cord. The spinal cord (sc) lies dorsally of the notochord (nc) whose ring like cells are characteristic. Above and below the median plane the V shaped transverse myosepta are visible. The horizontal myoseptum (not drawn on the sketch) forms on the level of the apex of the V's. The three labelled motoneurons indicate the identifying characteristics: The somas are positioned ventrally in the spinal cord and extend axons that elongate ventrally towards the horizontal myoseptum.

Figure 7.1

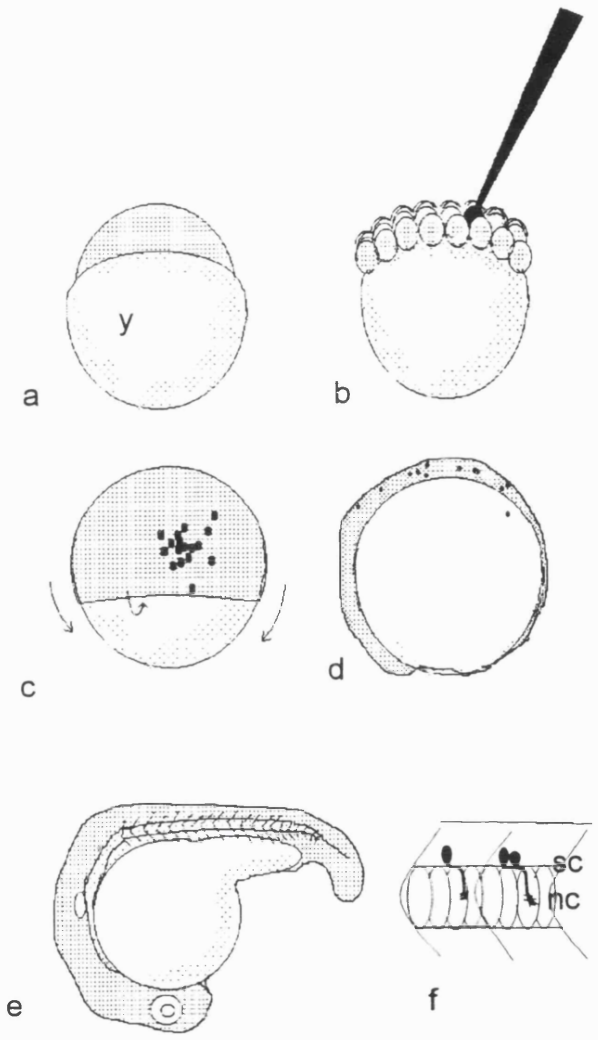

the cell orange. There was also no visible volume change. Within a few seconds after injection the fluorescence in the injected cell became fainter because of the diffusion of the dye within the cell and probably because it equilibrated with the low intracellular calcium concentration. Following the fate of injected cells for the next hours demonstrated that the vast majority of cells were not damaged but continued to divide normally, just as neighboring unlabelled cells. During the Gastrula Period (5-10 hpf) and later cells underwent extensive migration and rearrangement. This led to a wide scattering of the cell clone descending from the original cell, labelled in the early blastula period.(Fig 1 c,d). As a result it was usual to find labelled cells (from one clone) contributing to the epiblast layer (developing into ectodermal tissues) and hypoblast cells (giving rise to mesodermal and endodermal elements). It is only at the end of the blastula period (5 hpf) that cellular fate appears to be restricted to individual tissue types (Kimmel et al., 1990). However, from the 16 cell stage on there seems to be a higher likelihood for centrally lying blastomers to contribute to spinal cord cells (Strehlow et al., 1994). To maximise the number of labelled spinal cord neurons, I therefore injected, when possible, cells lying near to the center, the animal pole of the embryo. Until 16-17 hpf embryos were allowed to develop in darkness at 26 - 28°C, thereafter they were transferred to the stage of the confocal microscope and screened for the presence of labelled cells. Labelled cells were found in all three germ layers in all regions of the embryo. There appeared to be a higher density in the spinal cord but this was not tested statistically. In general, cells were strongly labelled and easily visible with either conventional epifluorescence optics or in the scanning mode of the confocal microscope. Examples of labelled non neuronal cells that could be readily identified were notochord cells, cells in the myotome and sclerotome, floorplate cells and epidermal cells. Labelled nerve cells in

the spinal cord at 17 hpf, that is before axogenesis, could be recognized with a fair degree of certainty by their size and position. After they had extended axons neurons could be unequvocally identified. Primary motoneurons were seen in approximately one out of 5 to 10 embryos aged 17 to 24 hours (Figure 7.2 a,b). Usually several motoneurons in the same and adjacent segments were labelled. Cell bodies of primary motoneurons were relatively large at ~10um in diameter and located in the ventral third of the spinal cord. The large axons (2 µm diameter) left the spinal cord on the ventral border and advanced to the level of the horizontal myoseptum. Gowth cones were clearly visible as distinctive enlargement at the tip of neurites. Examples of other early neurons in the spinal cord are the sensory Rohon Beard cells, which were the most dorsally located neurons in the spinal cord with descending and ascending neurites (Figure 7.2 c,d). Figures 7.2 e and f show an example of a ventral longitudinal descending (VeLD) neuron. These cells were found in the ventrolateral cord with an axon that run ventrally for a short distance and then descended caudally. The morphology of fluorescent neurons was apparently identical to that described previously from unmanipulated animals (Bernhardt et al., 1990). This indicates that neither calcium-green dextran as a substance, nor the additional calcium buffering capacity it represented, was incompatible with normal nerve cell development. Furthermore, the laser scanning process in the following experiments (5 to 15 scans every 30 seconds, with the laser set to minimum power) did not damage the cells. During the scanning cells continued to migrate actively over the field of view and neurites continued to elongate.

Figure 7.2

Examples of spinal neurons labelled with calcium green dextran. a,c,d, are transmitted light photomicrographs of segments of the spinal cords of zebrafish embryos of up to 24 hpf. Green overlays mark the exact position of labelled cells in the spinal cord. b,d,f. show detailed fluorescence pictures of the neurons of interest. All calibration bars are 10 µM **a)** A group of labelled cells in the ventral aspect of the spinal cord. One cell has extendend an axon ventrally beyond the level of the horizontal myoseptum and can thus be identified as a caudal primary motoneuron (CaP). **b)** Detail of (a) clearly showing the large growth cone of the CaP and the characteristic thickening of the axon at the level of the horizontal myoseptum. **c)** A sensory Rohon-Beard neuron. These cells were the most dorsally located neurons in the spinal cord and typically extended one rostral and one caudal axon. Note the notochord and the V shaped transvers myosepta, which point rostrally **d)** Detail of (c) showing the cell body and the caudal axon with its large growth cone. **e)** A ventral lateral descending neuron (VeLD) in the ventral aspects of the spinal cord and dorsally a Rohon-Beard neuron. **f)** This is a detailed view of the same VeLD neuron. The axon takes initially a ventral course but then turns in a caudal direction.

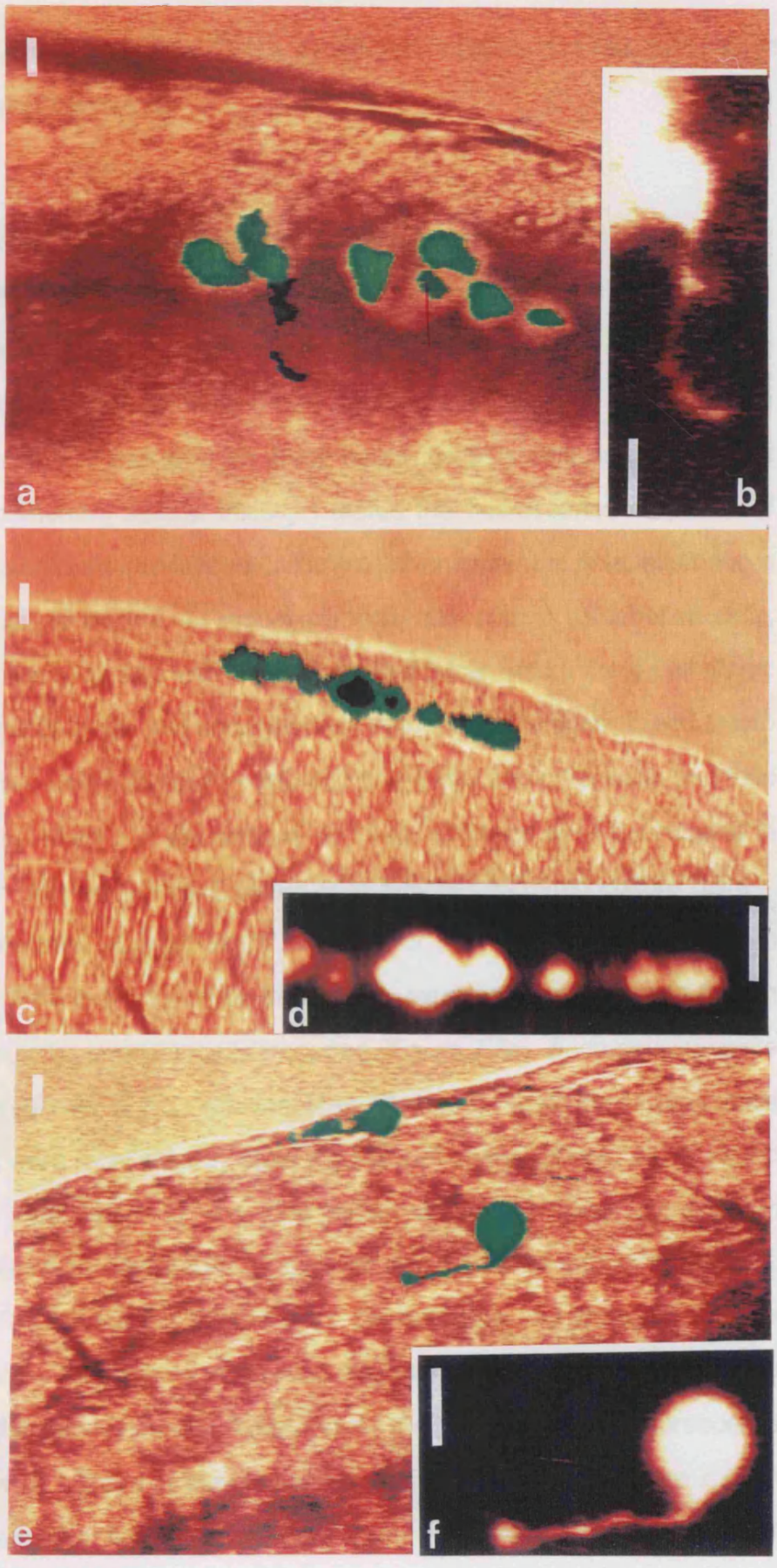
a
b
c
d
e
f

7.3 CALCIUM-GREEN IN CELLS OF 18 HPF EMBRYOS STILL RESPONDS TO CALCIUM CHANGES

These initial experiments proved that calcium-green dextran remained for at least 24 hours in developing neurons in concentrations high enough to allow visualisation. In the following experiment I tried to determine whether calcium-green dextran had preserved its ability to function as a calcium indicator dye after so many hours inside a cell, as this has not been documented before. Initially I tested the fluorescence response of the dye to calcium increases in a controlled environment in labelled nerve cells in culture dishes. To achieve a maximum number of labelled cells, embryos were injected with calcium-green dextran before the 8 cell stage. At this time cells are still connected via cytoplasmic bridges. Injection into one cell resulted therefore in diffusion of the dye into other cells and thus labelling of all cells in the embryo. At 16 hpf embryos were dissociated in a calcium free medium and plated onto polylysine coated culture dishes. Cells were then allowed to differentiate for 2 to 4 hours in L15 growth medium. After that time nerve cells which expressed neurites and growth cones could be unequivocally identified (Figure 7.3a). Such neurons were depolarised with a KCl solution (see Methods) while the fluorescence changes were monitored by scanning the cell every 320 ms. All 11 tested neurons responded to this depolarisation with a clear increase in fluorescence. In contrast in 10 cells of non neuronal morphology in the same fields of view the fluorescence did not show any changes. Figures 7.3 b,c show an example of a plated neuron before and 1600 ms after the start of the depolarisation. Averaged for the 11 neurons the fluorescence increased to 1.6 fold of the control value within 5 seconds (Figure 7.4). In some cells the fluorescence rose three fold indicating the maximum

dynamic range of calcium-green dextran that can be expected for further in vivo experiments.

Do cells in the intact organism also respond to calcium changes? To test this I considered that one of the most obvious cytosolic calcium rises can be found in contracting muscle fibers. Labelled muscles cells were easily recognised by their location and shape, spanning the chevron shaped myosepta longitudinally. Figures 7.3 d to h show two such muscle fibers in adjacent myomers. Muscle contractions occur spontaneously during the outgrowth of primary motoneuron axons after about 17 hpf but can also be triggered by inducing an escape behaviour (Fetcho & O'Malley, 1995). In the experiment shown, such an escape behaviour was triggered by increasing the temperature for a few seconds with a fan heater. As the embryos was embedded in 1% agar, muscle contractions did not result in gross movements, however, to preclude fluorescence artefacts from any remaining mobility the monitored muscle cells were focused at the brightest optical section prior to stimulation. The images of figure 7.3 d to h - acquired at 180 ms intervals - show the fluorescence changes associated with a stimulated contraction. (Only the upper muscle fiber contracted, the lower one located in a different myomere remained inactive.) In an average of three such contractions the fluorescence rose to a maximum of 2.7 (range 2.3 to 3.1) times of the baseline intensity. The amount of fluorescence increase is similar to the above described in vitro experiments and published values for the dynamic range of calcium-green dextran in cells (Fetcho & O'Malley, 1995).

Figure 7.3

Calcium green dextran in embryos more than 16 hpf still responds to calcium changes. **a)** Differential interference photomicrograph of a cultured neuron from an embryo dissociated at 16 hpf. Note the numerous filopodia on growth cone and axon. Calibration bar is 10 µM **b)** and **c)** Confocal fluorescence images of a calcium green labelled neuron in culture. Cells were labelled by injecting a 1 to 8 cell stage embryo with the dextran-bound dye. At 16 hpf embryos were dissociated and cells plated on culture dishes. b) is just before and c) 1600 ms after depolarisation with a solution containing 130 mM KCl, 2 mM $CaCl_2$ and 5 mM HEPES and a 10% dilution of the growth medium. The cell clearly responded with an increase in fluorescence. Fluorescence intensities are represented on a pseudocolour glow scale according to the colourbar in (i). The calibration bar is 10 µM. **d)** to **h)** Confocal fluorescence images on a pseudocolour glow scale of calcium green labelled muscle cells in a life embryo around 20 hpf. Muscle contractions associated with an escape behaviour were induced by increasing the temperature at the microscope stage with a fan heater. The images in this sequence depicting such a contraction in the upper muscle cell are 180 ms apart. (d) is just before the contraction in (e). the fluorescence in the upper muscle cell has clearly increased and then slowly declined again.calibration bar is 40 µM. **i)** This bar shows the pseudocolour glow scale used in (b) to (h) for the 255 possible on screen pixel-intensity values. An intensity of 0 is represented as black and the maximum intensity of 255 as white.

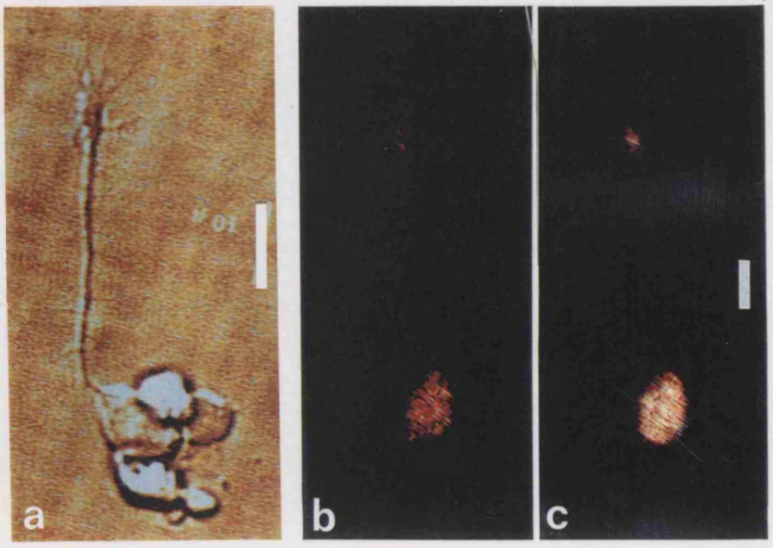
a
b
c

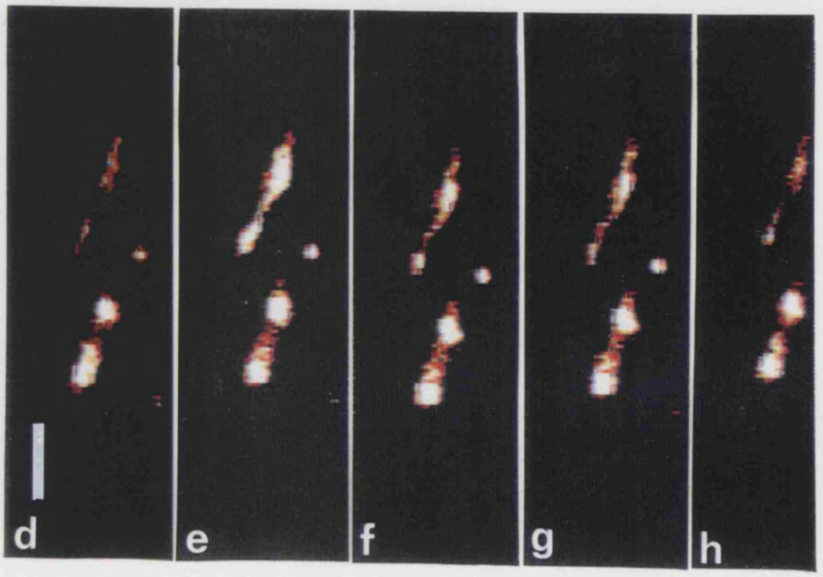
d
e
f
g
h


i

Figure 7.4

This histogram shows the average fluorescence increase in 11 calcium green labelled, cultured neurons when depolarised as seen in the example of figure 7.3 (b) and (c). The fluorescence intesities on the y-axis are expressed as ratios through the predepolarisation intensity values; errorbars are sem.

Figure 7.4

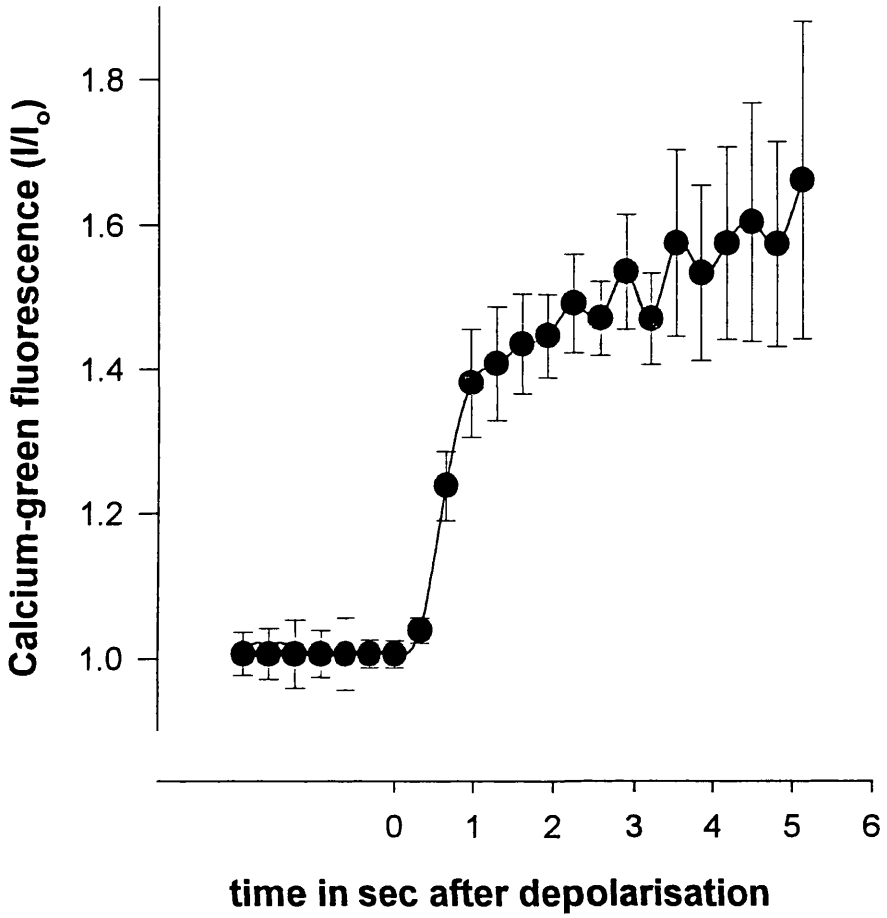
Calcium-green fluorescence (I/I$_0$)
1.8
1.6
1.4
1.2
1.0
0
1
2
3
4
5
6
time in sec after depolarisation

7.4 SPONTANEOUS CALCIUM WAVES IN DEVELOPING MOTONEURONS

Having established that calcium-green dextran reports calcium changes under the given experimental condition, I turned my attention to monitoring calcium dynamics in developing motoneurons which were among the most frequently labelled cells in the spinal cord. This section only describes preliminary experiments on 14 motoneurons. In these initial experiments labelled motoneurons with clearly recognizable axons and growth cones were selected. Fluorescence intensities were monitored by acquiring stacks of 5 to 15 images spanning the whole cell every 30 seconds usually for a duration 30 minutes. In three out of these 14 motoneurons (all from different embryos) I observed spontaneous fluorescence increases which I will describe in the following paragraphs.

One of these three motoneurones is shown in Figure 7.5. The fluorescence intensities are displayed on a pseudocolour scale according to the colourbar in (j). The growth cone has reached the horizontal myoseptum and during the observation period the axon continued to elongated both in a rostral and caudal direction (compare for instance (a) with (i) (rostral is up and right on the image). Images (a) to (d) illustrate a fluorescence wave that was propagated along the axon in a distal direction, that is down and to the left on the image. This wave phenomenon was even more clearly visible when images were displayed on the screen of the confocal computer as a movie (that is in rapid sequence). The wave appeared to travel at a speed of around 5 μm per minute. The sequence of images (e) to (h), which are displayed at a lower intensity gain than (a) to (d), show an example of a fluorescence increase affecting the whole cell simultaneously. Such fluorescence increases which were also observed in a second motoneuron lasted between 2 and

3 frames this is between 0.5 and 2 minutes. Figure 7.6 demonstrates the fluorescence changes observed in the third motoneuron which was still in the early stages of extending an axon. The cell body is in the centre of the image and the growth cone on the left. During the 30 min monitoring period there were 11 fluorescence increases in the growth cone which lasted 1 to 2.5 minutes each. Two of these waves are seen in the figure starting in image (b) and (g). These waves appeared to be transmitted to the cell body with a delay of two frames that is at an estimated speed of 5 to 10 μ per minute. These waves as in the other two cells were more easily observed in a movie on the screen of the computer.

7.5 Discussion of results

The pupose of this of this study was to develop a system capable of monitoring calcium changes during nerve cell development in an intact organism. In contrast to cell culture experiments which can only study nerve cells in a necessarely simplified condition, an *in vivo* system could help clarify which processes in a normal, physiological development are really associated with calcium signals. Zebrafish embryos were chosen because they offered a number of advantages for this task: They are almost transparent thus allowing microscopic investigations. They are convenient to maintain and produce large quantities of eggs. At 24 hours of development the zebrafish spinal cord is a simple system with only a limited number of cells in each segment. Finally, the zebrafish nervous system has been extensively studied in recent years providing a good fundament of knowledge to draw from. (Eisen, 1991; Kimmel, 1993;

Figure 7.5

Spontaneous calcium waves in a calcium green labelled motoneuron. Images seen are the average of stacks of 15 confocal scans which were in this case 1 µm apart and are thus recordings from the whole depth of the cell. Fluorescence intensities are shown on a pseudocolour scale as encoded in the colour bar in **(j)** An intesity of zero is seen as blue and 255 as purple. Numbers in the lower left corners are minutes passed since start of recording. Calibration bar is 10 µM. The motoneuron has extended its axons toward the horizontal myoseptum. **a)** to **d)** show a slow fluorescence wave travelling down the axon within 2 minures. **e)** to **h)** shows a wave affecting the cell soma and the growth cone simultaneously. The fluorescence increase is seen in two frames (f and g) and lasted therefore at least 0.5 minutes. The intensity gain of (e) to (h) is lower than in (a) to (d) to display the fluorescence changes in the cell soma. **i)** shows the motoneuron 10 minutes after (a). The cell has clearly extended a branch in a rostral (up and right) direction.

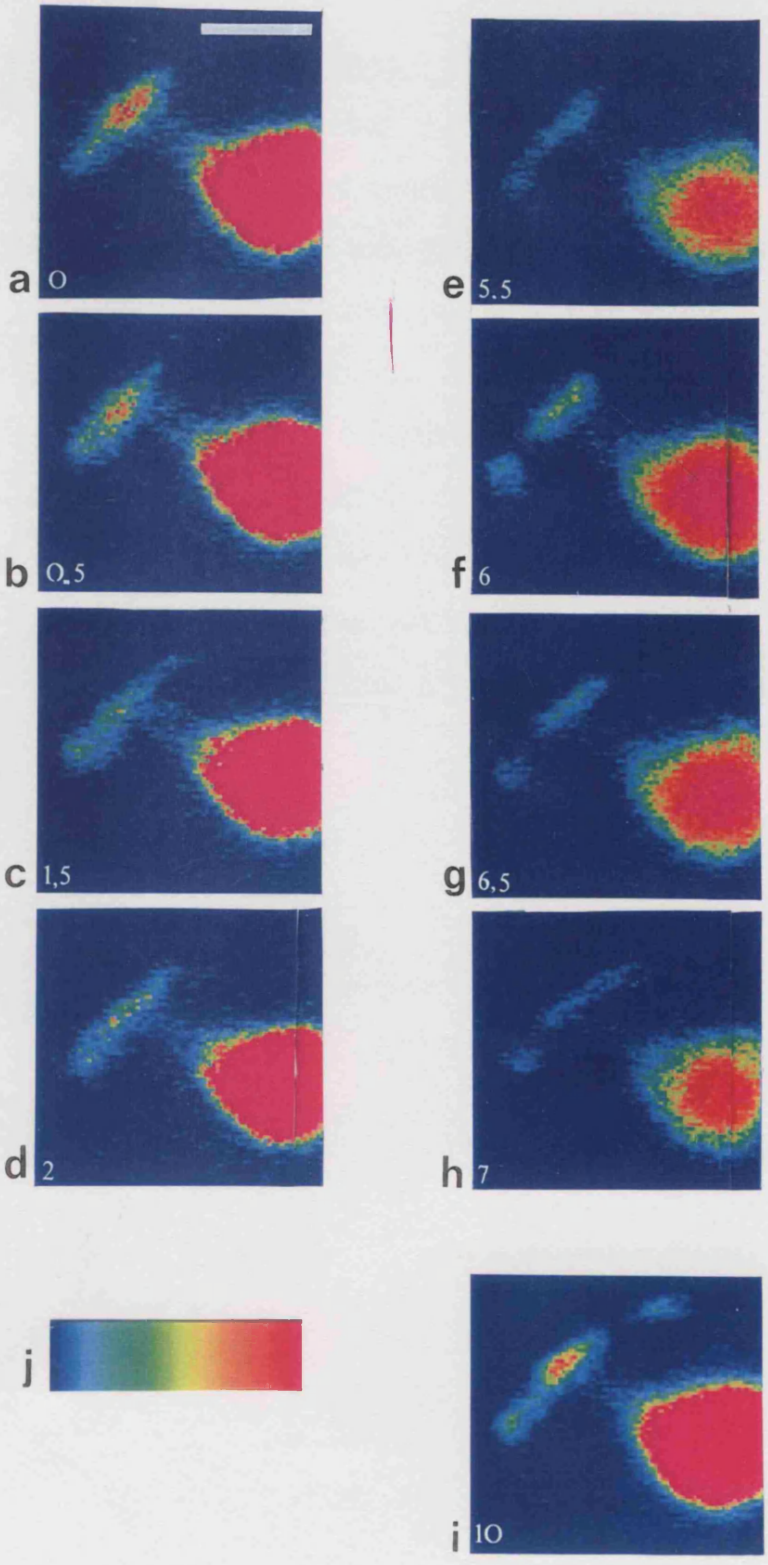
a 0
b 0,5
c 1,5
d 2
e 5,5
f 6
g 6,5
h 7
i 10
j

Figure 7.6

Spontaneous calcium waves originating in the growth cone of a motoneuron. Images are averages of 5 scans 3 µm apart so that the recording is from the whole depth of the cell. Fluorescence intensities are shown on a pseudocolour scale as encoded in the colour bar in (**k**). **a)** to **j)** is a continuous sequence, with 30 seconds intervals between images; the calibration bar is 10 µm. The growth cone lies to the left in the image and the cell soma to the right. The round cell in the upper right corner is a separate cell. A fluorescence wave is starting in the growth cone in (b) and lasts for 4 frames that is at least 2 minutes. At the same time this fluorescence increase is transmitted with a delay to the cell soma to the right. In (g) a second wave starts.

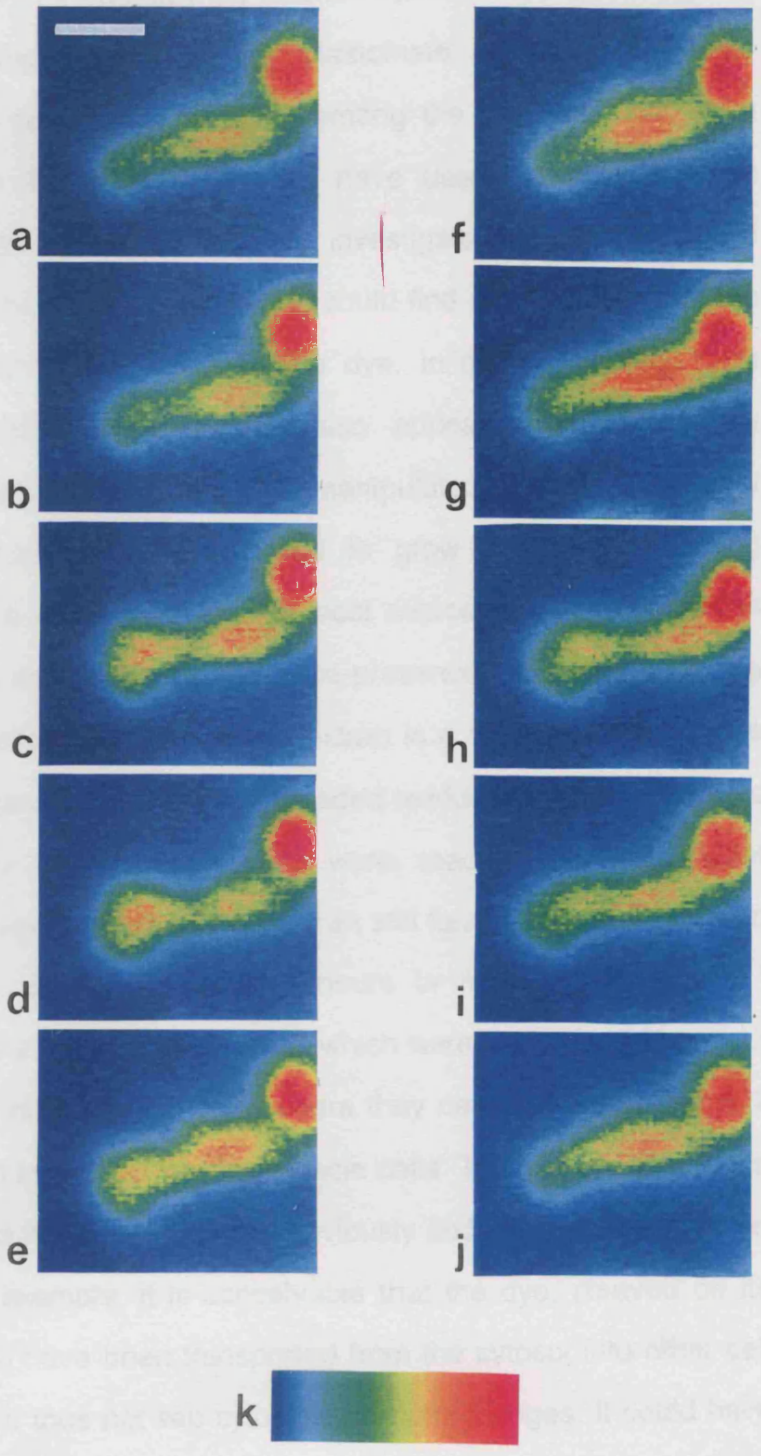
a
b
c
d
e
f
g
h
i
j
k

Easter et al., 1994). I introduced the calcium indicator dye calcium-green dextran by injecting it into an early blastomere cell. 15 hours later developing nerve cells could be found among the daugther cells as a matter of chance. Eisen et al., (1986) have used this method, with fluorescein dextran as a marker, to investigate the morphological development of motoneurons *in vivo* and could find no indication that the normal development was altered by the dye. In my experiments cells labelled with calcium-green dextran also appeared morphologically normal when compared to neurons in unmanipulated embryos (Bernhardt et al., 1990). Morover cells continued to grow and migrate during observation with a laser scanning confocal microscope. This indicates that labelled cells are not damaged by the presence of the dye or during the scanning process. Calcium-green dextran is a suitable indicator dye for these experiments as it was not degraded markedly in up to 22 hours in the cytoplasm and labelled cells were readily visualised. Most importantly however, calcium-green dextran still functioned as a cytosolic calcium indicator dye, even after 16 hours or more inside a cell. I demonstrated this in labelled nerve cells which were transferred from a 16 hour old embryo into a culture dish (where they developed for another 2 to 4 hours) and in *in vivo* contracting muscle cells This feature of calcium indicator dyes has not been reported previously and could not been taken for granted. For example, it is conceivable that the dye, cleaved off its dextran tail, could have been transported from the cytosol into other cell compartments and thus not see cytosolic calcium changes. It could have been that the dye although itself still fluorescent had lost its ability to report calcium-binding.

In much older posthatching zebrafish embryos it is possible to use a different approach to label already developed motoneurons. Fetcho et al.

(1995) injected calcium-green dextran into muscles and observed that motoneurons were retrogradely labelled by diffusion along the axon. Using this method the authors could demonstrate that muscle activity was associated with a calcium increase in innervating primary and secondary motoneurons. However, it is evident that such a method is not suitable if developing motoneurons before synaptogenesis or if other nerve cells are to be studied. Other authors labelled neurons in dissected *Xenopus* (Gu et al., 1994) or chick (O'Donovan et al., 1994) spinal cords with the membrane premeable acetoxy-methyl form of the calcium indicator dyes Fluo-3 and Fura-2. The disadvantages of this method is that as all cells are labelled the outline of individual cells can only vaguely be determined and it seems not possible to visualize axons or growth cones.

In contrast to the above mentioned methods the injection of precursor cells as described here appears to be a non damaging way of introducing calcium dyes into individual developing nerve cells and gives excellent morphological results.

Calcium changes in developing motoneurons

Having developed a suitable technique, I began experiments to study calcium dynamics in developing neurons *in situ*. Although these experiments only involved a small number of cells at this point, the results of spontaneous transients are interesting enough, I think, to be included in this chapter. Motoneurons were chosen because they were frequently labelled, easily identified and their morphological development is best described of all spinal neurons (Eisen et al., 1986; Myers et al., 1986). In three out of 14 monitored motoneurons I observed clear long lasting calcium increases or waves in the range of 0.5 to 2 minutes duration. These waves could either occur in the cell body or in growth cones and

Table III: Spontaneous calcium transients in dev. nerve cells during neurite outgrowth
Review of some studies

Preparation	Characterisation of transients	Mechanisms of $[Ca]_i$ elevation	Comments	References
cultured *Helisoma* neurons, only looked at growth cones	•incidence increased by addition of brain conditioned medium from 10% to 40-45% of growth cones •peak amplitude of ~100nM or 50% above baseline •duration of one transient: 8-12 min •frequency: ~10 per hour	•Transients are blocked by 50µM La^{3+} and appear at the same time in development as spontaneous electrical activity	Transients are coincident with initiation of neurite elongation and increase rate and extent of neurite outgrowth but are not essential for outgrowth.	Williams and Cohan 1993
Xenopus spinal neurons *in vitro* and *in situ*	**Spikes:** •occur in cell soma and travel rapidly throughout cell at action potential speed. •incidence: 38 - 75% of all cells in young neurons declining to 19% in mature cultures. •frequency declined from 2.4 to 1.6 per hour •amplitude of ~700nM or 400% above baseline (50nM). •peak in <5sec and decay with τ of ~11sec	•abolished by removal of $[Ca^{2+}]_o$, TTX, >50µM Ni^{2+} and 10µM ω-conotoxin •caffeine sensitive stores contribute to elevation of calcium	Spikes are essential for normal neurotransmitter expression and K channel maturation.	Gu et al 1994, Gu and Spitzer 1995
	Waves: •in soma and growth cone but only few (large ones) were propagated (speed: 30-70 sec/50 µm) •higher incidence and frequency in growth cones but similar between young and mature neurons (40-80% and 1.9 per hour) •amplitude of ~175% (up to 600%) •rise for > 30 sec and decay over ~2-4 min	Waves were sometimes triggered by spikes; not influenced by blocking VOCC (Ni^{2+} and Co^{2+} at low conc) and by TTX but abolished by removal of extracellular calcium and 5 mM Ni^{2+}; not inhibited by glutamate antagonists and depolarisation	Modulation of wave activity above and below the endogenous frequency down- and up-regulates neurite extension.	
chick DRG cultures	•transients only ever observed in growth cones, never in somata; •incidence: 29% (during 20 min observation) in 2mM $[Ca^{2+}]_o$ but 67% in 20 mM $[Ca^{2+}]_o$. frequency: ~8/hr •transients propagated with declining amplitude into neurites at speed of 22 µm/10sec •amplitude: from 100nM $[Ca^{2+}]_i$ (baseline) to ~150 nM (peak) •delay to peak <20 sec, duration ~1min ;	Ca^{2+} influx through non VOCC required: 100 µM La^{3+}, 1mM Ni^{2+} and removal of $[Ca^{2+}]_o$ blocked transients while inhibitors of L,N, and T-type channels (ω-conotoxin, verapamil, nifedipine, and 50µM Ni^{2+}) had no effect. IP_3 sensitive stores seem to buffer $[Ca^{2+}]_i$ during transients; in contrast caffeine sensitive stores contribute to $[Ca^{2+}]_i$ elevation	Growth cone migration was markedly reduced in the 10 min following a transient.	Gomez et al. 1995

could slowly travel throughout the cell with an estimated speed of around 5 µM per minute. In the cell shown in figure 7.5 the observed calcium waves were associated with an elongation of the axon during the monitoring period whereas this was not the case with the other two motoneurones.

Spontaneous calcium transients have been observed in a number of *in vitro* experiments (Holliday & Spitzer, 1990; Holliday et al., 1991; Gu & Spitzer, 1993; Komuro & Rakic, 1993; Lawrie et al., 1993; Gu et al., 1994; Gomez et al., 1995; Gu & Spitzer, 1995). These spontaneous transients can be divided according to their time course into short and long lasting ones. I shall call short lasting ones 'spikes' and longer transients 'waves' in accordance with the terminology used by Gu et al. (1994). Short lasting spikes, below ~ 30 sec, are generated by electrical activity (Lawrie et al., 1993; Gu et al., 1994). In addition to culture experiments they were also observed *in vivo* (Yuste et al., 1992; Gu et al., 1994; O'Donovan et al., 1994). Longer lasting calcium waves, lasting over several minutes, were reported by a number of investigators in cultured neurons (Williams & Cohan, 1993; Gu et al., 1994). Gu and al. (1994) noticed these waves also *in situ,* in Xenopus spinal cord preparations, but due to the high noise levels associated with Fluo-3 AM loading, could not describe them further. The mechanisms responsible for generating these waves are still unclear. Both Gu et al. (1994), and Williams & Cohan (1994) found an influx of calcium ions across the membrane critically important for waves, but this did not involve membrane depolarisation in *Xenopus* neurons. Gomez et al. (1995) investigating calcium transients on an intermediate timescale (~1 min) in chick dorsal root ganglion cells, stressed the importance of calcium release from internal stores, in addition to an influx of calcium through the membrane. In *Xenopus* neurons waves started both in cell

bodies and growth cones and could be propagated if calcium reached high enough levels (Gu et al., 1994; Gu & Spitzer, 1995). In other experiments calcium waves were only generated in growth cones but never in the cell body (Williams & Cohan, 1994; Gomez et al., 1995). Spontaneous calcium transients seem to convey specific information, perhaps encoded in the kinetics and frequencies of these transients. Whereas calcium spikes were critical for the general electrophysiological maturation of neurons (Gu et al., 1995) waves were found to inhibit neurite elongation (Gomez et al., 1995; Gu & Spitzer, 1995).

The experiments on zebrafish motoneurons described here are still in their early stages. It seems to me that the direction of future work should be guided by two questions. What are the cellular mechanisms responsible for the calcium waves and what is their physiological significance? Regarding the mechanisms it will be necessary to study the origin of the calcium. Are voltage gated or other types of calcium channels on the plasmalemma involved and what is the contribution of intracellular stores? Such experiments involve the search for conditions that specifically suppress spontaneous wave activity by using for example blockers of calcium channels, inhibition of action potentials or blockers of internal calcium release. To evaluate the developmental importance of spontaneous calcium waves it will be necessary to corellate wave activity to specific events in the development by monitoring intracellular calcium levels continuously over longer periods. Events that could be asociated with calcium wave signalling might be the initiation of axons from the unpolarised cell, arrival of the growth cone at guidepost locations where navigational decisions have to be made and the arrest of neurite elongation and synapse formation. Finally it would be of interest whether blocking of wave activity has any effect on the normal development. In conclusion it can be hoped that such experiments shed further light on the complex role of calcium as a second messenger in neuronal development.

REFERENCES

(1) Al-Mohanna, F, Cave, J and Bolsover, SR (1992). A narrow window of intracellular calcium concentration is optimal for neurite outgrowth in rat sensory neurones. Brain Res Dev Brain Res, 70, 287-90.

(2) Altman, D. G. (1991). Practical statistics for medical research. London: Chapman and Hall

(3) Altman, J (1992). Programmed cell death: the paths to suicide. Trends Neurosci, 15, 278-80.

(4) Bading, H, Ginty, DD and Greenberg, ME (1993). Regulation of gene expression in hippocampal neurons by distinct calcium signaling pathways. Science, 260, 181-6.

(5) Bandtlow, CE, Schmidt, MF, Hassinger, TD, Schwab, ME and Kater, SB (1993). Role of intracellular calcium in NI-35-evoked collapse of neuronal growth cones. Science, 259, 80-3.

(6) Bedlack, RJ, Wei, M and Loew, LM (1992). Localized membrane depolarizations and localized calcium influx during electric field-guided neurite growth. Neuron, 9, 393-403.

(7) Bentley, D, Guthrie, PB and Kater, SB (1991). Calcium ion distribution in nascent pioneer axons and coupled preaxonogenesis neurons in situ. J Neurosci, 11, 1300-8.

(8) Bentley, D and O'Connor, TP (1994). Cytoskeletal events in growth cone steering. Curr Opin Neurobiol, 4, 43-8.

(9) Bernhardt, RR, Chitnis, AB, Lindamer, L and Kuwada, JY (1990). Identification of spinal neurons in the embryonic and larval zebrafish. J Comp Neurol, 302, 603-16.

(10) Berridge, MJ (1993). Inositol trisphosphate and calcium signalling. Nature, 361, 315-25.

(11) Berrow, NS, Campbell, V, Fitzgerald, EM, Brickley, K and Dolphin, AC (1995). Antisense depletion of beta-subunits modulates the biophysical and pharmacological properties of neuronal calcium channels. J Physiol Lond.

(12) Bliss, TV and Collingridge, GL (1993). A synaptic model of memory: long-term potentiation in the hippocampus. Nature, 361, 31-9.

(13) Bokvist, K, Eliasson, L, Ammala, C, Renstrom, E and Rorsman, P (1995). Co-localization of L-type Ca2+ channels and insulin-containing secretory granules and its significance for the initiation of exocytosis in mouse pancreatic B-cells. Embo J, 14, 50-7.

(14) Bolsover, SR, Gilbert, SH and Spector, I (1992). Intracellular cyclic AMP produces effects opposite to those of cyclic GMP and calcium on shape and motility of neuroblastoma cells. Cell Motil Cytoskeleton, 22, 99-116.

(15) Burgoyne, RD, Graham, ME and Cambray, DM (1993). Neurotrophic effects of NMDA receptor activation on developing cerebellar granule cells. J Neurocytol, 22, 689-95.

(16) Burgoyne, RD and Morgan, A (1995). Ca2+ and secretory-vesicle dynamics. Trends in Neuroscience, 18, 191-196.

(17) Cherubini, E, Gaiarsa, JL and Ben, AY (1991). GABA: an excitatory transmitter in early postnatal life. Trends Neurosci, 14, 515-9.

(18) Cohan, CS, Haydon, PG and Kater, SB (1985). Single channel activity differs in growing and nongrowing growth cones of isolated identified neurons of Helisoma. J Neurosci Res, 13, 285-300.

(19) Collins, F, Schmidt, MF, Guthrie, PB and Kater, SB (1991). Sustained increase in intracellular calcium promotes neuronal survival. J Neurosci, 11, 2582-7.

(20) Colquhoun, D (1987). Practical Analysis of single channel records and the interpretation of single channel recordings. In N. B. Standen, P. T. A. Gray and M. J. Whitaker (Eds.), Microelectrode Techniques; The Plymouth Workshop Handbook (pp. 83-136). Cambridge, UK: The Compant of Biologists Limited.

(21) Cosgrove, C and Cobbett, P (1991). Induction of temporally dissociated morphological and physiological differentiation of N1E-115 cells. Brain Research Bulletin, 27, 53-58.

(22) Dai, Z and Peng, HB (1993). Elevation in presynaptic Ca2+ level accompanying initial nerve-muscle contact in tissue culture. Neuron, 10, 827-37.

(23) Davenport, RW and Kater, SB (1992). Local increases in intracellular calcium elicit local filopodial responses in Helisoma neuronal growth cones. Neuron, 9, 405-16.

(24) Davis, L, Rheder, V and Kater, SB (1992). Autonomous Activities of the neuronal growth cone. In P. C. Lerourneau, S. B. Kater and E. R. Macagno (Eds.), The nerve growth cone (pp. 133-150). New York: Raven Press Ltd.

(25) Daxer, A (1993). Characterisation of the neovascularisation process in diabetic retinopathy by means of fractal geometry: diagnostic implications. Graefes Arch Clin Exp Ophthalmol, 231, 681-6.

(26) Desarmenien, MG and Spitzer, NC (1991). Role of calcium and protein kinase C in development of the delayed rectifier potassium current in Xenopus spinal neurons. Neuron, 7, 797-805.

(27) Diebold, RJ, Koch, WJ, Ellinor, PT, Wang, JJ, Muthuchamy, M, Wieczorek, DF and Schwartz, A (1992). Mutually exclusive exon splicing of the cardiac calcium channel alpha 1 subunit gene generates developmentally regulated isoforms in the rat heart. Proc Natl Acad Sci U S A, 89, 1497-501.

(28) Doherty, P, Singh, A, Rimon, G, Bolsover, SR and Walsh, FS (1993). Thy-1 antibody-triggered neurite outgrowth requires an influx of calcium into neurons via N- and L-type calcium channels. J Cell Biol, 122, 181-9.

(29) Doherty, P and Walsh, FS (1994). Signal transduction events underlying neurite outgrowth stimulated by cell adhesion molecules. Curr Opin Neurobiol, 4, 49-55.

(30) Dolphin, AC (1995). The G.L. Brown Prize Lecture. Voltage-dependent calcium channels and their modulation by neurotransmitters and G proteins. Exp Physiol, 80, 1-36.

(31) Easter, SS, Burrill, J, Marcus, RC, Ross, LS, Taylor, JSH and Wilson, SW (1994). Initial tract formation in the vertebrate brain. Progress in Brain Research, 102, 79-89.

(32) Eisen, JS (1991). Developmental neurobiology of the zebrafish. J Neurosci, 11, 311-7.

(33) Eisen, JS, Myers, PZ and Westerfield, M (1986). Pathway selection by growth cones of identified motoneurones in live zebra fish embryos. Nature, 320, 269-71.

(34) Eisen, JS, Pike, SH and Romancier, B (1990). An identified motoneuron with variable fates in embryonic zebrafish. J Neurosci, 10, 34-43.

(35) Fetcho, JR and O'Malley, DM (1995). Visualization of active neural circuitry in the spinal cord of intact zebrafish. J Neurophysiol, 73, 399-406.

(36) Fields, RD, Guthrie, PB, Russell, JT, Kater, SB, Malhotra, BS and Nelson, PG (1993). Accommodation of mouse DRG growth cones to electrically induced collapse: kinetic analysis of calcium transients and set-point theory. J Neurobiol, 24, 1080-98.

(37) Fields, RD, Neale, EA and Nelson, PG (1990). Effects of patterned electrical activity on neurite outgrowth from mouse sensory neurons. J Neurosci, 10, 2950-64.

(38) Fisher, RE, Gray, R and Johnston, D (1990). Properties and distribution of single voltage-gated calcium channels in adult hippocampal neurons. J Neurophysiol, 64, 91-104.

(39) Forti, L and Pietrobon, D (1993). Functional diversity of L-type calcium channels in rat cerebellar neurons. Neuron, 10, 437-450.

(40) Fox, AP, Nowycky, MC and Tsien, RW (1987). Single-channel recordings of three types of calcium channels in chick sensory neurones. J Physiol Lond, 394, 173-200.

(41) Franklin, JL, Sanz, RC, Juhasz, A, Deckwerth, TL and Johnson, EJ (1995). Chronic depolarization prevents programmed death of sympathetic neurons in vitro but does not support growth: requirement for Ca2+ influx but not Trk activation. J Neurosci.

(42) French, AS and Stockbridge, LL (1988). Fractal and Markov behaviour in ion channel kinetics. Canadian Journal of Physiology and Pharmacology, 66, 967-970.

(43) Fritschy, JM, Paysan, J, Enna, A and Mohler, H (1994). Switch in the expression of rat GABAA-receptor subtypes during postnatal development: an immunohistochemical study. J Neurosci, 14, 5302-24.

(44) Fukushima, Y and Hagiwara, S (1985). Currents carried by monovalent cations through calcium channels in mouse neoplastic lymphocytes. Journal of Physiology, 358, 255-284.

(45) Funte, LR and Haydon, PG (1993). Synaptic target contact enhances presynaptic calcium influx by activating cAMP-dependent protein kinase during synaptogenesis. Neuron, 10, 1069-78.

(46) Galli, C, Meucci, O, Scorziello, A, Werge, TM, Calissano, P and Schettini, G (1995). Apoptosis in cerebellar granule cells is blocked by high KCl, forskolin, and IGF-1 through distinct mechanisms of action: the involvement of intracellular calcium and RNA synthesis. J Neurosci, 15, 1172-9.

(47) Gallin, WE and Greenberg, ME (1995). Calcium regulation of gene expression in neurons: the mode of entry matters. Current Opinion in Neurobiology, 5, 367-374.

(48) Goldberg, DJ and Burmeister, DW (1989). Looking into growth cones. Trends Neurosci, 12, 503-6.

(49) Goldberger, AL, Rigney, DR and West, BJ (1990). Chaos and fractals in human physiology. Sci Am, 262, 42-9.

(50) Gomez, TM, Snow, DM and Letourneau, PC (1995). Characterisation of spontaneous calcium transients in nerve growth cones and their effect on growth cone migration. Neuron, 14, 1233-1246.

(51) Gordon-Weeks, PR and Mansfield, SG (1992). Assembly of microtubules in growth cones: the role of microtubule associated proteins. In P. K. Letourneau SB; Macagno, ER (Eds.), The nerve growth cone (pp. 55-64). Raven Press.

(52) Gottmann, K, Dietzel, ID, Lux, HD, Huck, S and Rohrer, H (1988). Development of inward currents in chick sensory and autonomic neuronal precursor cells in culture. J Neurosci, 8, 3722-32.

(53) Gottmann, K and Lux. HD (1990). Low- and high-voltage-activated Ca2+ conductances in electrically excitable growth cones of chick dorsal root ganglion neurons. Neuroscience Letters, 110, 34-39.

(54) Griffith, WH, Taylor, L and Davis, MJ (1994). Whole-cell and single-channel calcium currents in guinea pig basal forebrain neurons. J Neurophysiol, 71, 2359-76.

(55) Groden, DL, Guan, Z and Stokes, BT (1991). Determination of Fura-2 dissociation constants following adjustment of the apparent Ca-EGTA association constant for temperature and ionic strength [published erratum appears in Cell Calcium 1991 Jul;12(7):522]. Cell Calcium, 12, 279-87.

(56) Grynkiewicz, G, Poenie, M and Tsien, RY (1985). A new generation of Ca2+ indicators with greatly improved fluorescence properties. J Biol Chem, 260, 3440-50.

(57) Gu, X, Olson, EC and Spitzer, NC (1994). Spontaneous neuronal calcium spikes and waves during early differentiation. J Neurosci.

(58) Gu, X and Spitzer, NC (1993). Low-threshold Ca2+ current and its role in spontaneous elevations of intracellular Ca2+ in developing Xenopus neurons [published erratum appears in J Neurosci 1994 Mar;14(3 Pt 1):following table of contents]. J Neurosci, 13, 4936-48.

(59) Gu, X and Spitzer, NC (1995). Distinct aspects of neuronal differentiation encoded by frequency of spontaneous Ca2+ transients. Nature, 375, 784-787.

(60) Gunderson, RW and Barrett, JN (1980). Characterisation of the turning response of dorsal root neurites toward Nerve Growth Factor. Journal of Cell Biology, 87, 546-554.

(61) Hamill, OP, Marty, A, Neher, E, Sakmann, B and Sigworth, FJ (1981). Improved patch-clamp techniques for high-resolution current recording from cells and cell-free membrane patches. Pflugers Arch, 391, 85-100.

(62) Hatten, ME and Mason, CA (1990). Mechanisms of glial-guided neuronal migration in vitro and in vivo. Experientia, 46, 907-16.

(63) Haydon, PG and Zoran, MJ (1994). Retrograde regulation of presynaptic development during synaptogenesis. J Neurobiol, 25, 694-706.

(64) Hell, JW, Westenbroek, RE, Warner, C, Ahlijanian, MK, Prystay, W, Gilbert, MM, Snutch, TP and Catterall, WA (1993). Identification and differential subcellular localization of the neuronal class C and class D L-type calcium channel alpha 1 subunits. J Cell Biol, 123, 949-62.

(65) Hendrickson, AE, Van, BJ, Mulligan, KA and Celio, MR (1991). Development of the calcium-binding protein parvalbumin and calbindin in monkey striate cortex. J Comp Neurol, 307, 626-46.

(66) Herman, MD, Reuveny, E and Narahashi, T (1993). The effect of polyamines on voltage-activated calcium channels in mouse neuroblastoma cells. J Physiol Lond, 462, 645-60.

(67) Hescheler, J and Schultz, G (1993). G-proteins involved in the calcium channel signalling system. Curr Opin Neurobiol, 3, 360-7.

(68) Hess, P (1990). Calcium channels in vertebrate cells. Annual Review of Neuroscience, 13, 337-56.

(69) Hess, P, Lansman, JB and Tsien, RW (1984). Different modes of Ca channel gating behaviour favoured by dihydropyridine Ca agonists and antagonists. Nature, 311, 538-544.

(70) Hofmann, F, Biel, M and Flockerzi, V (1994). Molecular basis for Ca2+ channel diversity. Annu Rev Neurosci, 17, 399-418.

(71) Holliday, J, Adams, RJ, Sejnowski, TJ and Spitzer, NC (1991). Calcium-induced release of calcium regulates differentiation of cultured spinal neurons. Neuron, 7, 787-96.

(72) Holliday, J and Spitzer, NC (1990). Spontaneous calcium influx and its roles in differentiation of spinal neurons in culture. Dev Biol, 141, 13-23.

(73) Horn, R (1991). Estimating the nuber of channels in patch recordings. Biophys J, 60, 433-439.

(74) Hymel, L, Striessnig, J, Glossmann, H and Schindler, H (1988). Puriefied skeletel muscle 1,4-dihydropyridine receptor forms phosphorylation-dependent oligomeric calcium channels in planar bilayers. Proceedings of the National Academy of Sciences of the United States of America, 85, 4290-4294.

(75) Ishida, I and Deguchi, T (1983). Effect of depolarizing agents on choline acetyltransferase and acetylcholinesterase activities in primary cell cultures of spinal cord. J Neurosci, 3, 1818-23.

(76) Isom, LL, DeJongh, KS and Caterall, WA (1994). Auxiliary subunits of voltage gated ion channels. Neuron, 12, 1183-1194.

(77) Issa, NP and Hudspeth, AJ (1994). Clustering of Ca2+ channels and Ca(2+)-activated K+ channels at fluorescently labeled presynaptic active zones of hair cells. Proc Natl Acad Sci U S A, 91, 7578-82.

(78) Jacobson (1991). Developmental Neurobiology. New York: Plenum Press.

(79) Johnson, BD and Byerly, L (1993). A cytoskeletal mechanism for Ca2+ channel metabolic dependence and inactivation by intracellular Ca2+. Neuron, 10, 797-804.

(80) Kasai, H and Neher, E (1992). Dihydropyridine sensitive and omega-conotoxin-sensitive calcium channels in a mammalian neuroblastoma-glioma cell line. Journal of Physiology, 448, 161-188.

(81) Kater, SB and Mills, LR (1991). Regulation of growth cone behavior by calcium. J Neurosci, 11, 891-9.

(82) Kimhi, Y, Palfrey, C, Spector, I, Barak, Y and Littauer, UZ (1976). Maturation of neuroblastoma cells in the presence of dimethylsulfoxide. Proceedings of the National Academy of Sciences of the United States of America, 73, 462-6.

(83) Kimmel, CB (1993). Patterning the brain of the zebrafish embryo. Annu Rev Neurosci, 16, 707-32.

(84) Kimmel, CB and Law, RD (1985). Cell lineage of zebrafish blastomeres. III. Clonal analyses of the blastula and gastrula stages. Dev Biol, 108, 94-101.

(85) Kimmel, CB, Warga, RM and Schilling, TF (1990). Origin and organization of the zebrafish fate map. Development, 108, 581-94.

(86) Kobrinsky, EM, Pearson, HA and Dolphin, AC (1994). Low- and high-voltage-activated calcium channel currents and their modulation in the dorsal root ganglion cell line ND7-23. Neuroscience, 58, 539-52.

(87) Koike, T, Martin, DP and Johnson, EJ (1989). Role of Ca2+ channels in the ability of membrane depolarization to prevent neuronal death induced by trophic-factor deprivation: evidence that levels of internal Ca2+ determine nerve growth factor dependence of sympathetic ganglion cells. Proc Natl Acad Sci U S A, 86, 6421-5.

(88) Komuro, H and Rakic, P (1992). Selective role of N-type Ca-channels in neuronal migration. Science, 257, 806-809.

(89) Komuro, H and Rakic, P (1993). Modulation of neuronal migration by NMDA receptors. Science, 260, 95-7.

(90) Kunze, DL and Ritchie, AK (1990). Multiple conductance levels of the dihydropyridine-sensitive calcium channel in GH3 cells. Journal of Membrane Biology, 118, 171-178.

(91) Lampe, PA, Cornbrooks, EB, Juhasz, A, Johnson, EJ and Franklin, JL (1995). Suppression of programmed neuronal death by a thapsigargin-induced Ca2+ influx. J Neurobiol, 26, 205-12.

(92) Larmet, Y, Dolphin, AC and Davies, AM (1992). Intracellular calcium regulates the survival of early sensory neurons before they become dependent on neurotrophic factors. Neuron, 9, 563-74.

(93) Lawrie, AM, Graham, ME, Thorn, P, Gallacher, DV and Burgoyne, RD (1993). Synchronous calcium oscillations in cerebellar granule cells in culture mediated by NMDA receptors. Neuroreport, 4, 539-42.

(94) Liebovitch, LS, Fischbarg, J, Koniarek, JP, Todorova, I and Wang, M (1987). Fractal model of ion channel kinetics. Biochimica et Biophysica Acta, 896, 173-180.

(95) Liebovitch, LS and Sullivan, JM (1987). Fractal analysis of a voltage-dependent potassium channel from cultured mouse hippocampal neurons. Biophysical Journal, 52, 979-988.

(96) Lipscombe, D, Madison, DV, Poenie, M, Reuter, H, Tsien, RY and Tsien, RW (1988). Spatial distribution of calcium channels and cytosolic calcium transients in growth cones and cell bodies of sympathetic neurons. Proceedings of the National Academy of Sciences of the United States of America, 85, 2398-2402.

(97) Madison, DV, Malenka, RC and Nicoll, RA (1991). Mechanisms underlying long-term potentiation of synaptic transmission. Annu Rev Neurosci, 14, 379-97.

(98) Mandelbrot, B (1967). How long is the coastline of Britain? Statistical self-similarity and fractional dimension. Science, 156, 636-638.

(99) Margiotta, JF and Gurantz, D (1989). Changes in the number, function, and regulation of nicotinic acetylcholine receptors during neuronal development. Dev Biol, 135, 326-39.

(100) Martin, DK and Cook, DI (1990). A direct-reading device for measurement of patch-clamp micropipette tip diameters. Pflugers Arch, 417, 255-8.

(101) Mattson, MP and Kater, SB (1987). Calcium regulation of neurite elongation and growth cone motility. Journal of Neuroscience, 7, 4034.

(102) McCarthy, RT and TanPiengco, PE (1992). Multiple types of high-threshold calcium channels in rabbit sensory neurons: high-affinity block of neuronal L-type by nimodipine. J Neurosci, 12, 2225-34.

(103) McCobb, DP, Best, PM and Beam, KG (1989). Development alters the expression of calcium currents in chick limb motoneurons. Neuron, 2, 1633-43.

(104) Meyer, A, Biermann, CH and Orti, G (1993). The phylogenetic position of the zebrafish (Danio rerio), a model system in developmental biology: an invitation to the comparative method. Proc R Soc Lond B Biol Sci, 252, 231-6.
For Miutz et al. see p. 180
(105) Moorman, SJ and Hume, RI (1993). Omega-conotoxin prevents myelin-evoked growth cone collapse in neonatal rat locus coeruleus neurons in vitro. Journal of Neuroscience, 13, 4727-4736.

(106) Moreau, M, Leclerc, C, Gualandris, PL and Duprat, AM (1994). Increased internal Ca2+ mediates neural induction in the amphibian embryo. Proc Natl Acad Sci U S A, 91, 12639-43.

(107) Morton, AJ, Hammond, C, Mason, WT and Henderson, G (1992). Characterisation of the L- and N-type calcium channels in differentiated SH-SY5Y neuroblastoma cells: calcium imaging and single channel recording. Brain Res Mol Brain Res, 13, 53-61.

(108) Myers, PZ, Eisen, JS and Westerfield, M (1986). Development and axonal outgrowth of identified motoneurons in the zebrafish. J Neurosci, 6, 2278-89.

(109) Mynlieff, M and Beam, KG (1992). Developmental expression of voltage-dependent calcium currents in identified mouse motoneurons. Dev Biol. 152, 407-10.

(110) Narahashi, T, Tsunoo. A and Yoshii, M (1987). Characterization of two types of calcium channels in mouse neuroblastoma cells. Journal of Physiology, 383, 231-249.

(111) Neely, MD and Gesemann, M (1994). Disruption of microfilaments in growth cones following depolarization and calcium influx. J Neurosci, 14, 7511-20.

(112) Neher, E and Zucker, RS (1993). Multiple calcium-dependent processes related to secretion in bovine chromaffin cells. Neuron, 10, 21-30.

(113) Nowycky, MC, Fox, AP and Tsien, RW (1985). Three types of neuronal calcium channel with different calcium agonist sensitivity. Nature, 316, 440-443.

(114) O'Donovan, M, Ho, S and Yee, W (1994). Calcium imaging of rhythmic network activity in the developing spinal cord of the chick embryo. J Neurosci.

(115) Ono, K and Fozzard, HA (1992). Phosphorylation restores activity of L-type calcium channels after rundown in inside out patches from rabbit cardiac cells. Journal of Physiology, 454, 673-688.

(116) Plummer, MR, Logothetis, DE and Hess, P (1989). Elementary properties and pharmacological sensitivities of calcium channels in mammalian peripheral neurons. Neuron, 2, 1453-63.

(117) Przywara, DA, Bhave, SV, Chowdhury, PS, Wakade, TD and Wakade, AR (1993). Sites of transmitter release and relation to intracellular Ca2+ in cultured sympathetic neurons. Neuroscience, 52, 973-86.

(118) Rakic, P, Cameron, RS and Komuro, H (1994). Recognition, adhesion, transmembrane signaling and cell motility in guided neuronal migration. Curr Opin Neurobiol, 4, 63-9.

(119) Randall, A and Tsien, RW (1995). Pharmacological dissection of multiple types of Ca2+ channel currents in rat cerebellar granule neurons. J Neurosci, 15, 2995-3012.

(120) Reber, BF and Reuter, H (1991). Dependence of cytosolic calcium in differentiating rat pheochromocytoma cells on calcium channels and intracellular stores. J Physiol Lond, 435, 145-62.

(121) Reboulleau, CP (1986). Extracellular calcium-induced neuroblastoma cell differentiation: involvement of phosphatidylinositol turnover. J Neurochem, 46, 920-30.

(122) Roberts, WM (1994). Localization of calcium signals by a mobile calcium buffer in frog saccular hair cells. J Neurosci.

(123) Robson, SJ and Burgoyne, RD (1989). L-type calcium channels in the regulation of neurite outgrowth from rat dorsal root ganglion neurons in culture. Neurosci Lett, 104, 110-4.

(124) Sakman, B and Neher, E (1983). Geometric parameters of pipettes and membrane patches. In B. Sakman and E. Neher (Eds.), Simgle-Channel Recording (pp. 37-52). New York: Plenum Press.

(125) Schilling, K, Dickinson, MH, Connor, JA and Morgan, JI (1991). Electrical activity in cerebellar cultures determines Purkinje cell dendritic growth patterns. Neuron, 7, 891-902.

(126) Scott, BS and Fisher, KC (1970). Potassium concentration and number of neurons in cultures of dissociated ganglia. Experimental Neurology, 27, 16-22.

(127) Scott, RH, Pearson, HA and Dolphin, AC (1991). Aspects of vertebrate neuronal voltage-activated calcium currents and their regulation. Progress in Neurobiology, 36, 485-520.

(128) Sheng, M, Dougan, ST, McFadden, G and Greenberg, ME (1988). Calcium and growth factor pathways of c-fos transcriptional activation require distinct upstream regulatory sequences. Mol Cell Biol, 8, 2787-96.

(129) Shuba, YM, Teslenko, VI, Savchenko, AN and Pogorelaya, NH (1991). The effect of permeant ions on single channel calcium channel activation in mouse neuroblastoma cells: Ion channel interaction. Journal of Physiology, 443, 25-44.

(130) Silver, RA, Lamb, AG and Bolsover, SR (1989). Elevated cytosolic calcium in the growth cone inhibits neurite elongation in neuroblastoma cells: correlation of behavioral states with cytosolic calcium concentration. J Neurosci, 9, 4007-20.

(131) Silver, RA, Lamb, AG and Bolsover, SR (1990). Calcium hotspots caused by L-channel clustering promote morphological changes in neuronal growth cones. Nature, 343, 751-4.

(132) Simpson, PB, Challiss, RAJ and Nahorski, SR (1995). Neuronal Ca2+ stores: activation and function. TINS, 18, 229-306.

(133) Snutch, TP and Reiner, PB (1992). Calcium channels: diversity of form and function. Current Opinion in Neurobiology, 2, 247-253.

(134) Soekarno, A, Lom, B and Hockberger, PE (1993). Pathfinding by neuroblastoma cells in culture is directed by preferential adhesion to positively charged surfaces. Neuroimage, 1, 129-144.

(135) Spitzer, NC (1991). A developmental handshake: neuronal control of ionic currents and their control of neuronal differentiation. J Neurobiol, 22, 659-73.

(136) Spitzer, NC, Debaca, RC, Allen, KA and Holliday, J (1993). Calcium dependence of differentiation of GABA immunoreactivity in spinal neurons. J Comp Neurol, 337, 168-75.

(137) Strehlow, D, Heinrich, G and Gilbert, W (1994). The fates of the blastomeres of the 16-cell zebrafish embryo. Development, 120, 1791-8.

(138) Streit, J and Lux, HD (1989). Distribution of calcium currents in sprouting PC12 cells. J Neurosci, 9, 4190-9.

(139) Sun, YA and Poo, MM (1987). Evoked release of acetylcholine from the growing embryonic neuron. Proc Natl Acad Sci U S A, 84, 2540-4.

(140) Takei, N and Endo, Y (1994). Ca2+ ionophore-induced apoptosis on cultured embryonic rat cortical neurons. Brain Res, 652, 65-70.

(141) Tessier-Lavigne, M (1994). Axon guidance by diffusible repellants and attractants. Curr Opin Genet Dev, 4, 596-601.

(142) Tsien, RY (1980). New calcium indicators and buffers with high selectivity against magnesium and protons: design, synthesis, and properties of prototype structures. Biochemistry, 19, 2396-404.

(143) Usowicz, MM, Sugimori, M, Cherksey, B and Llinas, R (1992). P-type calcium channels in the somata and dendrites of adult cerebellar Purkinje cells. Neuron, 9, 1185-99.

(144) Vigers, AJ and Pfenninger, KH (1991). N-type and L-type calcium channels are present in nerve growth cones. Numbers increase on synaptogenesis. Brain Res Dev Brain Res, 60, 197-203.

(145) Walicke, PA and Patterson, PH (1981). On the role of Ca2+ in the transmitter choice made by cultured sympathetic neurons. Journal of Neuroscience, 1, 343-350.

(146) Wall, PD and Gutnick, M (1974). Properties of afferent nerve impulses originating from a neuroma. Nature, 248, 740-743.

(147) Wang, X, Treistman, SN and Lemos, JR (1993). Single channel recordings of Nt- and L-type Ca2+ currents in rat neurohypophysial terminals. J Neurophysiol, 70, 1617-28.

(148) Wei, X, Neely, A, Lacerda, AE, Olcese, R, Stefani, E, Perez, RE and Birnbaumer, L (1994). Modification of Ca2+ channel activity by deletions at the carboxyl terminus of the cardiac alpha 1 subunit. J Biol Chem, 269, 1635-40.

(149) Westenbroek, RE, Hell, JW, Warner, C, Dubel, SJ, Snutch, TP and Catterall, WA (1992). Biochemical properties and subcellular

distribution of an N-type calcium channel alpha 1 subunit. Neuron, 9, 1099-115.

(150) Westerfield, M (1994). The Zebrafish Book. Eugene, OR: University of Oregon Press.

(151) Williams, EJ, Doherty, P, Turner, G, Reid, RA, Hemperly, JJ and Walsh, FS (1992). Calcium influx into neurons can solely account for cell contact-dependent neurite outgrowth stimulated by transfected L1. J Cell Biol, 119, 883-92.

(152) Williams, D and Cohan, C (1994). Calcium transients in growth cones and axons of cultured Helisoma neurons in response to conditioning factors. Journal of Neurobiology, 27, 60-75.

(153) Williams, EJ, Furness, J, Walsh, FS and Doherty, P (1994). Activation of the FGF receptor underlies neurite outgrowth stimulated by L1, N-CAM, and N-cadherin. Neuron, 13, 583-94.

(154) Williams, ME, Brust, PF, Feldman, DH, Patthi, S, Simerson, S, Maroufi, A, McCue, AF, Velicelebi, G, Ellis, SB and Harpold, MM (1992). Structure and functional expression of an omega-conotoxin-sensitive human N-type calcium channel. Science, 257, 389-395.

(155) Wilson, SW, Ross, LS, Parrett, T and Easter, SJ (1990). The development of a simple scaffold of axon tracts in the brain of the embryonic zebrafish, Brachydanio rerio. Development, 108, 121-45.

(156) Wisden, W and Seeburg, PH (1992). GABAA receptor channels: from subunits to functional entities. Curr Opin Neurobiol, 2, 263-9.

(157) Wolszon, LR, Rehder, V, Kater, SB and Macagno, ER (1994). Calcium wave fronts that cross gap junctions may signal neuronal death during development. J Neurosci, 14, 3437-48.

(158) Yavin, E and Yavin, Z (1974). Attachment and culture of dissociated cells from rat embryo cerebral hemispheres on polylysine-coated surface. J Cell Biol, 62, 540-6.

(159) Yuste, R, Peinado, A and Katz, LC (1992). Neuronal domains in developing neocortex. Science, 257, 665-9.

(160) Zheng, JQ, Felder, M, Connor, JA and Poo, M-m (1994). Turning of nerve growth cones induced by neurotransmitters. Nature, 368, 140-144.

(161) Zimprich, F, Gailey, M and Bolsover, SR (1994). Biphasic effect of calcium on neurite outgrowth in neuroblastoma and cerebellar granule cells. Brain Res Dev Brain Res, 80, 7-12.

(162) Zoran, MJ, Funte, LR, Kater, SB and Haydon, PG (1993). Neuron-muscle contact changes presynaptic resting calcium set-point. Dev Biol, 158, 163-71.

Mintz, IM, Venema, VJ, Swiderek, KM; Lee, TD, Bean,BP, Adams, ME (1992). P-type calcium channels blocked by the spider toxin omega-Aga-IVA. Nature, 355, 827-829.